Quality assurance of BOLD fMRI for use in diagnostic and presurgical mapping of brain activity

Anne-Lene Mathisen

Thesis submitted for the degree of
Master of Physics

Biophysics and medical physics,
Department of Physics,
University of Oslo

Interventional Centre,
Rikshospitalet,
Oslo University Hospital

June 2010

År

Tittel

Forfatter

http://www.duo.uio.no/

Trykk: Reprosentralen, Universitetet i Oslo

Abstract

Gradient-echo echo-planar imaging, GRE-EPI, is the most used imaging technique in functional magnetic resonance imaging, fMRI, based on the blood oxygenation level-dependent, BOLD, effect. BOLD fMRI exploits susceptibility differences between oxygenated and deoxygenated blood to detect neuronal activation. However, the sequence parameters which make GRE-EPI sensitive to the BOLD effect also make it sensitive to susceptibility artifacts such as geometric distortions and signal loss. Susceptibility gradients near air/tissue interfaces can severely compromise the detection power of the BOLD analysis in certain areas of the brain, especially in the orbitofrontal cortex and temporal lobes.

The objective of this project was to develop methods that could detect areas in the brain particularly sensitive to signal loss and geometric distortions and areas where the detection power of the BOLD analysis had been compromised as a result of susceptibility differences in the brain. The effect of susceptibility induced magnetic field inhomogenities on the image quality and on the BOLD sensitivity was investigated. Magnetic field maps were generated and used as a guide to detect areas at risk for artifacts. The field maps were also used to generate simulations of the image intensity and BOLD sensitivity.

BOLD fMRI has, since its inception, been a valuable part of brain research. The methods developed in this project were tested on data collected from the FRONT project. FRONT conducted BOLD fMRI analysis on patients with a known damage to the frontal lobe and on healthy controls. Magnetic field maps and simulated BOLD sensitivity maps were generated for a sample of the subjects.

BOLD fMRI has become an increasingly valuable tool for use in presurgical planning. Data from an epilepsy patient was collected. The BOLD analysis was conducted for the purpose of locating important centers, such as the language centre, in preparation of epilepsy focus resection. The patient had several metallic clips fastened in the scull, from previous operations, susceptibility differences from the clips, in addition to differences close to air/tissue interfaces, made the detection of BOLD signal challenging. Simulated BOLD sensitivity maps were generated to help in the presurgical planning.

It was found that the BOLD sensitivity maps together with image distortion maps, generated from the magnetic field maps, are useful tools for identifying problem areas in BOLD fMRI.

Acknowledgements

This thesis was written at the Interventional Centre at Rikshospitalet between August 2009 and June 2010.

I would first like to thank my supervisors Frédéric Courivaud and Atle Bjørnerud. When it came time for me to decide on the direction of my master's degree, I knew I wanted to do something worthwhile, and hopefully make a positive contribution to the field of medical physics. Thank you for providing me with such an interesting and important topic and for all the guidance you have given me along the way. To Tor Endestad and Inge Rasmussen; thank you for providing me with such interesting data to test my findings on. It's difficult to do MRI research without willing subjects; I would therefore also like to thank my volunteers. Special thanks go to my sister, Anette, for reading through my thesis, even though she had her own to worry about. I want to thank my parents, Petter and Lise, for their continued support. You have always been there for me and believed in me and that has helped me achieve the goals I have set for myself. And then there was Espen, thank you for helping me see the light when I was in the dark.

These 10 months have been extremely rewarding for me. I have learned so much, not just about BOLD fMRI, but also about myself. Even though I now embark on something completely different, I hope I can someday return to the exciting world of Magnetic Resonance Imaging.

I dedicate this thesis to my grandparents.

Contents

1 Introduction

Since Magnetic Resonance Imaging, MRI, was first proposed as an imaging technique by Mansfield (1), Lauterbur (2) and others, it has developed to become one of the most prolific and versatile imaging techniques; however, long imaging time has been seen as a limitation. Echo-planar imaging, EPI, was first conceived by Mansfield (3), but was little used initially because of its strenuous hardware demands. As the hardware has evolved, however, EPI has been a choice sequence in MRI whenever time is of the essence. When tracking an injection of contrast or following certain biological phenomena high time resolution is essential to obtain the desired information. However, the increase in speed achieved with EPI is often paid for in decreased image quality, both intravoxel dephasing and image distortion are common artifacts in areas affected by susceptibility differences due to a small bandwidth in the phase encoding direction.

The main application of echo-planar imaging today is functional magnetic resonance imaging, fMRI. In 1990, Ogawa et al. (4) discovered that EPI was sensitive to the signal changes caused by the blood oxygenation level-dependent, BOLD, effect. The active brain has a different proportion of oxyhemoglobin to deoxyhemoglobin than the resting brain. Echo-planar imaging has sufficient speed to detect these subtle differences. However, the physical phenomenon that makes BOLD work, magnetic susceptibility, is also what makes BOLD fMRI particularly exposed to image artifacts such as image distortions and signal loss (5). A homogenous magnetic field is essential for the image quality in magnetic resonance imaging and because of its sequence parameters that is especially true for EPI. Artifacts caused by an inhomogenous magnetic field and difference in susceptibilities between different anatomical structures may in some cases be corrected for by acquiring magnetic field maps (6), but total image correction cannot be achieved today, the correction methods that have been developed require the use of complicated methods (7). However, magnetic field maps do describe the inhomogenities that lead to artifacts in a good way. One of the goals of this project is therefore to employ such field maps to estimate the occurrence and scope of common BOLD fMRI artifacts.

The imaging parameters that make EPI so prone to artifacts are necessary to achieve an acceptable BOLD contrast, i.e., contrast between the resting and the active brain. Susceptibility related artifacts may conceal activation when in reality there is activation, or they may mimic activation in areas where there in reality is none; making the drawing of definite conclusions based on the images difficult (8). The field map used to detect and estimate susceptibility artifacts can also be employed to estimate the BOLD sensitivity; assessments of this kind could then be taken into account when BOLD studies are being conducted. Since its infancy the main application of functional MRI has been understanding brain function and organization (9). While these insights may potentially have relevance for clinical applications down the road, more direct uses for fMRI in patient treatment have been slow in materializing. Using fMRI for presurgical planning for removal of pathological brain regions, diagnosing for example Alzheimer's and rehabilitation therapy for stroke patients are all applications that are a reality today or are starting to come into the clinic (10).

As the system requirements needed for echo-planar imaging are becoming more commonplace, and hardware and software methods improve, the use of BOLD in clinical practice and research, as well as other fMRI based methods, will increase further.

1.1 Project goals

The goal of this project is to develop a post processing method that uses magnetic field mapping and magnetic resonance echo-planar imaging inherent properties to estimate:

1. The potential for artifacts and misregistration in EPI images used for BOLD fMRI

2. The BOLD sensitivity

The first point is important because it will flag areas in the EPI images where one should be hesitant in drawing definite conclusions. Such uncertainty maps could perhaps affect how surgeons chose to resect[1] pathological tissue in certain cases. The second aspect of the project is important to exclude false negative results in BOLD experiments. Both the amount of artifacts and the BOLD sensitivity in an imaging sequence is dependent on the individual patient anatomy and physiology. Patient specific assessment of the BOLD sensitivity is therefore useful to make the BOLD analysis more reliable.

Earlier studies where BOLD sensitivity calculations have been employed, have mostly been occupied with comparing different sequence protocols or parameters to optimize the BOLD experiment (11), (12), (13). In this project, the goal is instead to develop the use of BOLD sensitivity actively on a patient to patient basis, to assess the validity of conclusions drawn on the basis of the BOLD data.

[1] Surgical removal of a portion of any part of the body

2 Background

In the last 20 to 30 years magnetic resonance imaging (MRI) has become one of the most important imaging techniques in medicine. Especially in the field of brain research, MRI has played a dominant role.

In this chapter a brief review of MRI theory will be presented as well as a short introduction to the basics of brain anatomy and physiology.

2.1 Magnetic Resonance Imaging

The theory behind magnetic resonance imaging is quite comprehensive and only the main topics will be addressed here. The following is based on *The Physics of Magnetic Resonance Imaging* (14) and *Magnetic Resonance Imaging* (15).

2.1.1 Basic Principles of MRI

In magnetic resonance imaging, MRI, the magnetic properties of protons are exploited to visualize the internal structure of the human body. The human body is mainly comprised of water and each molecule of water consists of one oxygen atom and two hydrogen atoms. In addition, the macro-molecules that are important parts of the human anatomy also have protons as one of their constituents.

The basis for MRI is that protons have spin ½ and with that is associated a dipolar magnetic moment, μ. When placed in a magnetic field the spins will interact with that field in a way described by the Larmor-equation:

$$\boldsymbol{\omega_0} = \gamma \boldsymbol{B_0} \tag{2.1}$$

Equation 2.1 states that a spin in a magnetic field with flux density B_0 will interact with the field and presses with an angular frequency $\boldsymbol{\omega_0}$[2] around $\mathbf{B_0}$. γ is the gyromagnetic ratio and is a unique constant for each isotope possessing a spin, for hydrogen it is $\gamma/2\pi = 42.6 * 10^6$ Hz/T. When a sample containing spins is placed in a magnetic field the spins' magnetic moments will align with the field and precess around the axis of the field. Slightly more will align parallel than anti-parallel. This results in a net magnetization, $\mathbf{M_0} = \Sigma\boldsymbol{\mu}$, directed along the magnetic field. The magnetization is proportional to the number of spins and with a higher magnetic field a larger proportion of the spins will align parallel with the field and so contribute to the magnetization. In a state of equilibrium the time-dependent change of the magnetization vector **M** is described by the Bloch-equation:

$$\frac{d\boldsymbol{M}}{dt} = \gamma(\boldsymbol{M} * \boldsymbol{B}) \tag{2.2}$$

The equation states that the time dependent change in the macroscopic magnetization vector **M** will precess about the direction of the magnetic field **B** as it will always be perpendicular to both **B** and **M.**

In the state of equilibrium it will not be possible to detect the net magnetization as it is static along the direction of the field. In MRI a receiver coil is used to detect signal from the sample. Faraday's law of induction states that a varying magnetic field in the presence of a

[2] Vectors will be denoted by bold typeface

conducting loop, i.e. a coil, will induce a current in that loop. In its equilibrium state the magnetization is static and so $\mathbf{M_0}$ needs to be moved away from that state. To flip $\mathbf{M_0}$ away from the main magnetic field direction, a second coil, a transmitter coil, perpendicular to the $\mathbf{B_0}$-field, is used to generate a radio frequency pulse with the same frequency as the Larmor frequency of protons. The magnetic field, $\mathbf{B_1}$, of this excitation pulse will interact or resonate with the net magnetization and move it away from the direction of the $\mathbf{B_0}$-field with a precession motion around $\mathbf{B_1}$, and into the transverse plane around the axis of the transmitter coil. Away from its equilibrium state a torque is exerted on the magnetization that will lead to a precession motion as shown in Figure 2.1. The receiver coil will then be able to detect the signal from the sample as it is in motion relative to the opening of the coil.

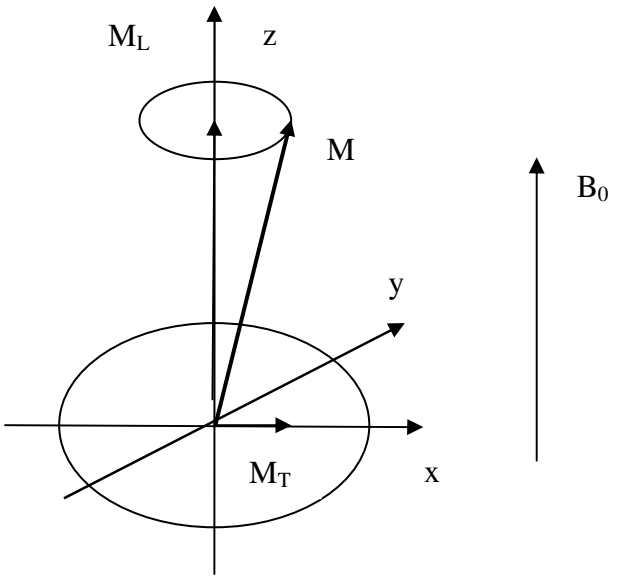

Figure 2. 1: After the net magnetization has been flipped away from the z-axis by the transmitter coil it will have a transverse component, $\mathbf{M_T}$, as well as a longitudinal one, $\mathbf{M_L}$, as it precesses about the z-axis. It is the transverse component that is detected by the receiver coil.

The motion of the magnetization vector is now determined by both $\mathbf{B_0}$ and $\mathbf{B_1}$:

$$\frac{d\boldsymbol{M}}{dt} = \gamma(\boldsymbol{M} * (\boldsymbol{B_0} + \boldsymbol{B_1})) \tag{2.3}$$

This will result in a more complex motion of the magnetization vector and it can be helpful to consider a rotating frame of reference. If this rotating frame of reference rotates around z with an angular frequency Ω, $\mathbf{B_0}$ and $\mathbf{B_1}$ will be constant and the effective magnetic field is given by:

$$\boldsymbol{B_{eff}} = \boldsymbol{B}_0 + \boldsymbol{B_1} + \frac{\Omega}{\gamma} \tag{2.4}$$

If the system rotates at the Larmor-frequency, that is $\boldsymbol{\Omega} = \boldsymbol{\omega_0}$, we have:

$$\frac{d\boldsymbol{M}}{dt} = \gamma(\boldsymbol{M} * \boldsymbol{B_1}) \tag{2.5}$$

The magnetization vector now has an angular velocity about the axis of $\mathbf{B_1}$ of:

$$\boldsymbol{\omega_1} = -\gamma \boldsymbol{B_1} \tag{2.6}$$

How far into the xy-plane the magnetization is flipped is dependent on the duration of the radio frequency pulse, t, ω_1 and B_1:

$$\alpha = t\omega_1 B_1 \tag{2.7}$$

The angle α is referred to as the flip angle and is the angle between the z-axis and **M**. For example; a flip angle of 90° would flip the magnetization entirely into the xy-plane.

2.1.2 Relaxation

As soon as the magnetization is affected by a RF pulse relaxation occurs. However, the relaxation that occurs while the pulse is applied can in most cases be neglected. When the radio pulse, also referred to as the excitation pulse, which is sent through the transmitter coil, is turned off, the magnetization will return to its equilibrium position aligned with the B_0-field. As it does so the receiver coil will detect an exponentially decaying signal called the free induction decay. The transverse component of the magnetization will decrease as the longitudinal component gradually regains its strength. There are two main components of the relaxation process.

Longitudinal relaxation

Longitudinal relaxation is also called T1 or spin-lattice relaxation. This process is caused by the spins giving up their energy to the surrounding environment or lattice. The magnetic moments of the spins then recover their longitudinal magnetization. The following equation describes this process:

$$M_L(t) = M_0\left(1 - e^{-t/T1}\right) + M_L(0)e^{-t/T1}) \tag{2.8}$$

In Equation 2.8, T1 is a measure of the time it takes for the longitudinal magnetization to regain $1\text{-}e^{-1} = 0.63$ of its equilibrium value. T1 relaxation is illustrated in Figure 2.2-A.

Transverse relaxation

Transverse relaxation is also called T2 or spin-spin relaxation. Immediately after the excitation pulse the spins' magnetic moments are parallel and precess in the same phase. But soon the spins will start to dephase leading to signal decay. There are two main processes that contribute to this. First, microscopic field inhomogenities caused by local susceptibility variations on a molecular level cause the spins to have slightly different Larmor frequencies. Second, in addition to the microscopic field inhomogenities, the main magnetic field will often not be completely homogenous. This can be because of an imperfect magnet or magnetic susceptibility variations between tissues. The first of these two effects is T2 decay, while both of the effects combined is referred to as T2* decay. The T2 relaxation process is described by the following equation:

$$\mathrm{M_T(t)} = \mathrm{M_T} * e^{-t/T2} \tag{2.9}$$

In Equation 2.9 T2 is a measure of the time it takes for the transverse magnetization to decay to e^{-1}=0.37 of its starting value. T2 relaxation is illustrated in Figure 2.2-B.

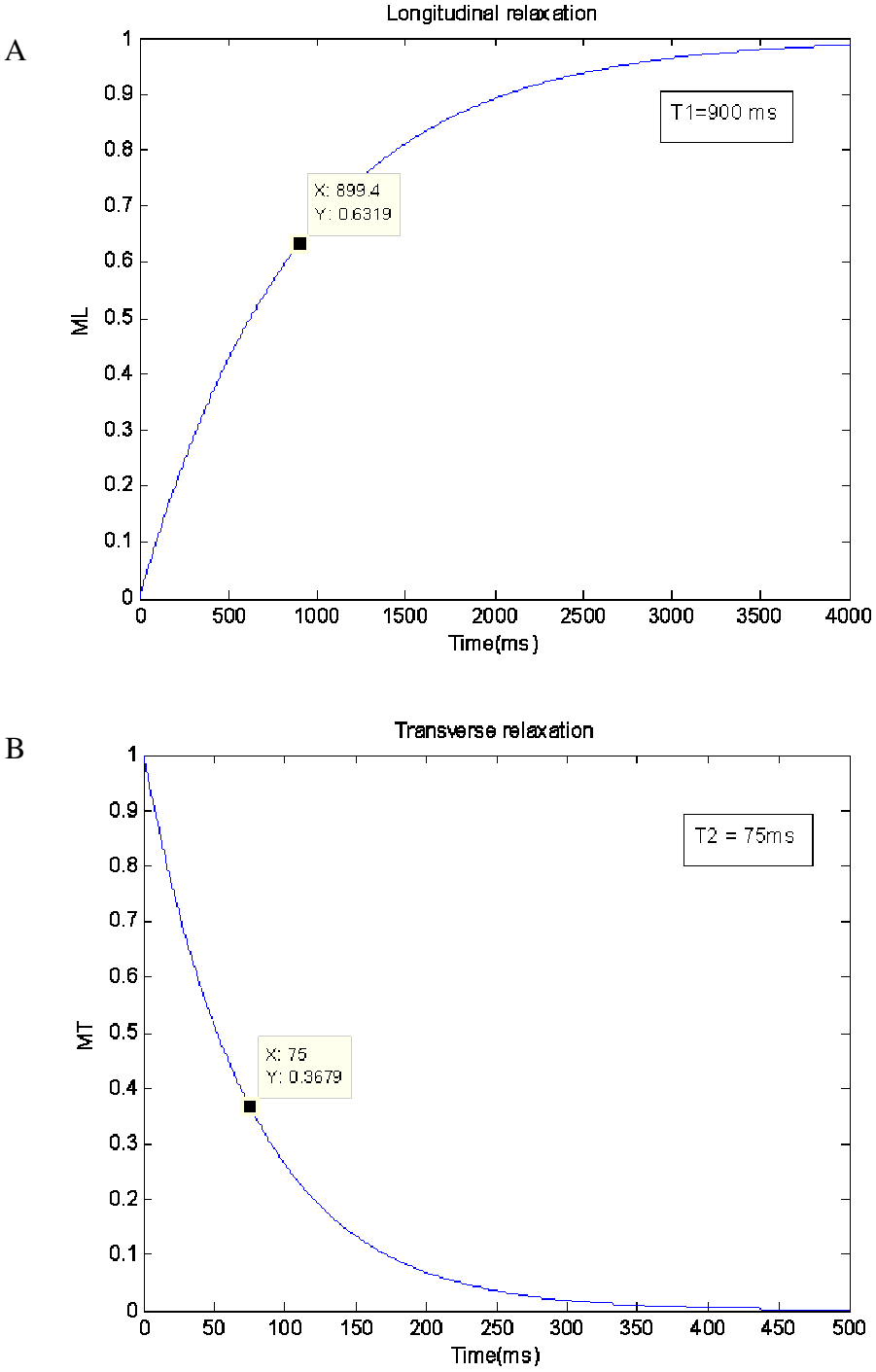

Figure 2. 2: The T1, A, and T2, B, relaxation processes after a 90^{o} excitation pulse where T1 is 900 ms and T2 is 75 ms. T1 and T2 are tissue dependent and are important parameters in the imaging process. Thus these recovery curves vary between tissues.

2.1.3 Image Formation

The situation so far has been that a single radio frequency pulse has excited the entire volume to be imaged; therefore the signal detected originates from the entire volume. It follows that this will not provide any real diagnostic information about the volume. It is necessary to locate the signal spatially in three dimensions. For this purpose magnetic field gradients are used. These gradients alter the magnetic field and make the Larmor-frequency a function of position. A gradient referred to as the slice-selection gradient makes it possible to excite one slice of the volume at a time. Only one plane within the object will have protons that are on resonance and will contribute to the signal. The axis which the slice selection direction is chosen to be along, is referred to as the z-axis. For an illustration of this process, see Figure 2.3.

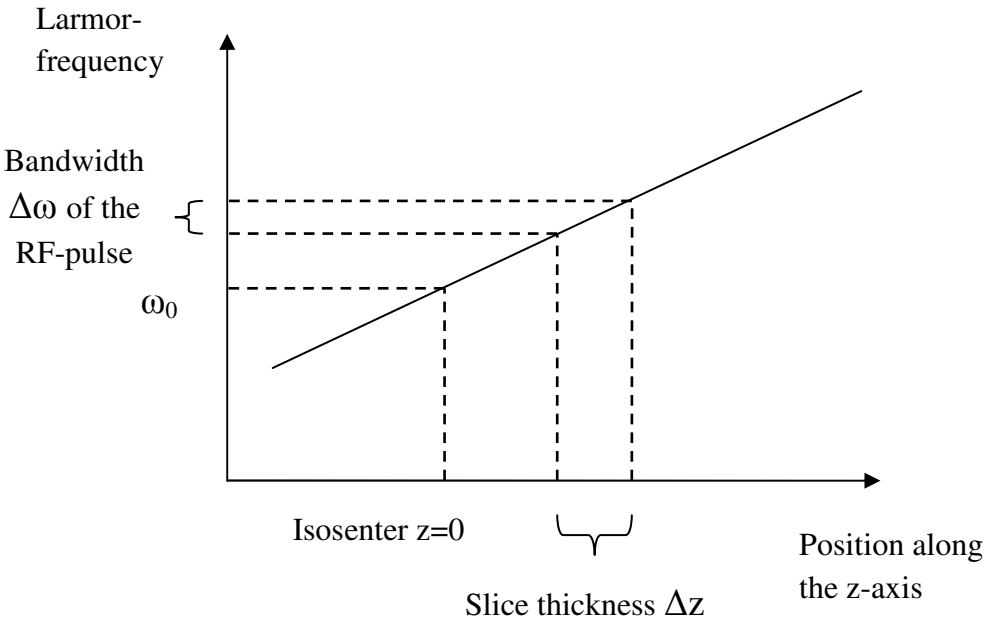

Figure 2. 3: The slice selection gradient creates a variation in the Larmor-frequency along the direction of the gradient by altering the magnetic field. The RF-pulse with bandwidth $\Delta\omega$ will excite only the spins within the slice Δz. In the isocentre the magnetic field is B_0.

Additional magnetic field gradients are then used to encode the selected slice in the two remaining directions. The phase encoding gradient and the frequency encoding gradient are always applied orthogonal to each other and the slice selection gradient. When the phase encoding gradient has been applied all spins that experienced the same magnetic field strength have the same phase. The frequency encoding gradient is applied during read-out of the signal with the result that all spins experiencing similar magnetic field strength have the same frequency.

After application of the gradients every pixel in the slice has a unique combination of phase and frequency. When data from the signal is collected it is stored as data points in k-space. One line of k-space is filled after every excitation, using a different phase encoding gradient for each line. The frequency encoding gradient is applied during read-out of the signal. Every point in k-space contains phase and frequency information from the whole slice

at a particular moment in time during read-out. k-space represents the spatial frequency distribution of the MR-image, with frequency information along the x-axis and phase information along the y-axis. Location in k-space is the integral of the applied gradients over time:

$$\boldsymbol{k} = \gamma \int_0^t \boldsymbol{G}(\tau) d\tau \tag{2.10}$$

In k-space, frequency amplitudes are represented in the time domain. To obtain a useful image, fast Fourier transform is employed to convert it into frequency amplitudes in the frequency domain. This is necessary because the gradients locate the signal spatially according to their frequency, not their time. The Fourier transform of k-space produces the distribution of the magnetization of the given slice at the time of measurement:

$$m(x,y) = \frac{1}{2\pi} \int_{k_x} \int_{k_y} M_T(k_x, k_y) e^{j(k_x x + k_y y)} dk_x dk_y \tag{2.11}$$

Thus, to form an image a Fourier transform is applied on k-space.

The use of gradient encoding is fundamental to image formation in MRI, but as only one point in k-space can be sampled at a time k-space speed is crucial in determining the total scan time.

2.1.4 Pulse Sequences

Different pulse sequences are used in the imaging process depending on the anatomy being imaged and what the desired result is. A pulse sequence is a combination of radio frequency pulses and gradient pulses applied so that k-space is sampled in a suitable way. The repetition time, TR and the echo time, TE, are parameters in any pulse sequence that are used to determine image quality and contrast. Different tissues will have different relaxation times and choosing these parameters carefully will give the MR images the desired contrast. This will be explained further in Section 2.2.1. TR is the time in ms between successive pulse sequences applied to the same slice and TE is the time in ms between excitation and read-out of the signal.

The Spin-Echo Sequence

In the spin-echo, SE, sequence a 90°-pulse is used to move the magnetization into the transverse plane. As soon as the pulse is turned off, a free induction decay is produced as spin coherence is reduced. This situation is shown in Figure 2.2-B. T2 decay ensues immediately and a 180°-pulse is applied to compensate for the dephasing caused by this effect. At a time TE after the excitation, maximum signal is induced in the receiver coil. This signal is called a spin-echo and will contain information about the T1 and T2 for the tissue as the T2* effect has been reversed by the 180°-pulse. The signal intensity for a SE sequence is given by:

$$SI \propto M_0 (1 - e^{-TR/T1}) e^{-TE/T2} \tag{2.12}$$

The Gradient-Echo Sequence

In the basic gradient-echo, GRE, pulse sequence a pulse is used to first flip the magnetization a certain angle away from the z-axis. But instead of using a second excitation pulse, gradients are used to refocus the echo. By omitting the refocusing pulse, a shorter TE and TR are possible. This saves precious time in the imaging process. But not using a refocusing pulse can have adverse effects on image quality, GRE sequences are generally more sensitive to artifacts caused by an inhomogeneous magnetic field than SE sequences, since the gradients will not refocus the dephasing in the same way that the 180°-pulse does. In GRE sequences, 'spoiling' is often applied prior to the application of the RF-pulse so that the transverse component of the magnetization is destroyed. Spoiling eliminates the effect of the residual transverse magnetization and leads to steady state longitudinal magnetization. The signal intensity for a 'spoiled' gradient-echo sequence is given by:

$$SI \propto M_0 \sin(\alpha) \frac{1 - e^{-TR/T1}}{1 - e^{-TR/T1} \cos(\alpha)} e^{-TE/T2*} \tag{2.13}$$

By varying the TR and TE of these sequences the image can be made sensitive to the T1 or T2 or T2* of the tissue, this is referred to as weighting and will be discussed more closely in Section 2.2.1.

2.2 Image Contrast

Image contrast is very important in MRI, as it is in all imaging techniques. It is essential to be able to distinguish different anatomical structures from each other as well as distinguish normal anatomy from pathology. By carefully choosing which pulse sequences and what parameters to use, the MRI sequence can be tailored to the specific needs of each exam. The following is taken from *MRI in practice* (16).

2.2.1 Weighting

The parameters T1 and T2/T2* vary between different tissues and anatomical features. As discussed in Section 2.1.2 the relaxation times T1 and T2 describe how the signal detected in the receiver coil regains its value along the z-axis and decays in the xy-plane, respectively. Figure 2.4 illustrates how the repetition time and the echo time, when selected appropriately, can have an impact on the image contrast.

As explained in Section 2.1.4 TR is the time between excitation pulses. TR is connected to T1-weighting of the image because it controls how much the longitudinal magnetization is allowed to regain its strength before the next excitation pulse is applied. As illustrated by Figure 2.4-A, a short TR will maximize the difference in T1 between the tissues. If a long TR is used both tissues' signal will have time to recover, eliminating the difference between the tissues. Setting short TR and TE will give a T1-weigthed image.

TE is the time between the excitation pulse and the peak of the echo; it controls how much the signal is allowed to decay before the signal is received. TE must be long enough so that the tissues' signal will have had time to decay. If the TE is short there will be little difference in the signals and therefore little contrast. A long TE and TR will produce an image with T2-weighting. T2*-weighting can be obtained by using a GRE sequence instead of an SE sequence.

A

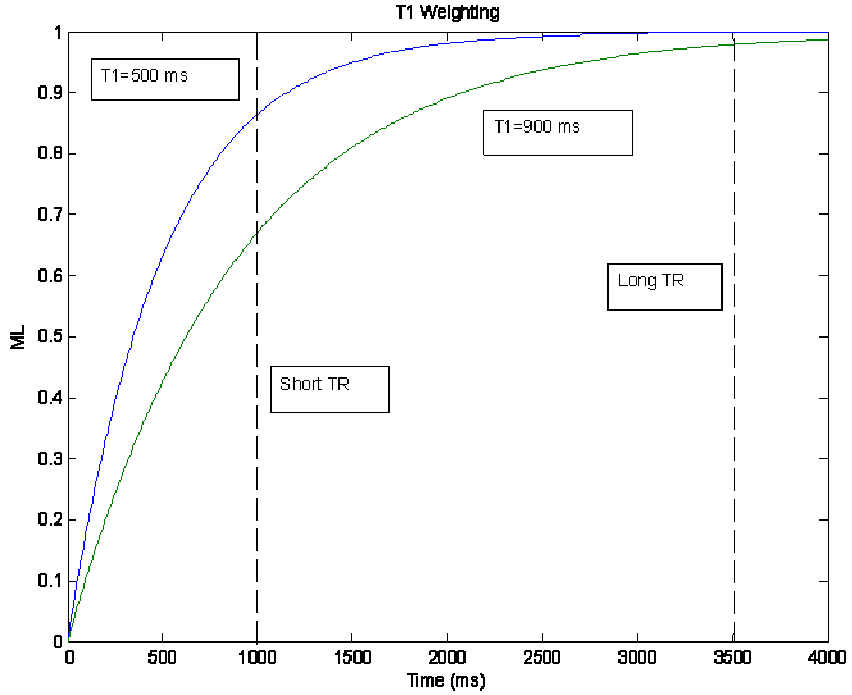

B

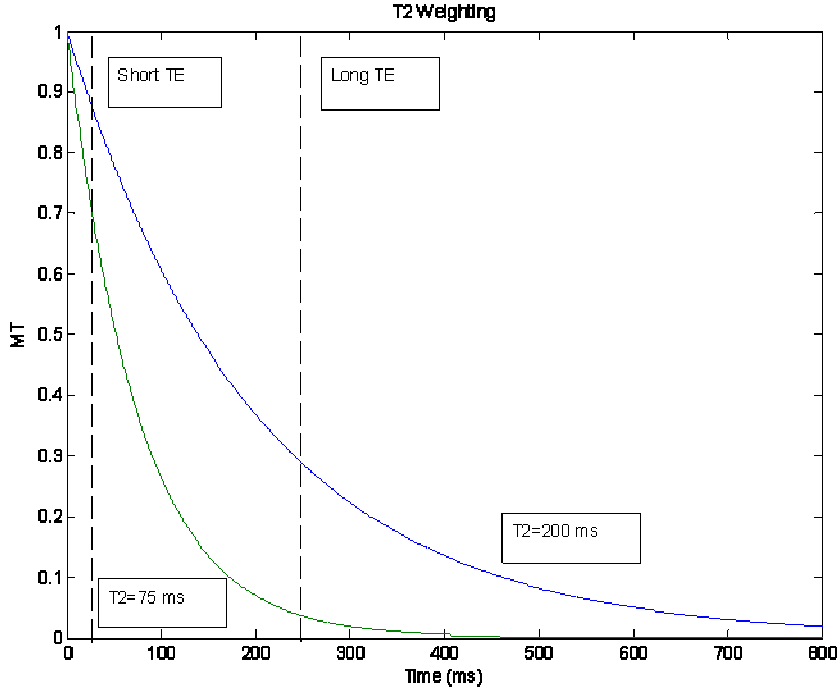

Figure 2. 4: Figure A illustrates the idea behind T1-weighting, keeping TR short will prevent the longitudinal magnetization from regaining all of its strength. Likewise, in B, for T2-weighting a long TE will let differences develop between the transverse magnetization of the tissues being imaged.

In addition to T1- and T2-weighting it is also possible to weight according to proton density. It is not as efficient as T1 and T2 as the difference in proton density for different tissues in the body is not very great. However, it can be useful at times and to achieve proton density weighting the other two effects must be diminished, so a long TR and short TE is chosen.

2.2.2 Contrast Agents

Although weighting the MR images towards T1 or T2 will induce a certain amount of contrast, it is dependent on there being a substantial difference in the relaxation times of the tissues being imaged. If this difference is not large enough, sufficient contrast may not be obtained. In these cases, contrast agents can be employed to enhance contrast. Contrast agents selectively alter the relaxation times of tissues by affecting the local magnetic environment in the tissue. They can shorten T1 or shorten T2; although all contrast agents to some extent do both, dose and imaging parameters can be chosen so that one or the other is preferred.

In addition, certain physiological parameters can be used as internal contrast; this will be discussed further in Section 3.1.

2.3 Echo-Planar Imaging

In many applications of MRI, time is an important factor in determining the nature and quality of the images. In the sequences discussed in Section 2.1.5, only one line of k-space is filled in every TR interval, in other words one excitation pulse is required for every phase encoding step. This method of generating an image is very time consuming and is in many cases not an acceptable approach. Rapid imaging techniques have therefore been developed to reduce scan time. *The Physics of Magnetic Resonance Imaging* (14) and *Magnetic Resonance Imaging* (15) is the basis for the following, unless otherwise is stated.

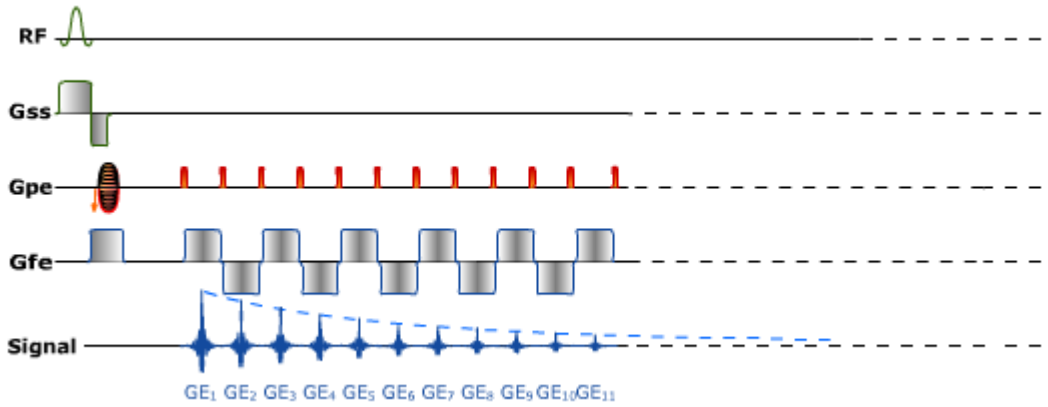

Figure 2.5: In the GRE-EPI sequence all of the lines in k-space are filled after only one excitation pulse. Following the initial 90°-pulse gradients are used to generate the first echo and refocus the signal again and again creating a train of echoes. In rapid imaging techniques the effective echo time is defined as the time between the excitation pulse and the time when the echo closest to the centre of K-space is formed. In SE-EPI a 180°-pulse is used to generate the first echo. The sequence diagram was taken from http://www.imaios.com/en/e-Courses/e-MRI/MRI-Sequences/echo-planar-imaging.

One of these fast imaging techniques is called echo-planar imaging, EPI, and is based on the gradient-echo sequence. In EPI, multiple lines of k-space are acquired after each excitation pulse by using gradients to refocus the magnetization again and again. In the extreme it is possible to fill k-space entirely after only one excitation; this is referred to as single shot EPI. Each line is acquired with a different phase encoding of the echo thereby covering k-space entirely. Because of this, echo-planar imaging has excellent time resolution. The sequence is illustrated in Figure 2.5.

In an EPI sequence the total path through k-space must be covered within the transverse relaxation time, T2*. If not the signal will decay before all the significant information can be acquired. In practice, this condition implies that k-space must be traversed within 100 ms, putting strict demands on the machine hardware, as powerful gradients are needed.

The special nature of the EPI sequence means that the expression in Equation 2.11 is no longer fully valid. T2* effects and inhomogenities in the magnetic field will affect the signal in a way described by:

$$m(x,y) = \frac{1}{2\pi}\int_{k_x}\int_{k_y} M_T(k_x,k_y)e^{j(k_x x+k_y y)}e^{-\frac{t}{T2^*}}e^{-j\Delta B(x,y)t}dk_x dk_y \tag{2.14}$$

In Equation 2.14, T2* is the transverse relaxation and ΔB is the inhomogenity in B0. They both affect the Fourier transform of the object and the consequences will be looked at closer Section 2.3.1.

2.3.1 Artifacts

Artifacts occur in all MRI images to some degree. Some can be obvious, while others are more subtle. It is important that they are understood and compensated for if possible. Using special techniques, some artifacts can be avoided while others can only be reduced. Echo-planar imaging is a very useful MRI technique when time is of the essence; however EPI is particularly sensitive to various imaging artifacts. The velocity through k-space in the phase encoding direction is much slower than in the read-out direction. Therefore artifacts caused by the T2* effect and field inhomogeneities have more time to affect the signal.

Blurring artifacts

In single shot EPI the echo is refocused many times in order to sample k-space entirely in a single TR interval. Since EPI sequences use gradients to refocus the echo and not RF pulses, spin-dephasing is not addressed. The transverse relaxation time is therefore described by T2*. During the sampling interval the refocused echoes will feel the effect of T2* differently depending on when they are sampled. T2* affects the Fourier transform of the object in such a way that blurring of the image occurs. By the time the outer k_y lines are sampled, the signal has almost completely disappeared. This effect is expressed by $e^{-t/T2*}$ in Equation 2.14.

Motion artifacts

MR imaging assumes that the object being imaged is fixed in space, but this is not always the case. It is not uncommon for the patient to move during the scan or for movement

within the body to occur, such as arterial pulsations. Motion artifacts often present itself as ghosting or blurring of the image. Since EPI has a very short acquisition time, each volume is usually free from motion artifacts; however, movement between successive volumes can occur. If differences in signal intensity are employed, for example to detect neural activity in BOLD fMRI, this can lead to erroneous detection of signal (8).

Patient movement can usually be reduced by using restraints and padding foams, especially in the case of brain scans. Other motion artifacts can be treated with post processing techniques, but are difficult to eliminate completely.

Chemical shift

When imaging areas containing both water and fat, misregistration of pixels containing fat can occur. Due to the different chemical environments of fat and water there is a 3.5 ppm chemical shift between the two. Protons in the different environments will precess at different frequencies and the scanner will mistake this difference as spatial difference causing misregistration. The artifact will be greater with increasing field strength and decrease with higher gradient strength. In addition, if a pixel contains elements of both water and fat the spins will acquire phase at different rates. The signal strength in these voxels will depend on whether the vectors are in or out of phase, it is therefore important to carefully choose an appropriate echo time.

Misregistration, which is an off-resonance effect, increases with smaller bandwidth. Increasing the bandwidth can therefore be a way of reducing these artifacts. In EPI sequences the bandwidth in the frequency direction is very high, but in the phase encoding direction the effective bandwidth can be very small. Therefore, to avoid serious artifacts, the fat signal is suppressed in EPI sequences.

2.3.2 Magnetic Susceptibility

Both chemical shift and susceptibility effects are caused by local deviations in the magnetic field. In the latter case the artifacts are linked to the different susceptibility properties of tissue versus for example air or bone. The chemical shift effect involves only two different frequencies. In contrast, susceptibility effects cause a range of different frequencies to develop.

Magnetic susceptibility is a quantity that describes the contribution made by a substance to the magnetic flux density in the presence of a magnetic field:

$$B_{eff} = (1 + \chi)B_0 \tag{2.15}$$

where χ is the susceptibility of the material. This contribution can be negative ($\chi < 0$), positive ($\chi > 0$) or zero ($\chi = 0$), for diamagnetic, paramagnetic and nonmagnetic materials respectively. The bulk susceptibility of human tissue is generally diamagnetic, water has a susceptibility of χ = -9 ppm; however, certain sub-structures in tissues can be less diamagnetic leading to potentially large differences in local susceptibility, and susceptibility gradients occur both in-plane and in the slice selection direction.

The difference in susceptibility between two regions leads to a field change, ΔB, this leads to a phase change, $\Delta\varphi$, which at the time of acquisition, TE, is given by:

$$\Delta\varphi = -\gamma\Delta BTE \tag{2.16}$$

The effects that develop as a result of the field inhomogeneities due to susceptibility effects will depend on the scale of the inhomogenities compared to the voxel dimensions of the volume, see Figure 2.6. Microscopic field inhomogeneities, 2.6-A, lead to dephasing, which leads to a shortened transverse relaxation time, T2*, see Section 2.1.2. The signal will decay faster in the presence of susceptibility effects, than if the field was completely homogenous.

Macroscopic field inhomogeneities, Figure 2.6-B, lead to two classes of image artifacts. The first artifact is image distortion. As discussed in Section 2.1.3, gradients are applied as a part of the image formation process. Susceptibility effects lead to additional gradients being present in the volume. These extra susceptibility gradients can cause spins to be incorrectly spatially localized in a way described by:

$$\delta x = \frac{\Delta \chi B_0}{G_x} \tag{2.17}$$

δx is a pixel shift along the direction of the applied gradient G_x because of a susceptibility induced field shift χB_0. The pixel dimension, Δx, in the direction of the gradient G_x is given by:

$$\Delta x = \frac{2\pi}{\gamma G_x TA} \tag{2.18}$$

where TA is the acquisition time. The pixel bandwidth is given by BW = 1/TA. For the pixel shift to be negligible relative to the pixel dimension, $\delta x << \Delta x$, the following condition must apply:

$$BW \gg \frac{\gamma \Delta \chi B_0}{2\pi} \tag{2.19}$$

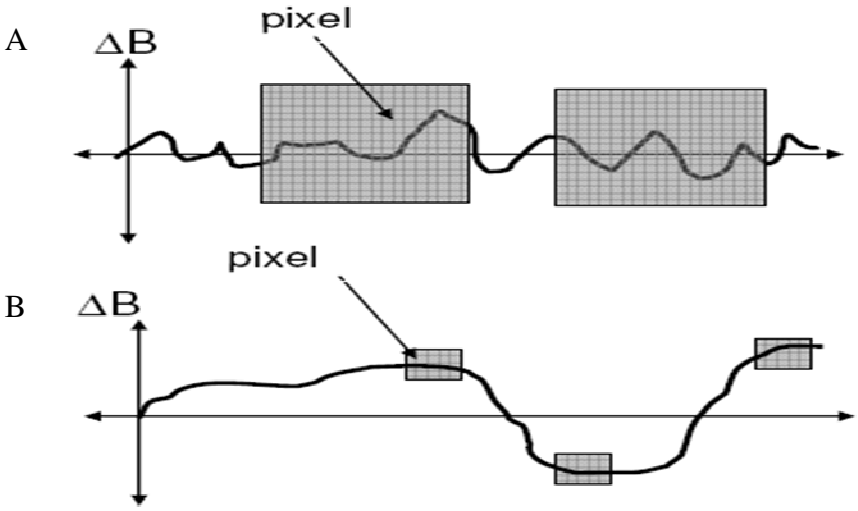

Figure 2. 6: The type of artifact the susceptibility effect will result in depends upon the properties of the susceptibility field. If the field has rapid field variations, a steep gradient, the result is likely to be signal dropout. The illustration was taken from *The Physics of Magnetic Resonance Imaging* by Bjørnerud (11).

In Equation 2.14, ΔB expresses the inhomogeneities in the magnetic field; the size of this deviation relative to the bandwidth will determine the amount of image distortion that occurs. In EPI the read-out bandwidth is usually very high due to a rapid sampling rate. But since there is only one excitation per slice k-space is travelled very "slowly" in the phase direction leading to a small pseudo-receiver bandwidth pr pixel. This small bandwidth makes EPI sequences especially vulnerable to susceptibility artifacts.

Geometric distortions caused by field inhomogenities can also occur in the slice selection direction. The effect of such a gradient is twofold as illustrated in Figure 2.7. First, the thickness of the excited slice is altered; second, the centre of the slice is shifted. Depending upon the direction of the slice-selection gradient and the susceptibility gradients, spins in the slice may not be excited, leading to signal void, or spins outside the slice may be excited leading to extra signal in some places (17). However, in EPI sequences, an interleaved scan order is often employed, implying that consecutive slices are acquired relatively far apart temporally, limiting the amount of geometric distortion in the slice selection direction.

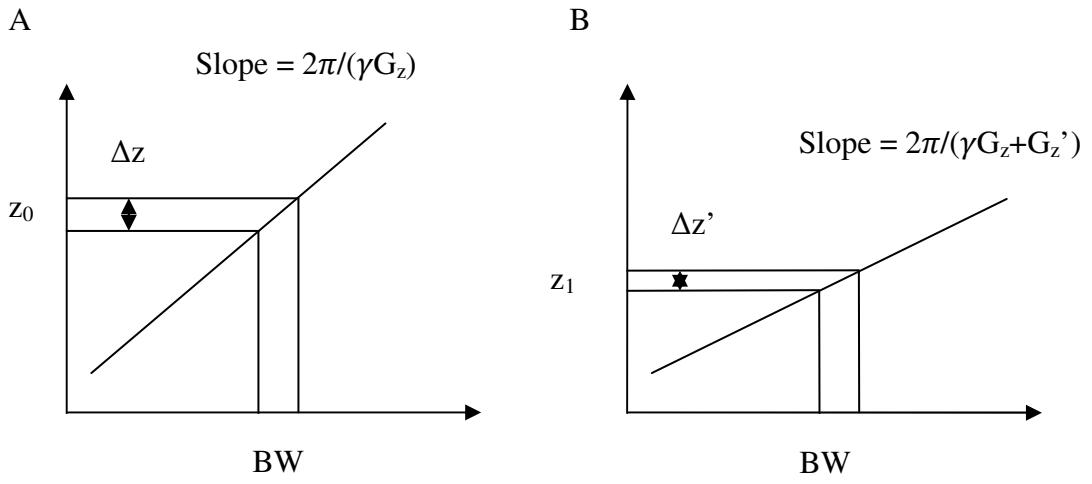

Figure 2. 7: A. The slice thickness, Δz, depends on the slice selection gradient, G_z, and the bandwidth, BW. B. An additional gradient in the slice selection direction will alter the slice thickness and the position of the excited slice.

Another artifact caused by macroscopic field inhomogenities is echo shifting (17). The additional gradient caused by susceptibility effects leads to a phase dispersion and a shifting of the echo so that it occurs at a time TE' instead of TE. This shifting of the echo can lead to a loss of signal intensity or a complete signal drop out if the echo is shifted completely outside the acquisition window. Again, this artifact is usually not a problem in the read direction in EPI because of the high sampling rate in that direction. However, the effect can be quite substantial in the phase encoding direction. The consequences for BOLD fMRI will be discussed in Section 3.1.2.

In spin-echo sequences, most of these effects are prevented due to the 180° refocusing pulse. Images generated using a gradient-echo sequence, however, are more sensitive to these artifacts since the echo is refocused using gradients the dephasing is not addressed.

2.3.3 Methods for Reducing Susceptibility Artifacts

Certain scan parameters can be adjusted to reduce artifacts that can occur because of the susceptibility gradients, as discussed in Sections 2.3.1 and 2.3.2, if not eliminate them completely. From Equation 2.16 it is obvious that a shorter TE will give the spins less time to dephase thereby increasing the signal strength. However, as will be discussed in Section 3.1.2, a long TE is sometimes necessary to achieve the acceptable results in BOLD fMRI studies. Increasing the image matrix resolution and using thin slices can significantly diminish the occurrence of susceptibility artifacts. Using multi shot EPI will also help, but since scan time will increase this is not always an option. A large pixel bandwidth will reduce distortion artifacts due to susceptibility effects, according to Equation 2.14. But in EPI sequences small bandwidths in the phase encoding direction are hard to avoid.

Shimming

Susceptibility artifacts will increase with an inhomogenous magnetic field and shimming is often used to make the field as homogenous as possible. Upon delivery from the factory, the MRI scanner has a magnetic field inhomogeneity of approximately 1000 ppm, while good quality imaging requires a maximum of 4 ppm. To achieve this, shim coils are used for active shimming and small pieces of metal are used for passive shimming. When the scanner is installed the shims are adjusted while scanning a phantom until optimum field homogeneity is achieved. In addition, in cases were a homogenous magnetic field is especially important, shimming can be specifically applied to the patient being scanned. Currents in the electromagnetic shim coils are suitably adjusted to ensure that the field is as homogenous as possible. However, magnetic susceptibility is an inherent tissue parameter and is impossible to suppress completely.

2.3.4 SENSE

As previously discussed, the small bandwidth in EPI makes the sequence especially susceptible to artifacts caused by magnetic field inhomogenities. The small bandwidth in the phase encoding direction is caused by the low velocity in which k-space is travelled in the k_y direction. SENSE stands for sensitivity encoding and is an imaging technique that acquires fewer lines in k-space while recording images simultaneously with multiple receiver coils. The receiver coils have known spatial sensitivities that are used to fill in the missing information, correctly reconstructing the image and preventing fold over artifacts that usually occur with under sampling of k-space. This technique allows the EPI sequence to be completed with a shorter scan time by a factor of 2 or higher, depending on the amount of receiver coils employed. This will in turn increase the bandwidth and reduce both motion and susceptibility artifacts. However, the signal to noise ratio, SNR, will also be reduced.

2.4 Anatomy and Physiology of the Human Brain

In neuroscience, obtaining high quality images of the brain is of the utmost importance and magnetic resonance imaging is one of the most important tools in this field, whether it is used for diagnostics or research purposes. The following is based on *Magnetic Resonance Imaging; Physical Principles and Sequence Design* (17) and *Introduction to Functional Magnetic Resonance Imaging* (18).

2.4.1 The Hemodynamic Response System

In functional magnetic resonance imaging the hemodynamic response is utilized to generate images that visualize brain function. As a patient is presented with stimulus or set to perform a task the brain activates and energy produced from glucose is needed. This production is mainly of the aerobic type, therefore the need for oxygen increases. The hemodynamic response is set into action, bringing oxygen to the activated areas, see Figure 2.8.

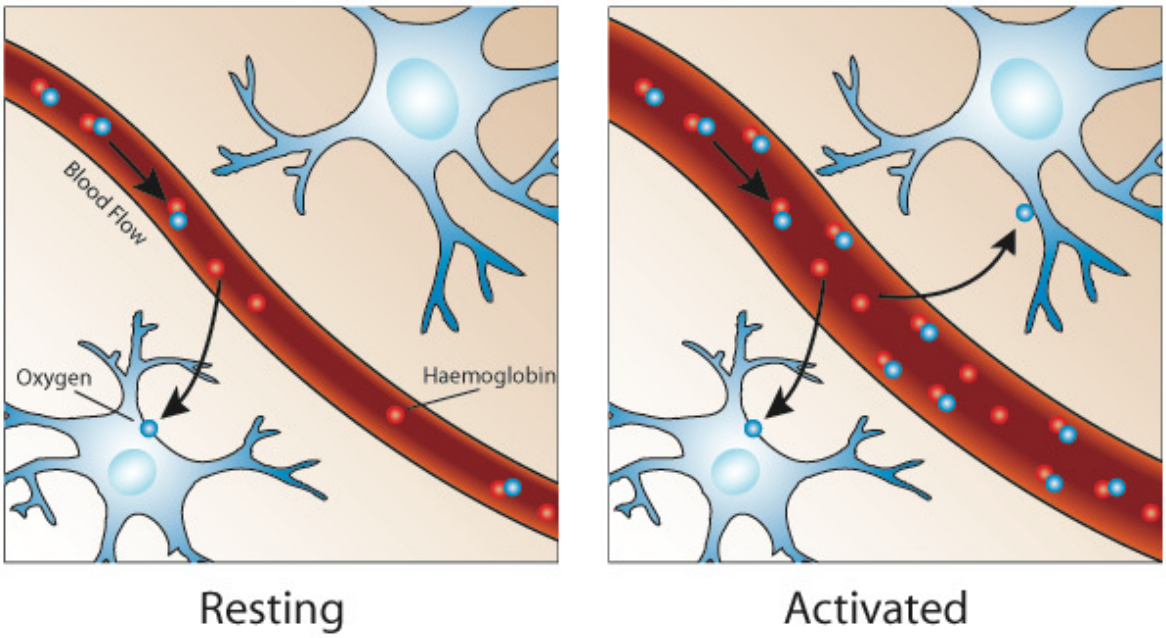

Figure 2. 8: As neurons are activated oxygenated blood is sent to the area, this response to brain activity overshoots the oxygen need, leading to an increase in the both the absolute and relative amount of oxygenated blood. The illustration was taken from http://www.psychcentral.com/lib/img/fmri_bold.jpg

Much of the iron in the blood can be found in the red blood cells or hemoglobin. Hemoglobin has two states, oxygenated or deoxygenated. Deoxyhemoglobin is paramagnetic because of the iron content in the molecule, while the oxygen in oxyhemoglobin shields the iron so that the molecule becomes diamagnetic. Fully oxygenated blood has about the same susceptibility as other brain tissues. As discussed in Section 2.3.2, susceptibility differences like this will distort the local magnetic field and lead to signal loss. Or put another way, decrease the transverse relaxation time, T2*.

Tissues that are metabolically active will have a different proportion of oxygenated blood to deoxygenated blood than surrounding quiescent tissues. The net effect of activation of a region in the brain is a net increase in the amount of oxygenated blood relative to deoxygenated blood, as the response overshoots the need. The result is a signal increase in areas that are activated, a transient rise in T2*, because of reduced susceptibility effects.

In Section 2.3.2 it was discussed how susceptibility gradients lead to unwanted artifacts in echo-planar imaging. Through functional magnetic resonance imaging, which will be further discussed in Section 3.1, susceptibility effects are taken advantage of to visualize brain activation.

2.4.2 Brain Anatomy

As discussed in Section 2.3.2, artifacts in echo-planar imaging can become a serious problem when the area being imaged contains tissues with different susceptibilities in close proximity to each other. The head mainly consists of three types of material: water, bone and air. Human tissues generally have a susceptibility of about -11 to -7 ppm, whereas air has susceptibility of 0.36. In EPI sequences this difference in magnetic susceptibility will often lead to severe artifacts in the vicinity of the sinuses and the petrous bone. When imaging the brain, especially the temporal lobes and the orbitofrontal cortex, distortions and even signal loss are common artifacts.

Thus, magnetic susceptibility is important in fMRI in two ways. First, it is utilized as a contrast to map brain activity as blood oxygenation changes with activation. Second, it is often the cause of disturbing artifacts in brain imaging especially at air-tissue interfaces. Although these artifacts constitute serious challenges, the usefulness of the BOLD response makes functional magnetic resonance imaging one of the most important tools in neuroscience today. Section 3.1 will look at how the physiological changes that follow brain activation are exploited in fMRI.

2.5 Clinical Applications of Functional Magnetic Resonance Imaging

BOLD fMRI was first conceived in the early 1990s (4), since then, the technique has been widely used for the investigation of the basic functions of the healthy human brain. However, the value of the clinical applications of BOLD is being increasingly recognized. One of the best validated applications has been, and remains, the use of BOLD fMRI in presurgical assessment of brain function for patients with epilepsy or brain tumors. Both these applications involve mapping brain function so as to facilitate planning of a surgical intervention.

Several other methods exist for mapping brain function: Electrocorticography, ECoG, consists of electrophysiological recordings in the brain. It is a demanding technique that is time consuming and requires that the patient be awake during the surgery. Since the technique is applied during surgery it cannot be incorporated in the presurgical planning. In addition, this method involves awake craniotomy, which can be very distressing and unpleasant for the patient. The Wada-test is also invasive and involves intra-arterial injection of barbiturates. This technique involves some risk and several days of hospitalization. Electroencephalography, EEG, measures neuronal activity directly via detection of electromagnetic fields. The technique has excellent temporal resolution; however, it requires complicated mathematical modeling and calculations and has limited accuracy. Advantages of fMRI include its non-invasiveness, repeatability and broad availability. Studies conducted comparing fMRI and other modalities; suggest good reliability of fMRI in locating functional areas (8).

2.5.1 Presurgical fMRI in Patients with Brain Tumors

Brain tumors are usually treated by surgery, radiation therapy, chemo therapy, or a combination of these treatment techniques. Whatever technique is employed, the primary goal is to remove as much of the tumor as possible while avoiding damage to important functions

of the brain. Surgery in the brain invariably carries a risk of post-surgical adverse effects. Although all brain areas are in some way functionally important; there are areas where damage inflicted during surgery, would have more serious consequences for the patient's quality of life after the surgery. Mapping the brain function of the patient helps with selection and planning of the appropriate treatment method. It is necessary that functional brain mapping is performed on an individual basis. Some individual factors such as gender, left or right handedness and multilinguality can affect cognitive brain functions. In addition the presence of a tumor will often lead to malformations in the brain (8).

2.5.2 Presurgical fMRI in Epilepsy

Epilepsy is a disorder of brain function that is characterized by recurring seizures with a sudden onset. The source of epilepsy can often be localized to the temporal lobe and in a limited number of cases surgical resection of focal epileptogenic lesions in the brain can be considered as a treatment (19).

Functional MRI can be useful in the treatment of epilepsy patients in a number of ways. When planning an operation the BOLD analysis can be used to determine what brain tissue holds major functions and may be affected by a surgical intervention. BOLD fMRI is especially used for lateralization of brain function. Lateralization involves determining which hemisphere of the brain controls a specific function, such as speech. In some instances, following an operation, the specialization of a function may move from one hemisphere to the other. This information may impact how future surgeries are performed.

In contrast to brain tumors, where malignant tumors have a mortality rate of about 80 %, epilepsy is not a life threatening condition, and information about possible deficits in cognitive or motor function as a result of surgical intervention, may affect the decision of whether or not to go through with the surgery. BOLD fMRI can also provide information about the localization of the epileptic focus (20).

The use of BOLD fMRI in presurgical planning is not yet an established and standardized procedure. Hopefully it can contribute to a reduction in the use of invasive mapping techniques, but for now it cannot completely replace techniques such as ECoG and Wada. Studies and clinical research trials need to be conducted to determine what positive effects BOLD fMRI presurgical planning can have on surgery-related morbidity and disease-related mortality (8).

3 Theory

3.1 Functional Magnetic Resonance Imaging

In magnetic resonance neuroimaging it is useful to separate between structural and functional imaging. Structural imaging images the anatomy of the brain and is used to diagnose large scale tumors and injuries. In functional imaging the goal is to map the function of the living brain and use this information to diagnose metabolic diseases and injuries on a smaller scale. Functional neuroimaging is also widely applied for research purposes.

The development of echo-planar imaging and other ultra-fast MRI imaging techniques has led to new applications, especially in neuroscience, that are not possible with conventional MRI sequences. Many of these new applications are collectively referred to as functional imaging techniques. Functional magnetic resonance imaging or fMRI is one such application. The following is taken from *Functional MRI* (20) and *Introduction to Functional Magnetic Resonance* (18), unless otherwise is stated.

In Section 2.4.1, it was discussed how when certain parts of the brain are activated, physiological changes in that area follow. In fMRI, susceptibility differences between oxygenated and deoxygenated blood are used to show what parts of the brain become activated following stimuli or the performance of tasks. The response detected in the fMRI image is called BOLD, blood oxygen level-dependant. Through the BOLD effect, contrast can be achieved between active and resting states of the brain.

3.1.1 The BOLD Response

In BOLD fMRI susceptibility differences between oxygenated and deoxygenated blood are utilized to look beyond the anatomy of the brain to show how different regions can be connected to specific types of activity. As discussed in Section 2.4.1, when parts of the brain activate several physiological changes occur. In summation, they lead to an increase of the amount of oxygenated blood and considering the susceptibility properties of oxygenated versus deoxygenated blood, the result is a slight signal increase in active areas. The BOLD response is dependent on both the physiological changes that follow brain activation and the physics of the MR imaging process.

Changes in three basic physiological parameters accompany brain activation, cerebral blood flow (CBF), cerebral blood volume (CBV) and the cerebral metabolic rate of oxygen utilization ($CMRO_2$). Cerebral blood flow, cerebral blood volume and the cerebral rate of oxygen utilization all increase with activation but affect the response in different ways. Thus the signal depends on these physiological changes in a somewhat complex manner. The exact nature of the response is still not completely clear, but there is a qualitative understanding of different aspects of the response. Figure 3.1 shows a schematic representation of a typical BOLD response to a short stimulus.

The initial dip of the response is mostly seen with magnetic field values of 3 T and above. It lasts about one second and is much smaller than the main response that follows. It can be interpreted as an immediate increase in $CMRO_2$ while the rest of the hemodynamic response system is somewhat slower in reacting to the stimulus. However, within seconds there is a steep rise in the BOLD response, usually to about two or three percent of baseline. It is believed that the initial dip can be a more precise spatial indicator of the activity than the main positive response.

The response reaches a steady level for the duration of the stimulus, then, as the stimulus is stopped there is an exponential decay of the signal below baseline. This undershoot is still not understood, but is most likely connected to an increase in CBV that persists even as blood flow drastically decreases, leading to susceptibility induced signal loss. After several seconds the signal returns to baseline. Repeated measurements and signal averaging are used to improve the signal to noise ratio and statistical analysis is used to detect the signal.

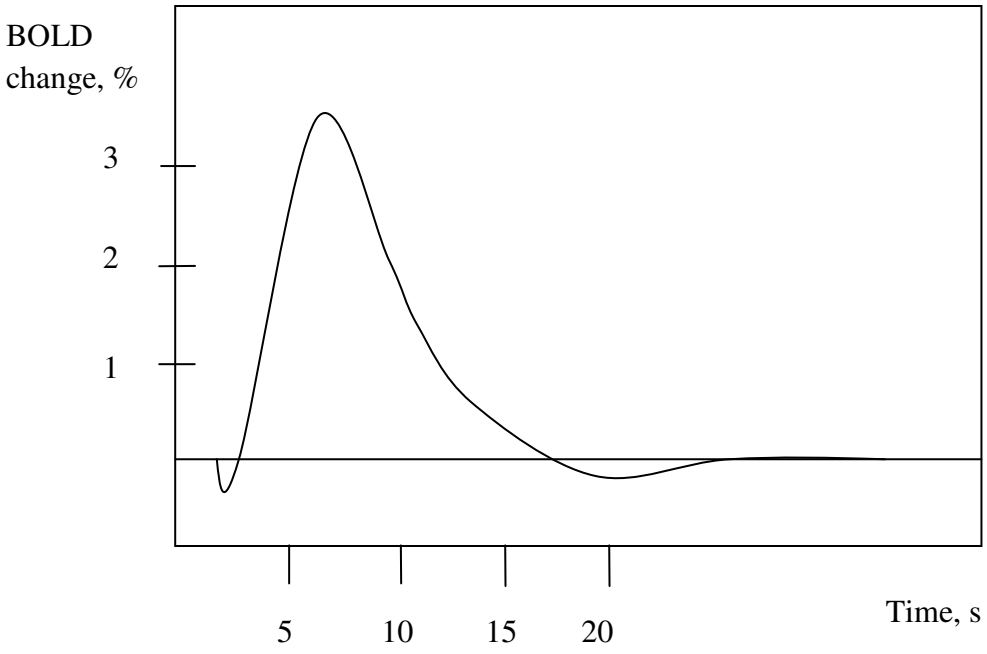

Figure 3.1: Following the neuronal stimulus there is an initial dip before a positive response. When the stimulus stops the signal undershoots before returning to baseline.

To derive useful information from the BOLD response the data needs to be processed through statistical analysis. An obvious way of processing the information would be to simply subtract the averages of the images recorded when no task is performed, the controls, from the average of the images recorded during the performance of the task. However, because of the complex nature of image noise, this method does not always work well. Instead, statistical parametric mapping has become the method of choice for analyzing BOLD fMRI data. To separate noise from true signal, the intrinsic variance of each voxel is mapped. Voxels with a large signal change together with large intrinsic variance will be suppressed, while voxels that have a large signal change compared to the intrinsic variance will remain. Voxels that have a signal change that is sufficiently greater than would be expected by chance alone are identified and marked as active. The result of the analysis will depend greatly on the threshold applied for significance. The t-test for statistical significance is often employed in BOLD fMRI analysis. It is briefly presented in Appendix B.

In the BOLD analysis there are broadly two main types of errors (8):

Type A: This type is referred to as a false positive, i.e., it is concluded that the voxel shows activation when in reality it does not.

Type B: This type is referred to as a false negative, i.e., it is concluded that there is no activity in the voxel when in reality there is.

Susceptibility artifacts of the kind described in Section 2.3.2, can contribute to both these types of errors. The BOLD analysis assumes that the noise in the BOLD measurements is normally distributed and independent; however, this is not always true. Some noise can be more structured and can even be stimulus-correlated. If this is the case, false positive activations can occur.

As seen from Figure 3.1 the response has a time frame of seconds and it is imperative that the sequence used to image it has excellent time resolution to adequately sample the response. For this reason echo-planar imaging is often employed in fMRI despite its vulnerability to artifacts.

3.1.2 BOLD Sensitivity

Since the signal increase is relatively small, only about 1 to 4 percent at 3 T, it is important to choose the imaging parameters with great care so as to maximize the potential contrast offered by the BOLD effect. Gradient-echo EPI sequences are used in order to maximize the signal change. The BOLD contrast is dependent on dephasing caused by susceptibility differences of oxygenated and deoxygenated blood. If a spin-echo sequence were to be used much of the dephasing would be corrected for and there would be little difference between areas with different blood oxygenation. Unless otherwise stated the theory from this section is taken from Deichmann et al. (21) and De Panfilis and Schwarzbauer (12).

The effective echo time is one of the most important parameters in determining the BOLD sensitivity, BS. Furthermore, BS will also depend on the image intensity, I:

$$BS_0 = TE * I \tag{3.1}$$

The image intensity in a gradient-echo EPI image is given by:

$$I \propto \rho * e^{-\frac{TE}{T2}*} \tag{3.2}$$

where ρ is the proton spin density. In the presence of susceptibility induced magnetic field inhomogeneities both the echo time and the image intensity will be affected. EPI sequences are often troubled by susceptibility effects, as discussed in Section 2.3.2; this must be taken into account when developing an expression for the BOLD sensitivity.

The susceptibility gradient can be decomposed into three main components, components in the slice selection direction, read-out direction and phase encoding direction; they will all affect the BOLD sensitivity in different ways. The effect of the gradient in the read-out direction is negligible because of the much higher bandwidth than in the phase encoding direction. The component of the gradient in the phase encoding direction, however, will cause a distortion of data in k-space affecting both the echo time and the image intensity, as discussed in Section 2.3.2, and therefore the BOLD sensitivity.

The following assumes a blipped EPI sequence with a positive phase encoding gradient for prephasing and negative gradient blips for stepping through k-space. In addition, the k-space coverage is assumed to be symmetrical. The effect of susceptibility gradients in the phase encoding direction is described by the dimensionless variable Q which depends on

several imaging parameters and the susceptibility gradient in the phase encoding direction G_{sp}:

$$Q = 1 - \frac{\gamma * \Delta t}{2\pi} * FoV * G_{sp} \tag{3.3}$$

where FoV is the field of view in the phase encoding direction and Δt is the inter echo spacing. If TC is the nominal echo time and I_0 is the image intensity in the absence of gradients then the actual echo time, TE, and image intensity, I, can be expressed by:

$$TE = \frac{TC}{Q} \tag{3.4}$$

$$I = \frac{I_0}{Q} * e^{-\frac{TE-TC}{T2*}} \tag{3.5}$$

Both TE and the image intensity are changed by a factor 1/Q; this reflects the effect of the gradient in the phase encoding direction on the sampling of k-space. The second term Equation 3.5 reflects the amount of T2* decay caused by the difference between TC and TE, normalized to give I the value of unity in the absence of gradients.

The slice-selection component of the susceptibility gradient also affects the BS through the image intensity but in a different way. The gradient will cause spin dephasing in a way dependent on TE and the slice thickness, Δz:

$$I = I_0 * e^{-\psi^2} \tag{3.6}$$

I_0 is the image intensity in the absence of susceptibility gradients and shimming gradients. ψ is given by:

$$\psi = \gamma * \frac{\Delta z}{4 * \sqrt{\ln(2)}} * (G_{SS} * TE + G_{comp} * \tau) \tag{3.7}$$

G_{SS} is the through-plane component of the susceptibility gradient. Susceptibility effects in the slice direction are often reduced by z-shimming, as described in Section 2.3.3. It is performed by applying gradient pulse, G_{comp}, of duration τ in the slice direction. If perfect shim is achieved the following will be true:

$$G_{SS} * TE + G_{comp} * \tau = 0 \tag{3.8}$$

and the susceptibility gradient in the slice direction will not affect BS. However, z-shimming is hard to achieve optimally for the entire volume image, generally perfect shim can only be obtained for a limited area at a time.

If both the phase and slice component of the susceptibility gradient are taken into account, combining Equations 3.1 and 3.4-3.6, the following new expression for the BOLD sensitivity is obtained:

$$BS = \frac{BS_0}{Q^2} * e^{-(TE-TC)/T2*} * e^{-\psi^2} \tag{3.9}$$

If the gradients alter TE to such a degree that the effective echo time is moved outside the acquisition window, no signal will be recorded and the BOLD sensitivity will be zero. Therefore the following condition must hold:

$$\mathrm{TC} - \frac{\mathrm{TA}}{2} \leq \mathrm{TE} \leq \mathrm{TC} + \frac{\mathrm{TA}}{2} \tag{3.10}$$

TA is the duration of the acquisition window. The BOLD sensitivity can experience two types of signal loss depending on the sign of the susceptibility gradient:

Type 1: $G_{sp} > 0$

In this case Q is less than 1 causing an increase in TE, the image intensity and BS. However, TE may increase to such a degree that it is shifted outside the acquisition window. In this case, the result will be complete signal dropout. With positive prephasing gradients, a positive susceptibility gradient will increase the effectiveness of the dephasing, and decrease the effectiveness of the negative rephasing lobe thereby shifting the echo temporally to the right.

Type 2: $G_{sp} < 0$

In this case Q will be positive and the image intensity, TE and the BOLD sensitivity will all be reduced. The effect on BS will be worse as it scales with Q^2. In this case the susceptibility gradient will make the dephasing lobe more effective and the rephasing lobe less effective, thereby reducing TE.

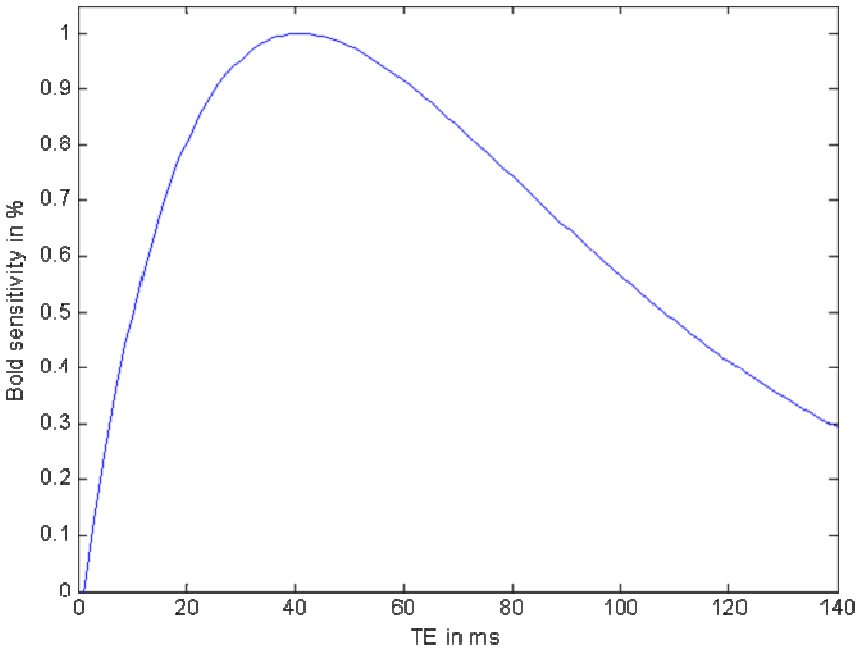

Figure 3. 2: TE dependence of BOLD sensitivity for T2* = 40 ms. BS is given in percentage of maximum value.

As seen from the discussion, TE is very important for what BOLD sensitivity can be achieved. Figure 3.2, derived from Equations 3.1 and 3.2, shows the BOLD sensitivity dependence for a certain T2*. A long echo time is beneficial for the BOLD contrast as the small susceptibility gradients that cause the BOLD effect have a longer time to develop, leading to a larger difference between areas with a larger fraction of oxyhemoglobin compared to areas with more deoxyhemoglobin. On the other hand, T2* decay is greater as TE increases and will lead to signal loss. As observed in Figure 3.2, and as follows from Equation 3.1 and 3.2, the TE that optimizes BS is TE = T2*. However, T2* varies across the brain and is often reduced by susceptibility gradients, therefore, to maximize the sensitivity to BOLD, TE should also be reduced.

3.2 Magnetic Field Maps

Many of the artifacts discussed in Section 2.3.2 appear as a consequence of an inhomogenous magnetic field. Although methods exist to limit inhomogeneities, they cannot be eliminated completely. In addition, it is not always straight forward to detect these artifacts, although some are obvious, others are more subtle. It is therefore important to develop techniques that can help detect artifacts and predict what consequences they imply for MR images. Magnetic field mapping is one of the tools that can be applied in this endeavor.
Field maps can also be used to determine the BOLD sensitivity in an fMRI study. As seen in Equation 3.3, the quantity Q depends on the susceptibility gradient in the phase encoding direction, G_{sp}. The quantity ψ depends on the susceptibility gradient in the slice selection direction. A map of these gradients across the slice can be acquired by taking the first derivative of the field map in the phase encoding direction, and the slice selection direction, respectively (13).

Magnetic field maps, or B0 maps, display the difference between the actual magnetic field and the ideal field strength, pixel by pixel; this difference can be denoted in Hz or T. To generate a B0 map, two phase images are acquired at different echo times. Since the echo time is longer for one of the images, that image will be more affected by the inhomogenous magnetic field and the phase will be larger. A B0 map given in T may be calculated according to Equation 3.11, while a map given in Hz can be calculated according to Equation 3.12 (6):

$$\Delta B_0(x,y) = \frac{\Delta\varphi(x,y)}{\gamma * \Delta TE} \tag{3.11}$$

$$\Delta f_0(x,y) = \frac{\Delta\varphi(x,y)}{2\pi * \Delta TE} \tag{3.12}$$

where $\Delta\varphi$ is the difference in phase for the same pixel in the two phase images. The difference in echo time between the two phase images, ΔTE, should be a multiple of the precession time for fat at the magnetic field strength, so that the signal from fat is equal in both acquisitions and will cancel when the two images are subtracted (22).
The field map can then be used to try to predict where artifacts are likely to occur in EPI images. For illustration purposes, assume a Δf_0 of 300 Hz and a bandwidth in the phase encoding direction of about 40 Hz. A discrepancy like this between the nominal field and the actual field in a pixel caused by susceptibility differences could lead to a pixel shift of about 7 in the phase encoding direction. With a pixel dimension of 3 mm this would lead to a special shift of over 2 cm.

3.2.1 Phase Unwrapping

The MRI signal is composed of real and imaginary components. Usually only the magnitude part of the MRI image is considered, but in some cases the phase image can yield useful information as discussed in Section 3.2. The article *Understanding phase maps in MRI* (23) is the basis for the following.

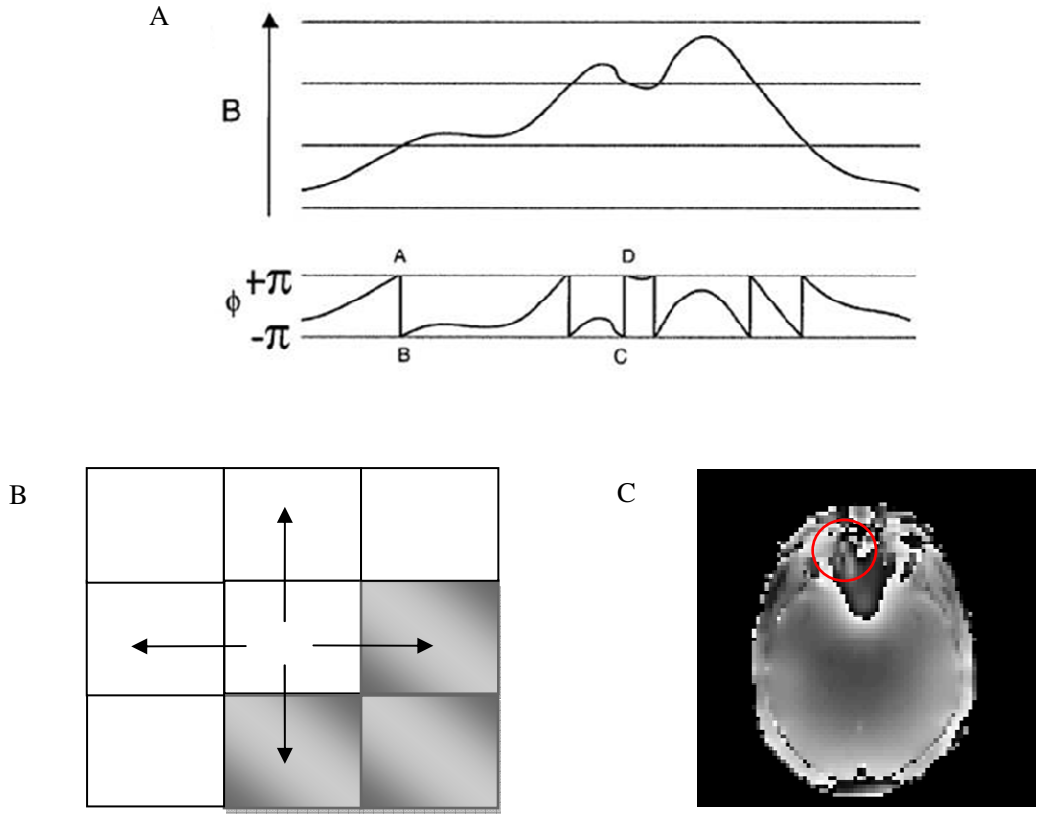

Figure 3. 3: A. In the phase image the pixels can only take values in the interval (-π,π] while the actual values can exceed this range. This results in abrupt changes between black and white in the image. B. A starting pixel is chosen and assumed to be unwrapped, the algorithm then moves through the image adding or subtracting modulo 2π as required. In B the pixels to the right and below the centre pixel would need to be unwrapped. C. The unwrapping process is made more complicated by inconsistencies in the phase image. The illustration in A is taken from *New Robust 3-D Phase Unwrapping Algorithms* by Cusack and Papadakis (38).

Phase can only be determined modulo 2π, usually in the interval (-π, π]. If larger phases evolve they will be wrapped back unto the interval, referred to as phase wrapping, see Figure 3.3-A. In phase images, phase wrapping will result in sudden transitions between black and white. The phase difference between two regions as a result of magnetic field differences was defined in Equation 2.16. Since the range is 2π, field deviances above $\Delta B_{0max} = 2\pi/\gamma\Delta TE$ will result in wrapped phase images. The phase images can therefore not be utilized directly to generate B0 maps; first the missing multiples of 2π must be obtained. The true phase in a point, φ can be expressed as:

$$\varphi = \varphi_1 + n * 2\pi \tag{3.12}$$

where φ_1 is the value of the pixel and lies in the interval $(-\pi,\pi]$, n is an integer. The process of finding the appropriate value of n for each pixel is referred to as unwrapping. Several different methods have been developed for this purpose. The basic principle is illustrated in Figure 3.3-B, beginning with a pixel, which is assumed to have the correct phase, all neighboring pixels are compared to it, to see if the difference in phase is above a threshold value. Depending on the sign and size of this difference a multiple of 2π will be added or subtracted to obtain the correct value.

An important part of the unwrapping process is defining the path that the algorithm should follow. Because of inconsistencies of the phase image, see Figure 3.3-C, the result yielded by the unwrapping procedure will usually not be independent of the path. A satisfactory result will depend on each pixel being given a measure of their quality, and in the unwrapping process high quality pixels will be unwrapped before low quality pixels. Some pixels may be kept out of the process altogether. The unwrapping algorithm developed for this project is described in Section 4.3.

4 Methods

The first goal of this thesis is to use field maps as a tool for estimating spatial misregistration in EPI images. B0 field maps are generated from phase images and because of their nature it is necessary to first unwrap these images. The methods for unwrapping phase images and generating field maps used in this thesis are self-produced.

The second goal of this thesis is to generate BOLD sensitivity maps to estimate the BOLD sensitivity of the fMRI images. The theory behind generating these maps was found in literature while the programs used to generate the maps were self-produced.

4.1 Test Subjects

One healthy male and one healthy female were used as volunteers for this project. Head restraints and padding were used on both subjects to reduce motion. Great care was also taken to make sure the subjects were in a comfortable position during scanning. Data was also collected from the FRONT project and from an epilepsy patient at the interventional center, see Section 4.8 and 4.9 respectively.

4.2 MRI Protocol

The experiments were carried out on a Phillips Achieva 3T MRI scanner located at the Interventional Centre at Rikshospitalet. The following frames were acquired in order:

- Survey protocol to obtain an overview and a reference scan to set the field of view
- T1 weighted 3D turbo gradient-echo for anatomical overview
- Dual-echo volume in the axial plane with two anatomical and phase images pr slice
- Dual-echo volume in the sagittal plane
- 3 fMRI volumes with different echo times
- 3 fMRI volumes with different water-fat shift

For the second volunteer an additional fMRI volume was acquired with the fat shift direction set to anterior, so that the effect of this parameter could be investigated.

The dual echo sequence was run to obtain phase images that could be used to generate field maps. The echo times were 3.2 and 5.5 ms, making ΔTE 2.3 ms, equal to the chemical shift between water and fat at 3T, thereby cancelling out the chemical shift effects when the two images were subtracted.

Table 4.1 displays an overview of the parameters used in the sequences. A total of six fast field echo EPI sequences were run with different parameters. The level of artifacts in EPI images rely heavily on especially the echo time, TE, and water fat shift, WFS, these parameters where therefore chosen to vary. Although the parameters were varied, the values are quite common for fMRI studies. A long repetition time will generally give increased signal, but will also limit the possible number of samplings. Common repetition times are around 2 to 4 s. All frames had the same geometry, including voxel size, gap and matrix size, to make the further processing easier.

Figure 3.2 shows the BOLD sensitivity dependence on echo time. Optimal TE for BOLD fMRI is widely recognized to be around the T2* value of the tissues being imaged, as discussed in Section 3.1.2. However, susceptibility effects lead to a variation of T2* values throughout the brain, often reducing them to below 30 ms. For these reasons the TE values

were chosen to be somewhat lower than the nominal value of T2* (24). Wansapura et al. (25), gives a T2* value of 51.8±3.3 for gray matter in the frontal regions of the brain for 3T, while Krüger et al. (26) gives a T2* value of 49 ms at 3T. In this project a T2* value of 50 ms was used.

As discussed in Section 2.3.1, the resonance frequencies between water and fat are different due to chemical shift. This will lead to a wrong spatial coding of the fat signal. Water fat shift is a parameter that sets the maximum pixels a fat signal can be shifted away from its correct position. In EPI sequences, the fat signal is shifted in the phase encoding direction and WFS is linked to the bandwidth in that direction. Setting WFS to a higher value will, when all other parameters are kept the same, decrease the bandwidth in the phase encoding direction. The fat shift direction can also be varied. If the fat shift direction is set to posterior then susceptibility effects will be in the opposite direction, anterior.

Table 4.1: Overview of the main parameters from the acquisitions.

Constant parameters					
# Slices/Gap between slices 36/0	FoV 240x240 mm^2	Voxel size 3x3x3 mm^3	Matrix 80x80	TR 2000 ms	Fat shift direction Posterior
Varying parameters					
WFS, TE=35ms 8.3 12 20			TE, WFS=8.3 30 ms 35 ms 40 ms		

SENSE, discussed in Section 2.3.4, was used in all of the fMRI sequences with a SENSE factor of two, thereby reducing the scan time by a factor of two. SPIR, spectral presaturation with inversion recovery, was used to suppress the fat signal as it would otherwise have caused serious chemical shift artifacts in the images. In SPIR, a frequency selective inversion pulse excites the fat tissues only; the main excitation pulse is applied at the zero crossing of the fat signal.

4.3 Preparing Data for Post Processing

The MR scanner stores all data in the DICOM[3] format. Nordic ICE was used to convert the images to a file format accepted by Matlab; nordic ICE also sorted the images into folders by sequence. Nordic image control and evaluation is an MR-image processing and analysis software that was used to display the images and generate and compare ROIs.

4.4 Unwrapping Algorithm

As discussed in Section 3.2.1, phase images usually need to be unwrapped before they can be made use of, for example to generate field maps. In this project a new algorithm for

[3] DICOM is an abbreviation for Digital Imaging and Communications in Medicine

iterative unwrapping of phase maps was developed using Matlab as a programming tool. Matlab is a fourth generation programming language especially suited for numerical calculations with many built in functions. Matlab version R2007a was used in this project. The code for this algorithm can be found in Appendix C.1, the main points will be described in this section.

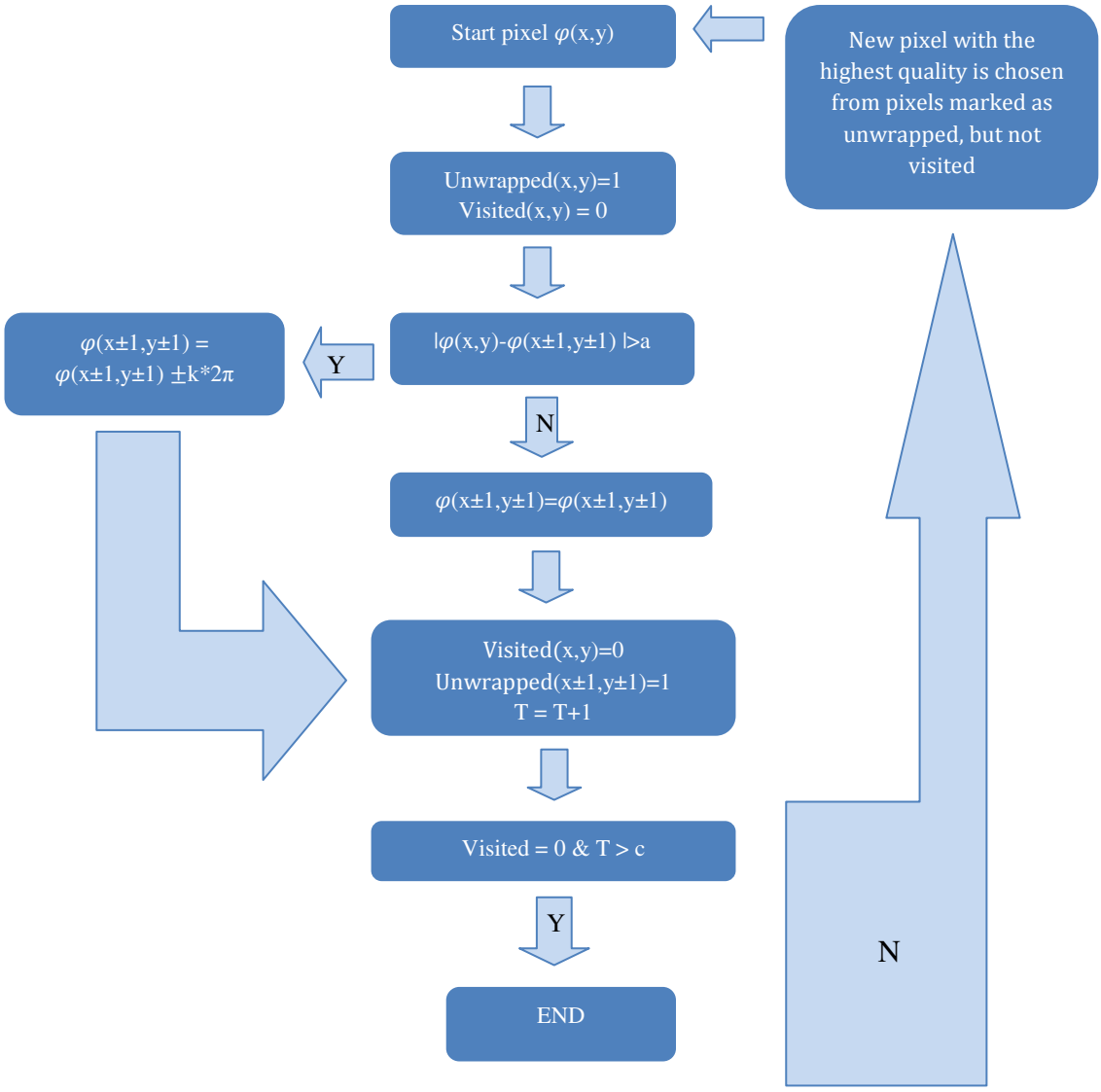

Figure 4. 1 Flow chart of the unwrapping procedure. T is a counting variable that is not allowed to exceed a threshold value c.

Throughout the algorithm pixels with zero signal are excluded to avoid problems. Two phase images are recorded for every slice; they were imported at the beginning of the program. The images first need to be rescaled to the range (-π, π]. As previously discussed in Section 3.2.1, the path chosen for the unwrapping procedure is critical for the result attained. Trial and error was employed for discovering the optimal path defining measure. Quality maps were generated separately for each image. In this project the quality of each pixel was

defined in two ways. As no single measure was found to be satisfactory, two different quality measures were developed to achieve the optimal result. Two unwrapping procedures were conducted on each phase image, one with the first quality measure as the path choosing mechanism and then a second time with the second quality measure defining the path. This increased the duration of the algorithm somewhat, but the quality of the unwrapping was significantly increased.

The first quality measure was based on the variance of the population of pixels closest to the pixel, the pixel itself and its eight neighbors:

$$k(x,y) = \frac{\sum_{x-1}^{x+1} \sum_{y-1}^{y+1} \left(\varphi(i,j) - \bar{\mu} \right)^2}{9} \tag{4.1}$$

φ(i,j) is the phase of the pixel, while $\bar{\mu}$ is the average of the nine pixels phase values. High variance of a pixel translates to low quality. The second measure of quality is also based on the variance but in addition includes gradients of the phase in the x and y directions:

$$q(x,y) = \frac{\sum_{x-1}^{x+1} \sum_{y-1}^{y+1} \left(\varphi(i,j) - \bar{\mu} \right)^2}{9} * \frac{\partial \varphi}{\partial x}(x,y) * \frac{\partial \varphi}{\partial y}(x,y) \tag{4.2}$$

$\frac{\partial \varphi}{\partial x}$ is the gradient of the phase in the x-direction and $\frac{\partial \varphi}{\partial y}$ is the gradient in the y-direction. These were calculated with a built in Matlab function, 'gradient'.

The pixel with the lowest value of k is chosen as the starting point for the first unwrap process, as this is seen as an indication of the pixel being in a relatively homogenous area of the magnetic field. Two matrices with similar dimensions as the phase image and quality map are then generated. The 'unwrapped' matrix tracks which pixels have been unwrapped, wrapped pixels are set to zero while unwrapped pixels are set to one. The starting pixel is marked with one. The 'visited' matrix shows which pixels have already been used as unwrapping pixels; these are set to zero while the others are marked with one. At the beginning of the algorithm all pixels are set to one. These two support matrices, 'unwrapped' and 'visited' made sure that no pixel was unwrapped more than once, and that the algorithm didn't get stuck on the same pixel, respectively.

The unwrapping process is described in Figure 4.1. The designated starting pixel is detected using the 'unwrapped' matrix since at this point; it is the only one set to one. The active pixel is then compared to its eight neighbors one at a time. If the difference is larger than a positive threshold value; n*2π is added to the value of the pixel being considered, the neighbor of the active pixel. n is an integer whose value is determined based upon the magnitude of the difference. If the difference is smaller than a negative threshold value; n*2π is subtracted from the value of the pixel. If the difference is within the thresholds the pixel value remains the same since no wrap has occurred. After this process n*2π has either been added to or subtracted from the pixel value, or the pixel value has not been changed at all. In any case the neighbor pixel is then marked as 'unwrapped'. After all the neighboring pixels have been compared the start pixel is declared as 'visited' and a new pixel is chosen to be the active pixel. The pixel chosen is the one with the lowest k value that has been marked as 'unwrapped', but not as 'visited'. The loop continues until all pixels are marked as 'unwrapped' or when a counting variable reaches a preset max value. The counting variable prohibits the possibility of the program ending up in a perpetual loop.

After the first unwrapping is completed, the 'visited' and 'unwrapped' matrices are reset and a new starting pixel is chosen based on its q value. The entire process is then repeated with the q values as the path guiding measure.

A problem that presented itself early in the process was that of inconsistencies in the phase images, as mentioned in Section 3.2.1. The quality measures shown in Equation 4.1 and 4.2 were optimized through a process of trial and error, but some artifacts in the images prevailed. The expression for the quality map gives quality values that correspond well to the intentions behind the design of the program in most cases. But in some cases, for example when inconsistencies exist, the measures lead to an unwarranted high quality for some pixels, leading to unsatisfactory unwrapping of the phase image, see Figure 4.2. For this reason an additional condition was added to the quality measures. Studying the quality map that Equation 4.2 gives; it was found that pixels in the area marked with the red circle, in Figure 4.2-A, had a higher quality than pixels marked with the green circle leading the pixels in the red area to be unwrapped first. The result can be seen in Figure 4.2-B. After a careful analysis of the values involved, a threshold was set; pixels with variance values above this threshold would have new values assigned to them so that they would be put in line ahead of the pixels involved in inconsistencies. The result of applying this threshold value can be seen in Figure 4.2-C.

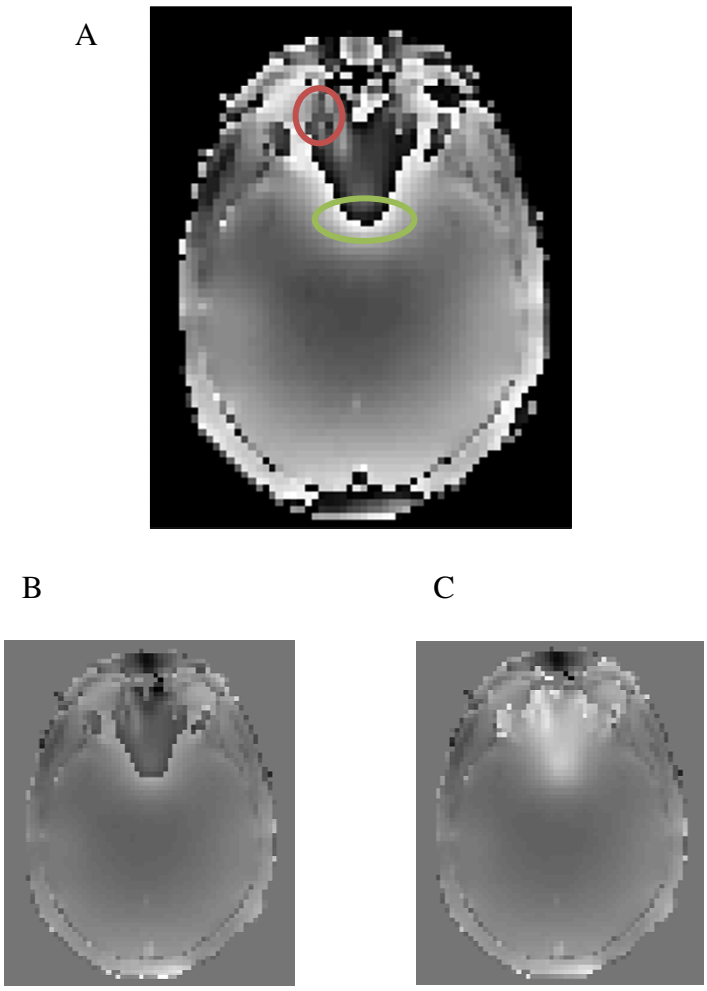

Figure 4. 2: A. The wrapped phase image with an inconsistency marked by the red circle. B. The unwrapped phase image when the inconsistency was not accounted for. C. The unwrapped phase image with the current method.

4.5 Field Maps

Once the phase images were unwrapped it was straight forward to use them for generating magnetic field maps. The connection between the phase images and field maps, shown in Section 3.2, reveals that it does not depend on any parameters that changed between the different EPI sequences, i.e. the echo time or the bandwidth. Therefore it was only necessary to generate one volume of field maps per subject. The field maps were saved to file in two different versions for their two different uses. When using the field maps for artifact analysis it was practical to give them the unit of Hz, making it easier to analyze the maps with varying bandwidths. The field maps were then generated using Equation 3.12. The field maps were also used in generating BOLD sensitivity maps, in this case it was useful to express the field difference in T, employing Equation 3.11 in Section 3.2. Matlab was again used to automate the process of generating and saving the field maps.

FSL was used to verify the accuracy of the self-produced field maps by generating magnetic field maps for control. FSL, FMRIB Software Library, is a software library containing image analysis and statistical tools for MRI, fMRI and DTI brain imaging data. The unwrapping algorithm used by FSL is called PRELUDE, details about this tool can be found in Section 4.12.1. SPM was used to convert the phase images and the Matlab generated field maps into NIFTI[4] files so they could be imported into FSL. SPM, Statistical Parametric Mapping, is a Matlab software package that uses statistical methods to analyze functional MRI data. The eight edition of SPM was used.

4.6 Artifact Analysis

After the field maps had been generated the next step was to use them in addressing the first main goal of the project: estimating areas in the EPI images particularly affected by susceptibility artifacts. To illustrate this effect, pixel shift maps were generated by dividing the axial field maps in Hz by the bandwidth pr pixel in the phase encoding direction; giving an indication of how far the magnetic field deviation could cause a spatial misregistration of a pixel. Using basic Matlab functions, maps were created where negative field differences were shown closer to blue while positive differences were shown in red. With these maps in hand, and knowledge of the fat shift direction, the likely shift and direction of the pixels in problem areas could be estimated. Nordic ICE was used to display the anatomical and EPI images and to generate and compare ROIs.

4.7 Generating T2* Maps

In addition to altering TE throughout the brain, as discussed in Section 3.1.2; susceptibility gradients also alter the value of T2*. Therefore, a map of T2* values across the volume was generated. The following equation was employed, (24):

$$T2^* = \frac{TE2 - TE1}{\ln(I1/I2)} \tag{4.4}$$

[4] NIFTI is an abbreviation for Neuroimaging Informatics Technology Initiative

TE1 and TE2 are echo times of two images acquired at different echo times, I1 and I2 are the intensities of these images. The anatomical images acquired together with the phase images in the dual echo sequence were used to generate the T2* maps. A Matlab routine was generated specifically for this purpose. This program included a programming code making a histogram of T2* throughout the slice. The code can be found in Appendix C.2. BET, an FSL brain extraction tool, was applied to the images so that only the relaxation times of the pixels within the brain were counted. Details about BET can be found in Section 4.12.2.

4.8 Generating BS Maps

Simulated BOLD sensitivity maps were generated from a self produced Matlab routine based on the model developed by Deichmann et al. (21), presented in Section 3.1.2. Figure 4.3 shows a flow chart of the process. The code can be found in Appendix C.3.

Equation 3.3 shows that the Q parameter is partly dependent on the field gradient in the phase encoding direction. Basic Matlab functions were used to generate maps of the gradient in the phase encoding direction from the magnetic field maps. Matrices showing each pixel's Q-value were then generated; these were then used to generate maps showing the actual TE in each pixel simply by dividing the nominal echo time, TC, by Q.

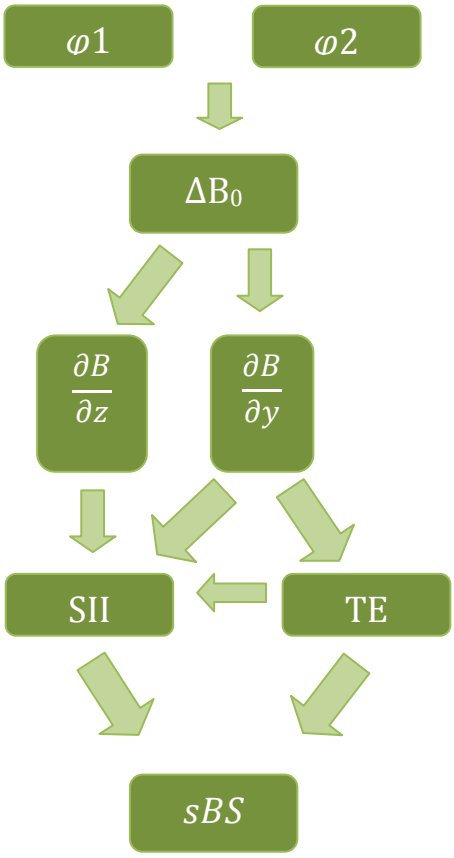

Figure 4. 3: Flow chart describing how BOLD sensitivity maps are generated. Two phase images are used to create a field map, the gradient in the y-direction is used to create echo time and simulated intensity maps, and these are then used to generate simulated BOLD sensitivity maps. $\frac{\partial B}{\partial y}$ is the susceptibility gradient in the phase encoding direction, G_{sp}, and $\frac{\partial B}{\partial z}$ is the susceptibility gradient in the slice encoding direction, G_{ss}.

To calculate gradient maps in the slice encoding direction a new Matlab routine was written, the code can be found in Appendix C.4. An additional dual echo sequence in the sagittal plane was acquired. The phase maps were unwrapped with the same routine used to unwrap the phase images taken in the transverse plane, described in Section 4.4. BET was performed on the field maps before MatLab's 'gradient' function was used to attain the component of the susceptibility gradient in the slice encoding direction. The gradient values in the sagittal images then had to be transformed into the transverse plane so they could be used when generating the BOLD sensitivity maps. SPM's coregistration tool was employed for this purpose. This tool is described further in Section 4.12.3.

Simulated intensity maps in the absence of shimming were generated according to the following equation, (11):

$$SII = \frac{I_0}{Q} * e^{-\frac{TE-TC}{T2*}} * e^{-\psi^2} \tag{4.5}$$

As explained in the previous chapter, values for T2* vary across the brain because of inhomogenities in the magnetic field. However, a constant T2* value was chosen since part of this variation is already included through the term for the susceptibility gradient in the phase encoding direction (12). In the absence of shimming, the following expression for ψ is found from Equation 3.7:

$$\psi = \gamma * \frac{\Delta z * TE}{4 * \sqrt{\ln(2)}} * G_{SS} \tag{4.6}$$

I_0 was set to 1 so that the resulting map would show SII relative to the intensity in the absence of susceptibility gradients. Finally, the simulated BS maps were generated using the following equation, (11):

$$sBS = SII * \frac{TE}{TC} \tag{4.7}$$

For all the maps, pixels were set to zero if TE was outside the acquisition window, since no signal can be detected in these cases. This is expressed through the following conditions:

$$G_{sp} > \frac{2\pi(1 - \frac{TC}{t_{start}})}{\gamma * \Delta t * FoV} \tag{4.8}$$

$$G_{sp} < \frac{2\pi(1 - \frac{TC}{t_{end}})}{\gamma * \Delta t * FoV} \tag{4.9}$$

These conditions follow from Equations 3.3, 3.4 and 3.10. t_{start} and t_{end} is the time at which the acquisition starts and ends respectively. If the susceptibility gradient was outside of the

interval set up by Equations 4.8 and 4.9, the BOLD sensitivity would be zero. A gradient outside this interval would indicate that the effective echo had been shifted outside of the acquisition window.

4.9 Case Study: FRONT

FRONT is a collaboration project between Rikshospitalet, Sunnaas Rehabilitation Hospital and the Department of Psychology at the University of Oslo. The project investigates patients with known damage to the frontal lobe, caused by violent injury, stroke or cancer. A combination of electroencephalographic, EEG, recordings, BOLD fMRI and behavioral tests are employed in this effort. As has been previously discussed, BOLD fMRI studies of the frontal lobe are especially exposed to susceptibility artifacts because of its proximity to bone and air-filled sinuses (26).

Data from the FRONT project was acquired and used to test the methods developed in Section 4.8. The results found were contrasted to the BOLD analysis made in the FRONT project. Special interest was taken in comparing areas were FRONT had not found activity, to see if these were areas where the simulated BOLD sensitivity maps show a low level of sensitivity. It was anticipated that false negative results, as discussed in Section 3.1.1, could be detected. Table 4.2 shows the parameters used in the EPI sequence. A water fat shift of 14.9 pixels corresponds to a bandwidth in the phase encoding direction of 29.1 Hz.

Tabell 4. 2: Overview of the parameters used for the EPI sequence in the FRONT project.

Parameters							
# Slices/Gap between slices	FoV	Voxel size	Matrix	TR	TE	WFS	Fat shift direction
30/0.5	224x224 mm^2	2x2x3 mm^3	112x112	2250 ms	30 ms	14.9	Posterior

Data was collected from 8 patients and 17 healthy controls. The sequences acquired by the FRONT project were not the same as the sequences presented in Section 4.2. Instead of a dual echo sequence, a B0 field map sequence was run. In this sequence, the scanner generates the field maps directly in Hz. This technique does not account for phase wrapping, so some wraps could be observed in some of the images. ΔTE was 2.6 ms, as opposed to the dual echo sequence described in Section 4.2, where ΔTE was 2.3 ms in order to avoid chemical shift effects. In the B0 map sequence, the water fat shift parameter was set to 1.1 pixels, with a pixel dimension of 2 mm this corresponds to a shift of not quite 0.5 cm. A shift of this magnitude is unlikely to cause problems when the magnetic field maps are generated.

In addition, the project had not acquired any images in the sagittal direction. The methods described in Sections 4.8 require field maps in both the sagittal and axial directions to generate BOLD sensitivity maps. New methods were developed so that susceptibility gradient maps in both directions could be generated from the axial volume alone. The multi-planar reconstruction tool in nordic ICE, was used to reconstruct a volume in the sagittal direction. Neither volume was unwrapped, so some of the lower slices had wrapped regions, these however occurred in regions where susceptibility gradients led to complete loss of BOLD sensitivity.

Brain activity maps were collected for two of the subjects, one patient and one healthy control. The maps were imported into Nordic ICE, and overlaid onto the BOLD sensitivity maps for further analysis. The maps were generated on the basis of a Go-success paradigm designed to test the inhibition of the subjects. The subjects were given a command and within a limited amount of time were either told to stop or given the go ahead. Since the frontal region of the brain is important for this type of cognitive function, it was predicted that the patients would underperform compared to the healthy controls. This particular experiment was designed so that if the subject failed to inhibit the initial task when the order was given to stop, the subject was given increasingly longer to react so that eventually all subjects were successful.

4.10 Case Study: Epileptic Patient

For this project, data was collected from a young epileptic patient that had undergone several operations, and additional procedures were being considered. The patient underwent a BOLD exam and dual echo sequences in both the sagittal and axial directions were added to the protocol. BOLD sensitivity maps were generated on the basis of these sequences. The parameters employed in the EPI sequence are listed in Table 4.3. A water fat shift of 10.3 pixels corresponds to a bandwidth in the phase encoding direction of 42.1 Hz. Unwarping of geometric distortions was not conducted on the EPI images.

Tabell 4. 3: Overview of the parameters used in the EPI sequence for the BOLD exam on the epileptic patient.

Parameters							
# Slices/Gap between slices	FoV	Voxel size	Matrix	TR	TE	WFS	Fat shift direction
35/0	240x240 mm^2	3x3x3 mm^3	80x80	3000 ms	30 ms	10.3	Posterior

The patient considered in this project had two metallic clips in her scull from previous surgeries. The BOLD analysis was to be a part of the presurgical planning for an additional surgery. The goal was to locate the language center, so as to limit the risk of damaging it during the operation. The BOLD experiment was set up as a block experiment with alternating task and rest periods. Different language tests were performed by the patient during the task periods. The main goal of the tests was to lateralize the language centre and to investigate if it had managed to relocate to the opposite hemisphere. It needed to be demonstrated that the language area was at a ‘safe’ distance from the anatomic location of the epileptic focus.

The exam resulted in activity maps showing where activity had been detected. Figure 4.4-A shows the two areas, in each hemisphere, where activity was expected to appear. The goal of the surgery was within this area on the right side. Figure 4.4-B shows an anatomical image, and the site of previous surgeries can clearly be seen. If the activity maps were to show activity in this region it would be a contraindication for surgical intervention. If the surgery was to be conducted the ECoG technique of mapping brain activity would have to be applied. As explained in Section 4.5, this technique requires the patient to be awake during the operation. This process can be very unpleasant for the patient and leads to a significant

increase in the duration of the surgery. Especially considering the young age of the patient, it would be preferable if this option could be avoided.

According to the method described in Section 4.8, simulated BOLD sensitivity maps were generated in order to decide the reliability of the BOLD analysis, especially in regions close to the language center. Activity maps from the BOLD analysis were acquired for comparison with the BOLD sensitivity maps.

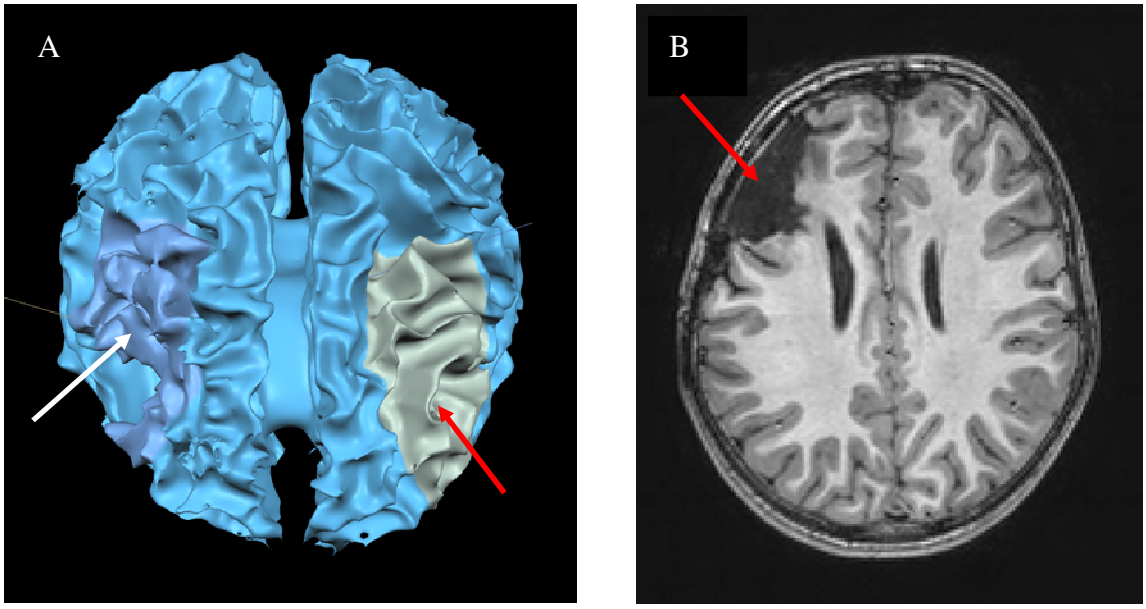

Figure 4. 4: A. Highlighted areas are where the language centre is expected to be. B. Anatomical image of the brain. The area where tissue is missing is close to the light gray area in A, highlighted by the red arrows. It is near this area that the epileptic focus is located.

4.11 Phase preparation for dual echo sequence

For the dual echo sequences used to generate the field maps and pixel shift maps, the MRI scanner applied preparation phases resulting in an intensity offset across the slices. This implies that slices away from the isocentre would have slightly offset values. Therefore, the field maps and pixel shift maps presented in Sections 5.1-5.3, 5.6 and 5.8 will not be completely accurate. However, the general tendency illustrated by the maps will still hold.

A preparation phase was also applied to the B0 maps collected from the FRONT project. However, a rescaling across the slices was performed by the scanner eliminating the offset. The results presented from the FRONT project in Section 5.7 are therefore more accurate.

As only the gradients of the magnetic field maps are used to generate the simulated BOLD sensitivity maps their validity should not be affected by these preparation phases.

4.12 Specifications about the FSL and SPM Programs used

Some of the tools in FSL and SPM were used in the analysis of the results.

4.12.1 PRELUDE

PRELUDE stands for phase region expanding labeller for unwrapping discrete estimates. The input is a wrapped phase volume with corresponding anatomical volume. PRELUDE then performs a 3D phase unwrapping of the image and the output is a single unwrapped volume. The algorithm uses a region-merging approach to optimize a cost function that penalizes phase differences across boundaries. The whole volume is divided into N regions, none of them containing any phase wrappings. A cost function is then defined and used to decide which two and two regions should be merged (27).

4.12.2 BET

BET stands for brain extraction tool. It takes MR brain images and separates it into two parts; the actual brain and the areas outside the brain, for example skull, skin and eyes. The output is a binary mask where voxels found to contain elements of the brain are marked as one and all other voxels are marked as zero. BET begins with a sphere centered at the centre of the brain. The sphere is made up of many triangles that are stepwise moved until the sphere eventually traces out the brain surface (28).

4.12.3 Coregistration

Coregistration or image registration is the process of transforming different sets of image data into one coordinate system. The coregistration method used by SPM is based on the work of Collignon et al. (29), however the interpolation method described in that paper was slightly changed to give a smoother cost function. The output of the program is an affine transformation matrix giving the coordinates of the source volume as linear transformations of the reference volume coordinates.

5 Results and Analysis

In illustrating the results only images from one subject at a time are shown. The images that are chosen represent the general tendency found in both of the subjects. In the following, if nothing else is specified, the fMRI volume with TE=35 ms and WFS=8.3 is used as a default volume for generating results.

The results presented in Sections 5.7 and 5.8 are presented according to radiological convention. The other results are presented such that the subject's left is left in the image and vice versa.

5.1 Verifying Self-produced Field Maps

The field maps generated in this project are fundamental to both of the two main goals. As the field maps are used in estimating BOLD sensitivity and in estimating the potential for artifacts, it is crucial that the accuracy of the maps be validated. The field maps were generated using the method laid out in Sections 4.4 and 4.5, hereafter referred to as the Matlab method. The PRELUDE algorithm in FSL was employed to generate control maps, hereafter referred to as the FSL method.

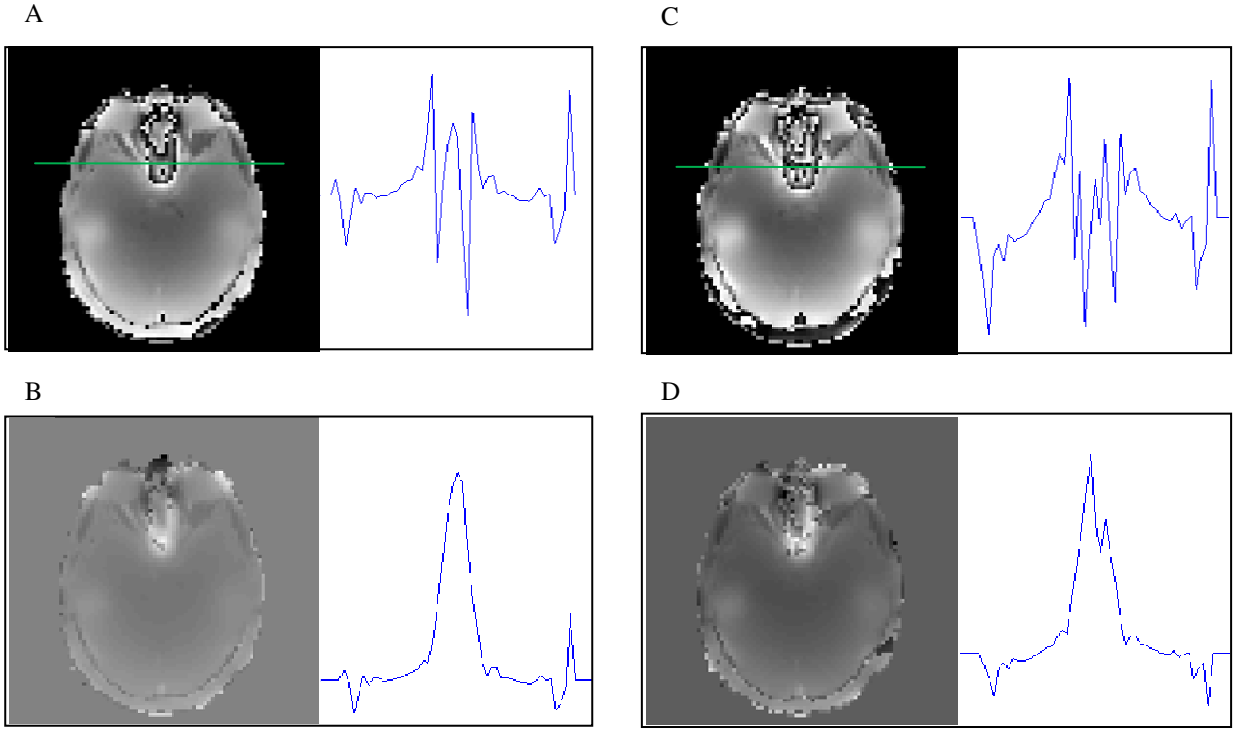

Figure 5. 1: A. wrapped phase image of slice 11 acquired with a short echo time and the line profile of the green line. B. The unwrapped phase image of slice 11 and the new line profile. C and D show the same thing for the same slice with a long echo time. The peak for the line profile of the first unwrapped image, B, is at about 8, while the line profile of the second image, D, has a peak just over 12.

The most demanding part of generating field maps is the unwrapping of the phase images. Figure 5.1-A shows a wrapped phase image together with its corresponding line profile. Figure 5.1-B shows the unwrapped phase image and the new line profile. Figure 5.1-C and Figure 5.1-D show the same thing for a phase image acquired with a longer echo time.

The line profiles show the phase value across the image. Comparing Figure 5.1-A and C it can be observed that larger phases have had time to develop in C, resulting in a more complex situation seen in the middle of the unwrapped line profile.

The next step in generating the field maps was simply to subtract the two unwrapped phase images, using Equation 3.12 to get the field deviation in Hz. Figure 5.2 shows the FSL generated field maps, A, together with the field maps generated in Matlab, B, for two different slices. The two slices have been selected to illustrate the most common deviances found in the Matlab maps compared to the FSL generated maps. The field maps seem for the most part to match well. The black arrows in Figure 5.2-B highlight a typical example of the most common irregularity found in the comparison between the two maps. These incorrectly unwrapped regions are almost always in close proximity to the skull if not in the scull itself. The other type of deviances, highlighted by the white arrow in Figure 5.2-B, is found in places where the original phase maps were especially complicated. It can be observed that the FSL maps also have some aberrations in these regions.

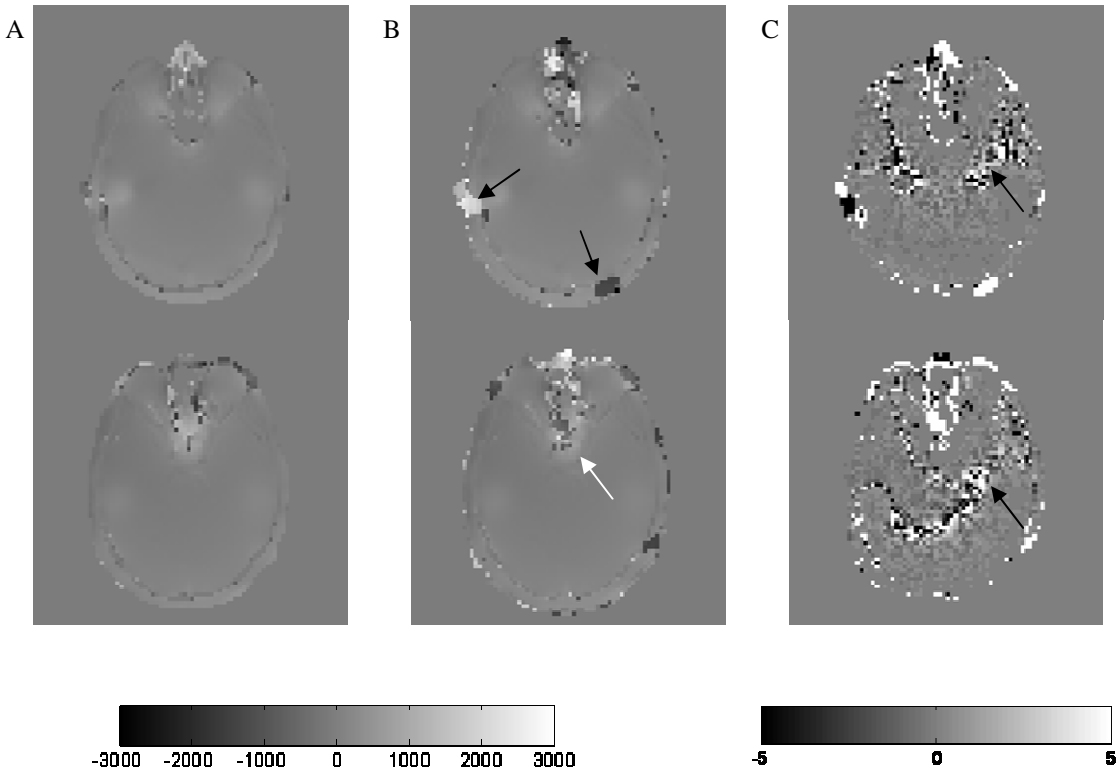

Figure 5. 2: A. The field maps generated by FSL for two different slices. B. The Matlab generated field maps. C. The difference between the FSL maps and the Matlab maps in percent. The field maps are in rad/s as that is the unit of the FSL generated maps.

Figure 5.2-C shows the percent deviation between the FSL map and the Matlab map. Generally the deviation is seen to be small except in areas highlighted by the black arrows. Both methods generate field maps with the maximum deviation from the main magnetic field being in the range of 2-4 ppm.

5.2 Ability of Field Maps to Predict Artifacts

One of the main goals of this project was to use maps of deviations in the B0 field to estimate the potential for artifacts, such as misregistration and signal loss, in EPI images. Figure 5.3 shows anatomical images, A, EPI images, B, and field maps in Hz, C, for four different slices. The anatomical images are considered to be nearly free from artifacts and can be seen as a control.

There is a clear relation between the predicted field difference of the field maps and the amount of artifacts in the EPI images. The effect of the field deviations will depend on parameters such as the echo time and the bandwidth in the phase encoding direction. The EPI images in Figure 5.3 were acquired with a TE of 35 ms and a bandwidth of 52.3 Hz/pixel. In the EPI images both distortions and complete signal drop can be seen to occur in areas that have high positive or negative values on the field map.

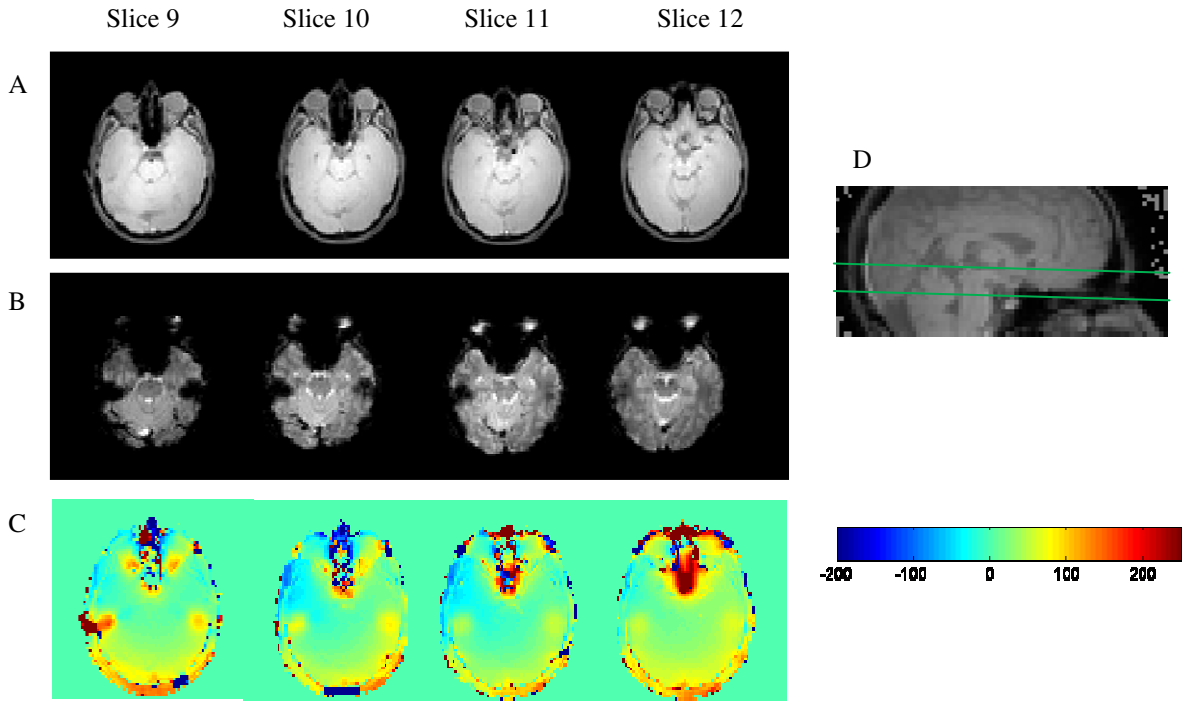

Figure 5. 3: A. The anatomical images for four different slices. B. The EPI images for the same slices. C. The field maps in Hz. D. Marks the position of the slices in the brain.

The direction in which the pixels will possibly be shifted depends on the parameter fat shift direction. This parameter is set by the operator and denotes in which direction fat containing pixels will be shifted as a result of chemical shift. It can only be determined along one axis for a particular sequence. For the scan shown in Figure 5.3, the fat shift direction was set to posterior, meaning fat containing pixels would be shifted to the back of the brain. Susceptibility artifacts are shifted to the opposite direction from chemical shift artifacts. The effect of the parameter fat shift direction will be more closely examined in Section 5.4.

5.3 The Effect of TE and Bandwidth on Artifacts

In the sequences used, the two main parameters that were varied were the effective echo time and water fat shift. Changing the water fat shift had the main effect of changing the bandwidth in the phase encoding direction. The correlation between these two parameters and the pervasiveness of artifacts in the EPI images were illustrated by observing the anatomic images together with the EPI images for the different values of the parameters.

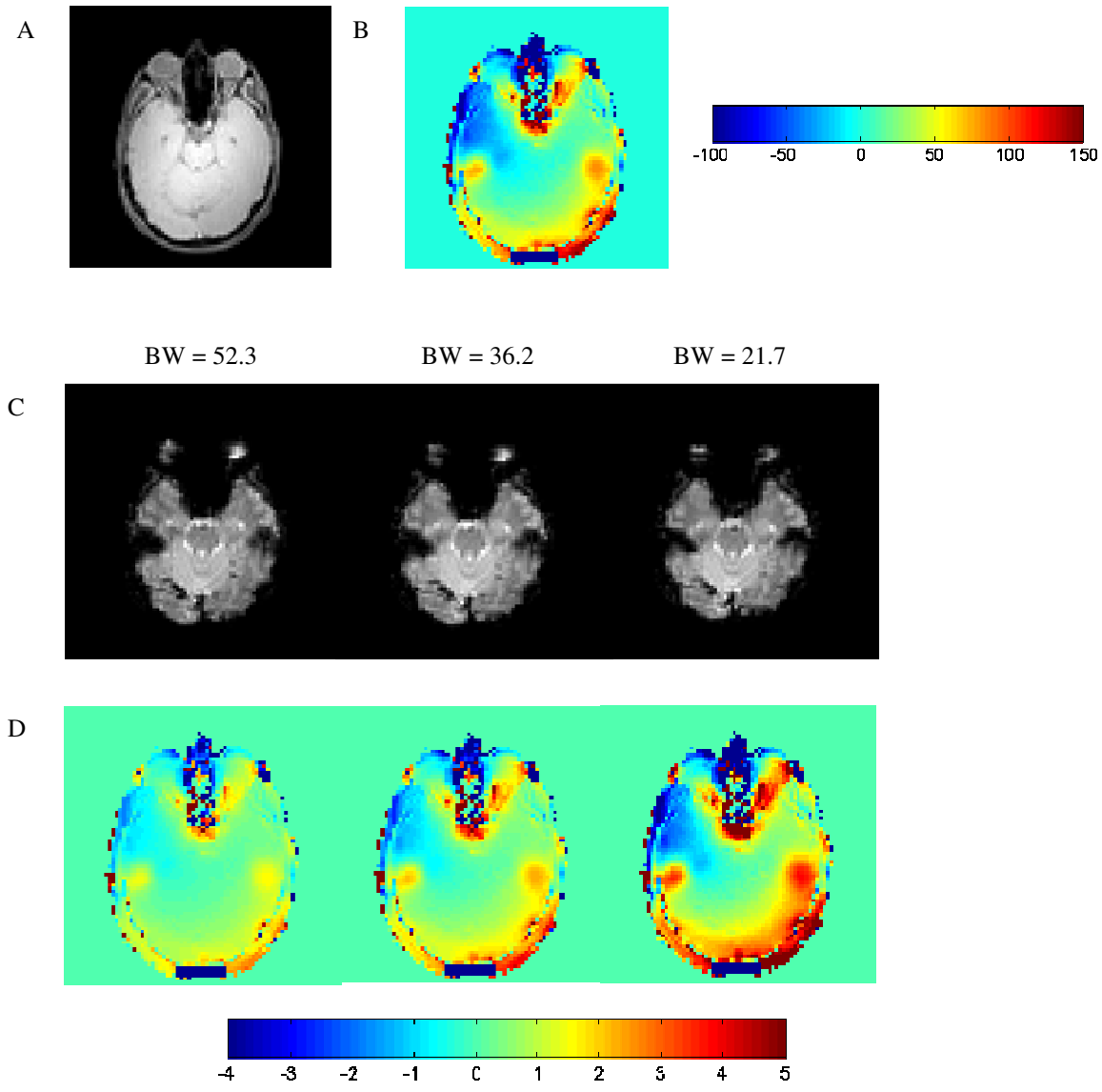

Figure 5. 4: A. The anatomical image of slice ten. B. The field map of slice ten given in Hz. C. EPI images for the same slice with three different bandwidths. D. Pixel shift maps for the three different bandwidths.

The top row in Figure 5.4 shows the anatomic image and the field map of a slice in Hz. The second row shows the EPI image for all three bandwidths and the bottom row shows the pixel shift maps. A tendency can be spotted in the images of more artifacts as the

bandwidth decreases. Both signal loss and distortions seem to be more present in the image with the smallest bandwidth. The pixel shift maps illustrates by how many pixels a pixel affected by geometric distortion can be expected to be misregistrated. The amount of pixels shifted a substantial length is clearly seen to increase with decreasing bandwidth. For the highest bandwidth, 52.3 Hz/pixel, most pixels have a negligible pixel shift of less than one pixel. As the bandwidth decreases and reaches 21.7 Hz/pixel, a substantial proportion of the pixels are likely to be shifted.

For the scan shown in Figure 5.4, the fat shift direction was set to posterior, the susceptibility artifacts are shifted to the opposite direction from chemical shift artifacts which in this case would mean the anterior. Upon closely examining the EPI images a slight blurring can be seen by the edge of the brain toward the front.

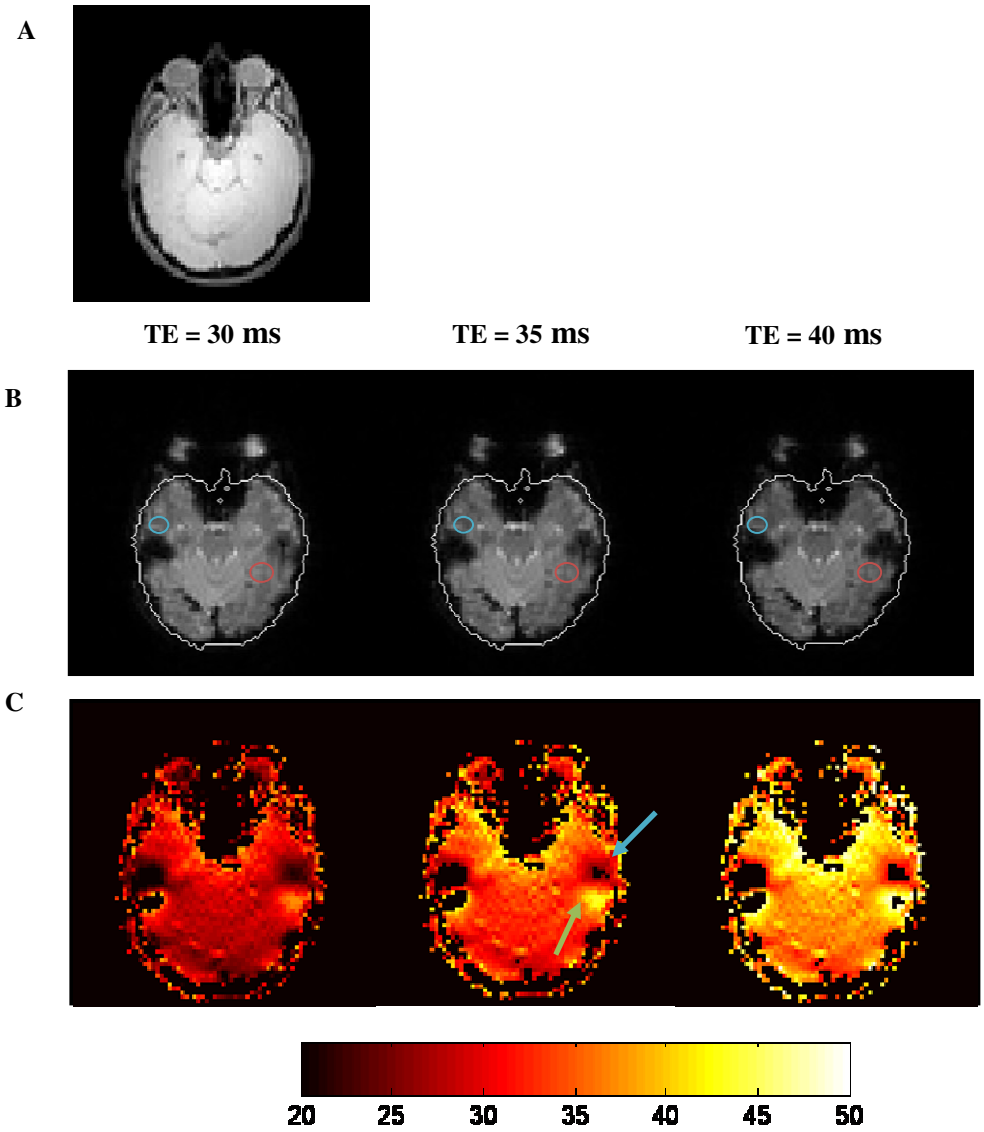

Figure 5. 5: A. The anatomical image of slice ten. B. EPI images at three different echo times with a contour of the brain acquired from the anatomical image overlaid. C. TE maps for the different echo times in ms, TE is set to zero if it falls outside of the acquisition window.

Table 5.1: Intensities for the ROIs marked in the EPI images in Figure 5.5. Only the relative value of the intensities is of interest, since they were rescaled upon entry to nordic Ice.

TE (ms)	Intensity	
	ROI red	ROI blue
30	897	798
35	868	781
40	844	728

Figure 5.5 shows the anatomical image, A, EPI images, B, and maps of the effective echo time, C, for the same slice acquired at three different echo times. The TE maps were generated as explained in Section 4.8. The quality of the EPI image is seen to decrease with increasing TE. Both a decrease of the intensity and an increase in the complete signal dropout can be observed. The signal dropout is especially evident on either side of the brain in the temporal lobe region. As Table 5.1 shows, the image intensity weakens with increasing echo time. The blue ROIs are placed in a region where the echo time is shorter than the nominal echo time, while the red ROIs indicate an area where the echo time is longer.

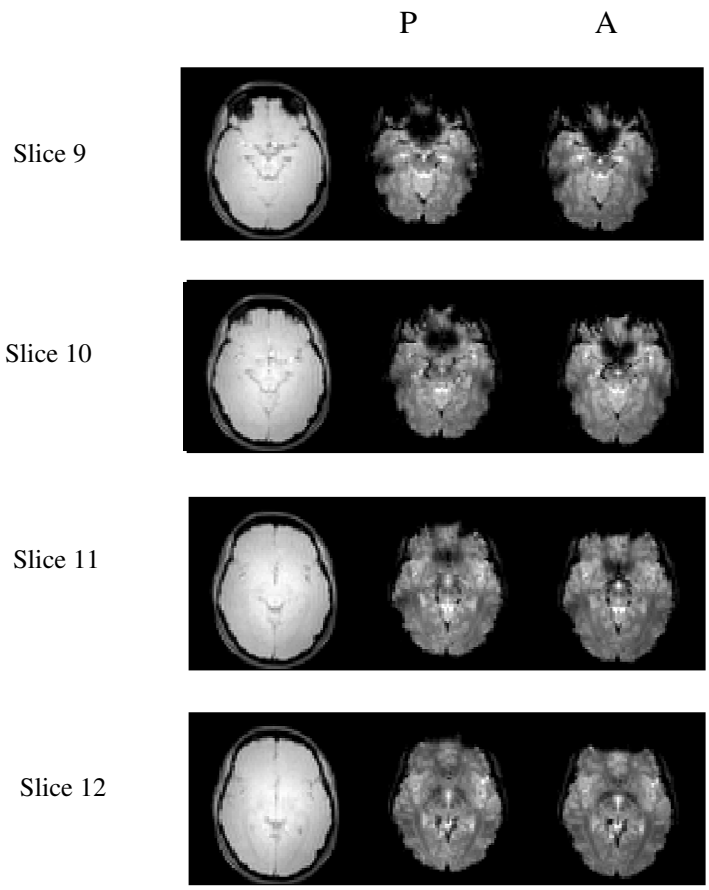

Figure 5. 6: Anatomical images, first column, and EPI images for both the posterior, second column, and the anterior, third column, fat shift direction.

5.4 Fat Shift Direction

The fat shift direction parameter controls in what direction fat is shifted relative to water in the presence of chemical shift effects. Susceptibility artifacts will be shifted in the opposite direction. Figure 5.6 shows anatomical images for four slices in addition to EPI images for the slices for both fat shift directions. The second row shows EPI images with the fat shift direction set to posterior, while in the third row the parameter is set to anterior. Throughout the sequences, the fat shift direction was set to posterior, with the exception of this one sequence to illustrate the effect of the parameter. Artifacts are seen to decrease higher up in the brain for both fat shift directions.

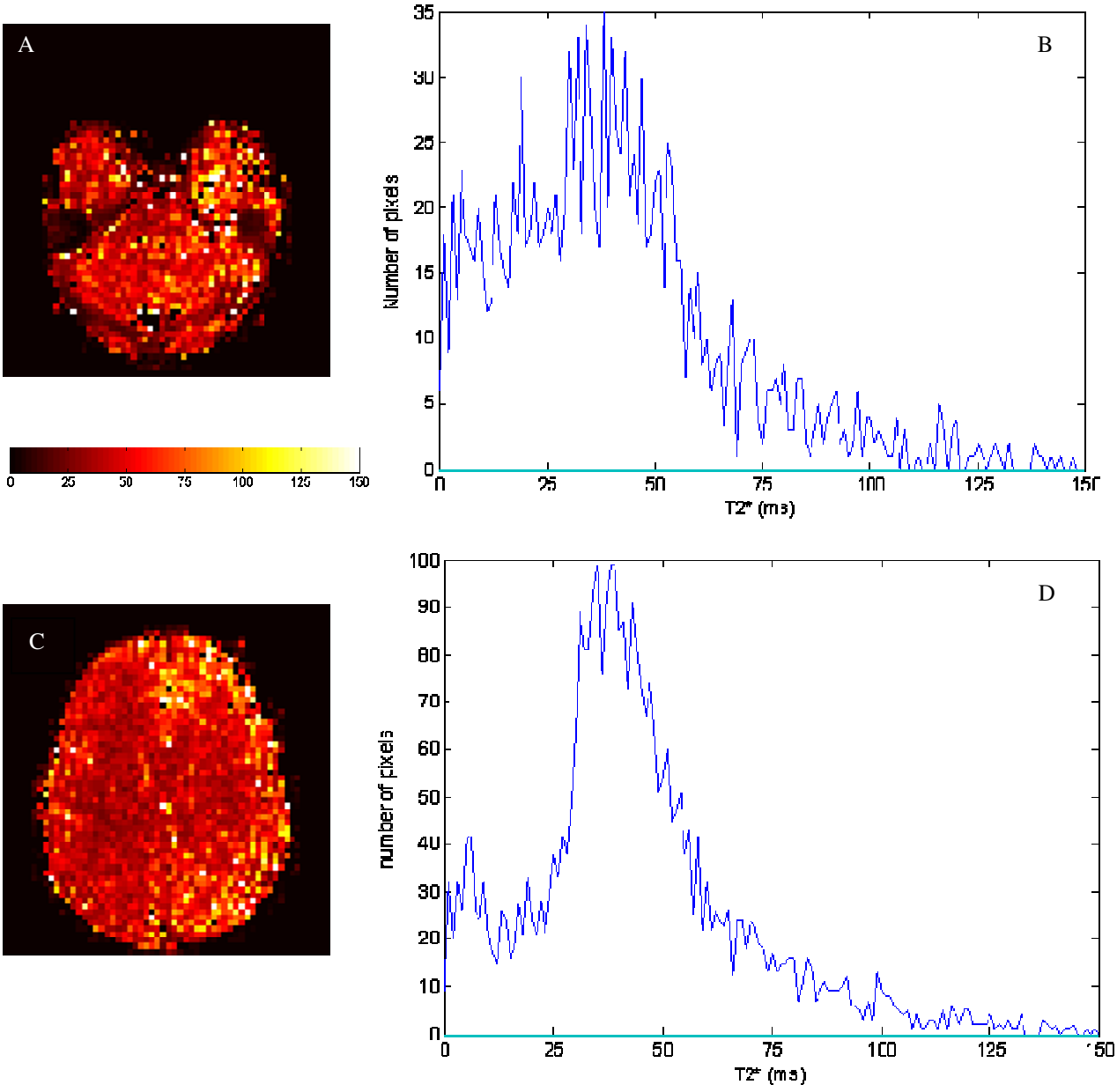

Figure 5. 7: A. T2* map from a slice in the lower part of the brain. B. Histogram showing the distribution of the T2* values from A. C. T2* map from a slice in the upper part of the brain. D. Histogram showing the T2* distribution from C.

5.5 Susceptibility Gradients Effect on T2*

The transverse relaxation time was accounted for in Section 2.1.2. For gradient-echo sequences, where spin-dephasing is not corrected for, susceptibility gradients in the volume being imaged contribute considerably to rapid signal decay and decreasing T2*.

Figure 5.7 shows T2* maps generated from Equation 4.4 with corresponding histograms. One slice from the lower part of the brain, A and B, and one slice from the upper part of the brain, C and D, have been selected. The lower slice is more affected by susceptibility gradients than the upper slice. The histograms show that the upper slice has T2* around 30 to 55 ms. In the lower slice however, the distribution of relaxation times is much more spread out, with T2* values below 30 and 20 ms.

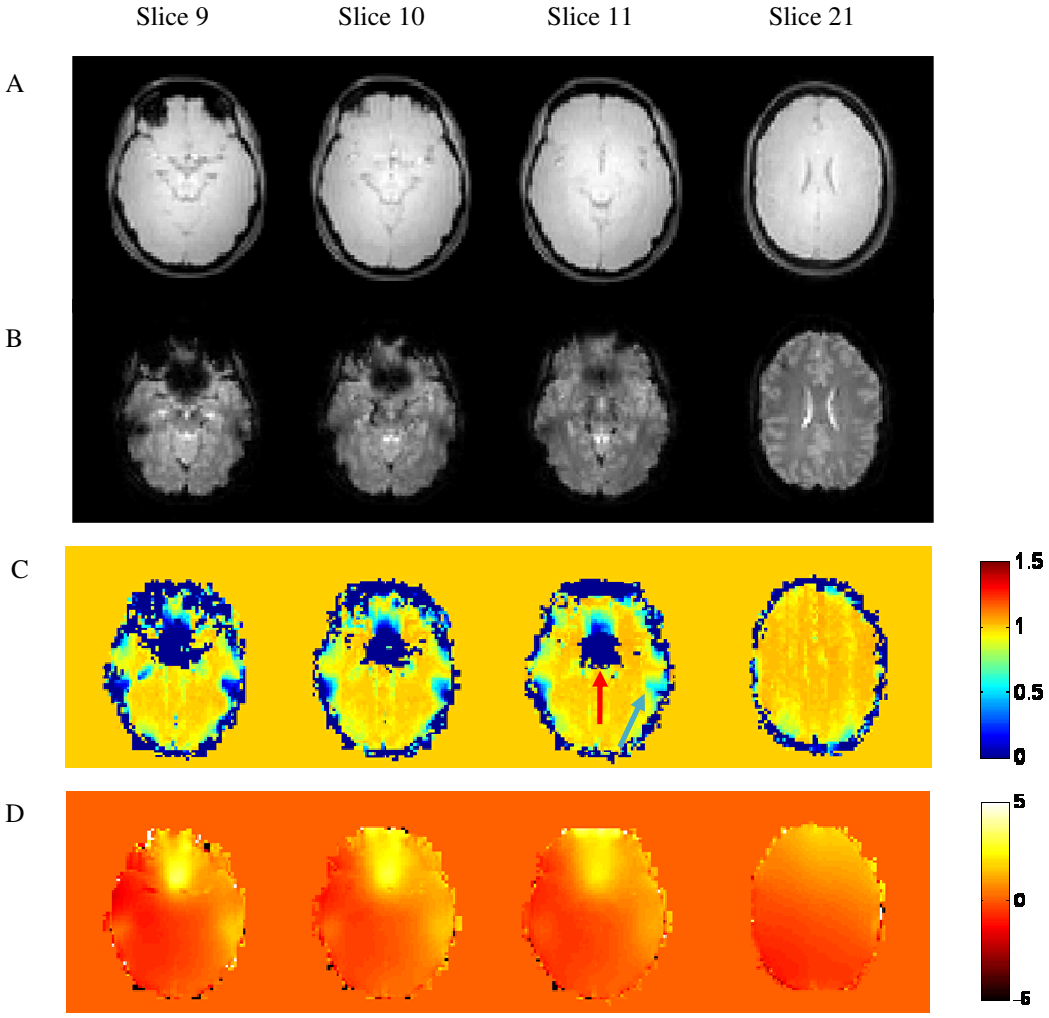

Figure 5. 8: A. Anatomical images for four different slices. B. EPI images. C. Simulated image intensity maps. D. Pixel shift maps.

5.6 BOLD Sensitivity Maps

Figure 5.8-A, B, C and D shows anatomical images, echo-planar images and simulated image intensity maps and pixel shift maps for four different slices, respectively. The maps were generated on the basis of Equation 4.5, with both the effects of through-plane susceptibility gradients and in-plane gradients taken into account. The intensity maps show a pixel's simulated intensity relative to the intensity expected in the absence of susceptibility gradients. Areas where the conditions set by Equations 4.8 and 4.9 did not hold were set to zero. The overall correlation between signal losses in the EPI images vs. the BOLD sensitivity maps was good.

The pixel shift maps were generated according to the method described in Section 4.6, from magnetic field maps expressed in Hz, and show the potential misregistration in the phase encoding direction. The fat shift direction was set to posterior, and so any shift due to susceptibility effects would be toward the anterior.

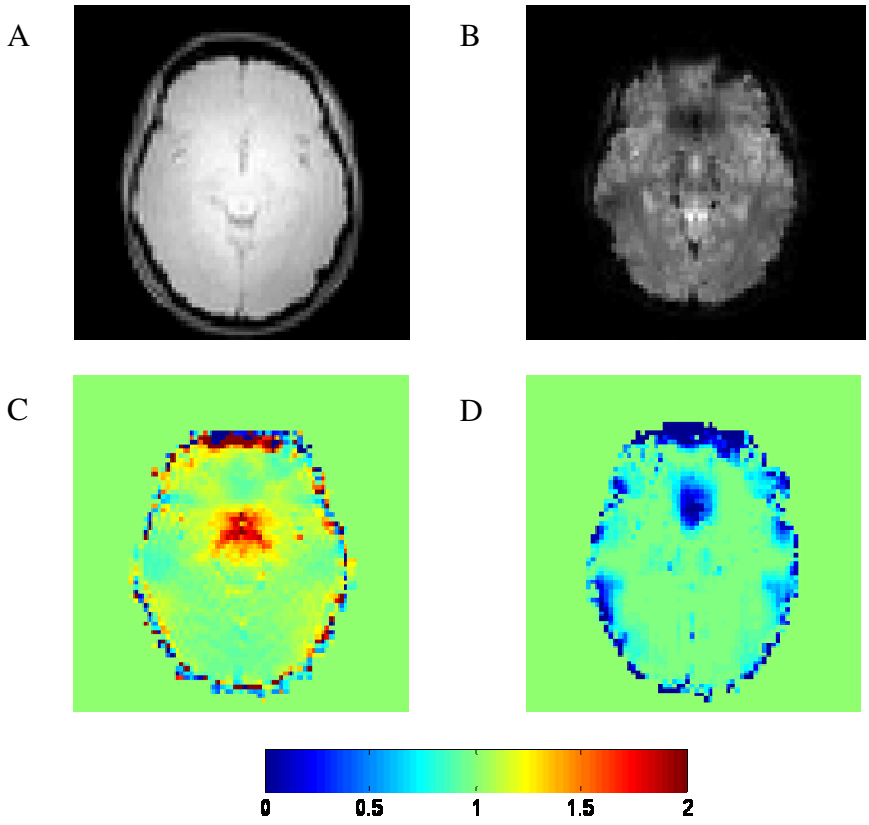

Figure 5. 9: A. Anatomical image of slice 11 B. EPI image C. Map showing the value of 1/Q D. Map showing the value of $e^{-\psi^2}$.

The image intensity is affected by in-plane susceptibility gradients and through-plane gradients. In Figure 5.8, the effects of both components are seen together, in Figure 5.9 the two components are considered separately. The effect of the gradient in the phase encoding direction on the image intensity is expressed by 1/Q, the parameter Q was defined in Equation 3.3, while the effect of the gradient in the slice direction is expressed by $e^{-\psi^2}$, ψ was defined in

Equation 4.6. For illustration purposes, the conditions set in Equations 4.8 and 4.9 were not applied to these maps. As seen from the expression for the effect of the through-plane gradient, Equations 4.5 and 4.6, this effect can only affect the image intensity negatively. The effect of the in-plane gradient can be both positive and negative depending on the polarity and magnitude of the gradient.

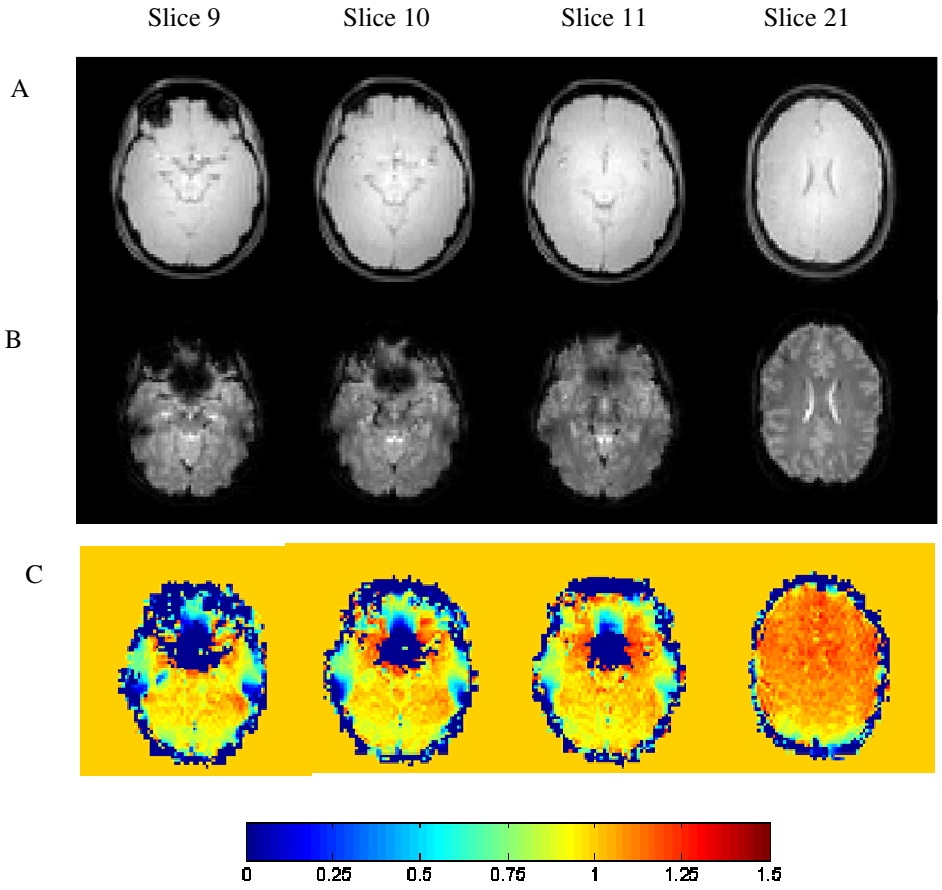

Figure 5. 10: A. Anatomical images B. EPI images C. BOLD sensitivity maps generated with susceptibility gradients in both the phase encoding and slice selection directions.

5.7 Case: FRONT

The results presented in this section are a sample of the analysis performed on the data collected from the FRONT project. The basis of the project was presented in Section 4.9

Figure 5.11 shows BOLD sensitivity maps, A, activity maps overlaid anatomical images, B, and activity maps overlaid BOLD sensitivity maps, C, from one patient, first row, and one healthy control second row. The activation maps display t-values from zero to 5.5. A t-value of 4 corresponds to a p-value of 0.001 for activation. The t-test for statistical significance is discussed briefly in Appendix B. Figure 5.12 shows the same images as Figure 5.11 for a slice lower down in the brain. Together with pixel shift maps, Figure 5.12-D. The scale for the t-values is the same as in Figure 5.11.

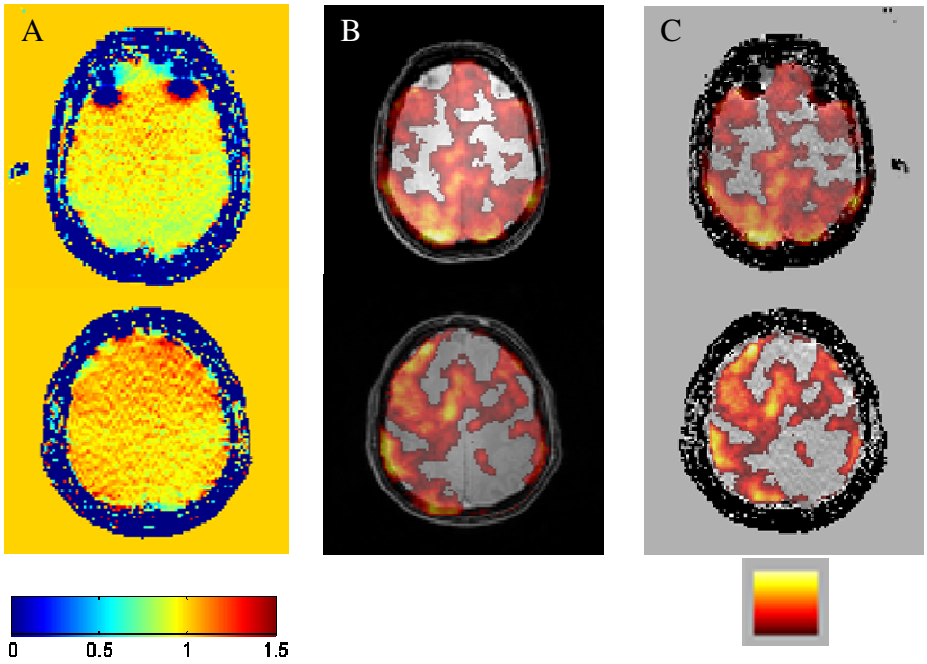

Figure 5. 11: A. BOLD sensitivity maps. B. Anatomical image with activity maps overlaid. C. BOLD sensitivity maps with activity maps overlaid.

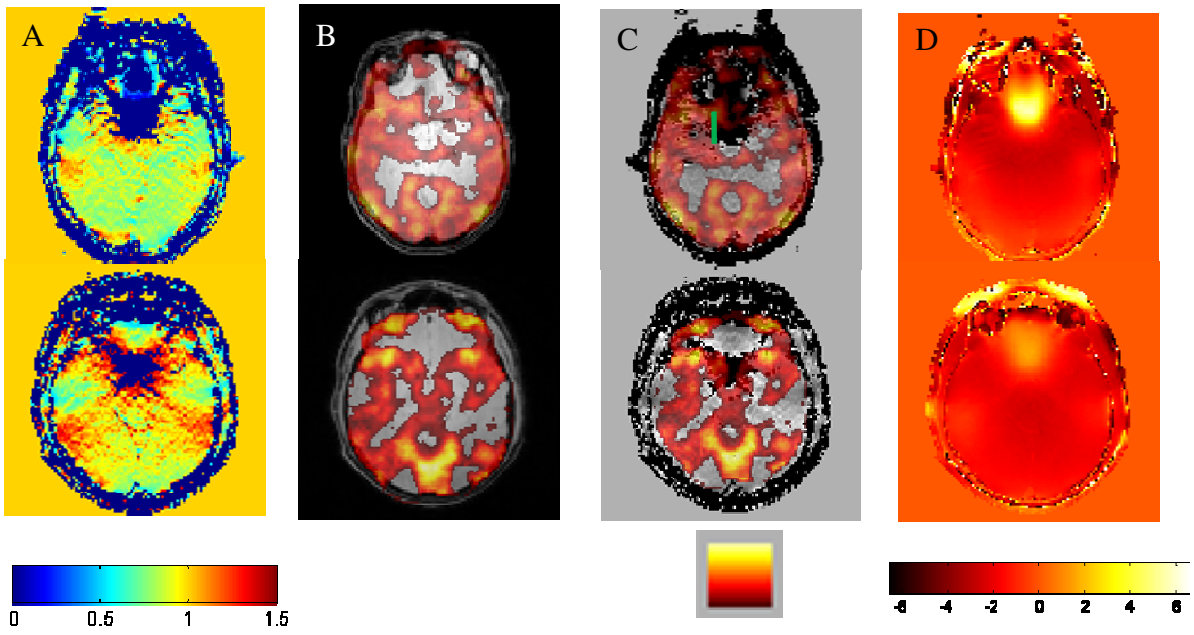

Figure 5. 12: A. BOLD sensitivity maps. B. Anatomical images with activity maps overlaid. C. BOLD sensitivity maps with activity maps overlaid. D. Pixel shift maps

5.8 Case: Epilepsy

The second case that was studied was a young epilepsy patient that had already undergone several operations. An additional intervention was planned; therefore it was necessary to conduct a new presurgical mapping of the activity near the temporal lobes. As a result of the previous operations several metallic clips were fastened to the scull. Figure 5.13-A shows a T1-weigthed anatomy image with an activity map overlaid, 5.13-B shows a BOLD sensitivity map in grayscale with the same activity map overlaid. The activity map was generated from a word generation paradigm. Figure 5.13-C shows a pixel shift map for the same slice shown in A and B.

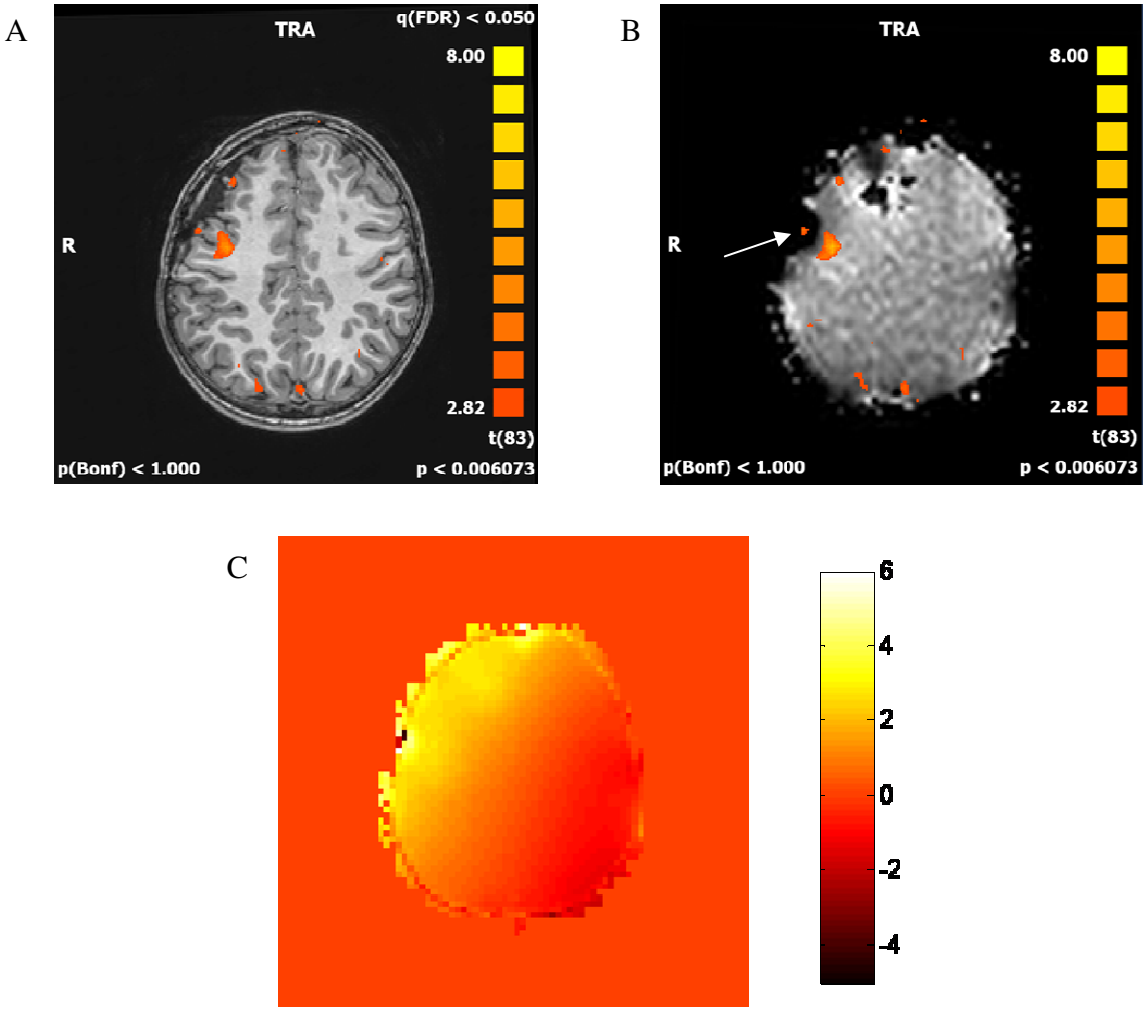

Figure 5. 13: A. The anatomical image with the activity map from the word generation test overlaid. B. The BOLD sensitivity map from the same slice as in A, with the same activity map overlaid. The color scale to the right in each image denotes the scale of the t-values for the activity map. A higher t-value suggests a more robust analysis. C. A pixel shift map generated from a magnetic field map of the slice. The color scale is in pixels.

Figure 5.14 shows a BOLD sensitivity map with the activity map from the antonym paradigm overlaid. Figure 5.15 shows a simulated BOLD sensitivity map, C, and a pixel shift

map, D, generated for this patient, together with anatomy, A, and EPI images, B, for comparison. Some effects of the clips can be seen in the anatomy images, as well as in the EPI images. Visual inspection of the simulated BOLD sensitivity maps in Figure 5.15, give a certain indication of what areas in the brain where caution should be taken in interpreting the BOLD results.

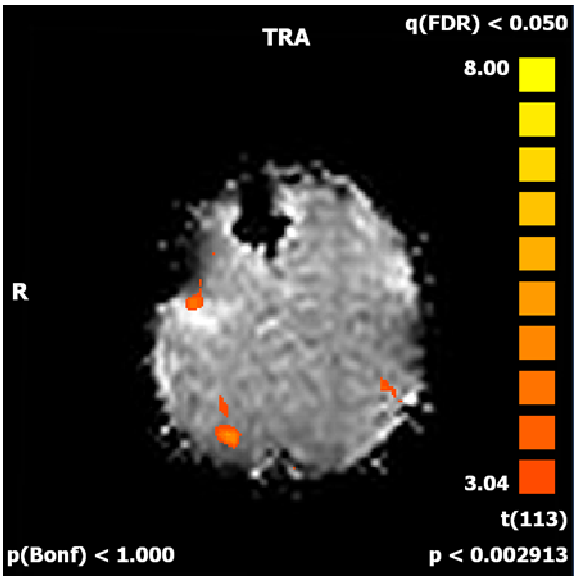

Figure 5. 14: The BOLD sensitivity map with an activity map from a antonym paradigm overlaid.

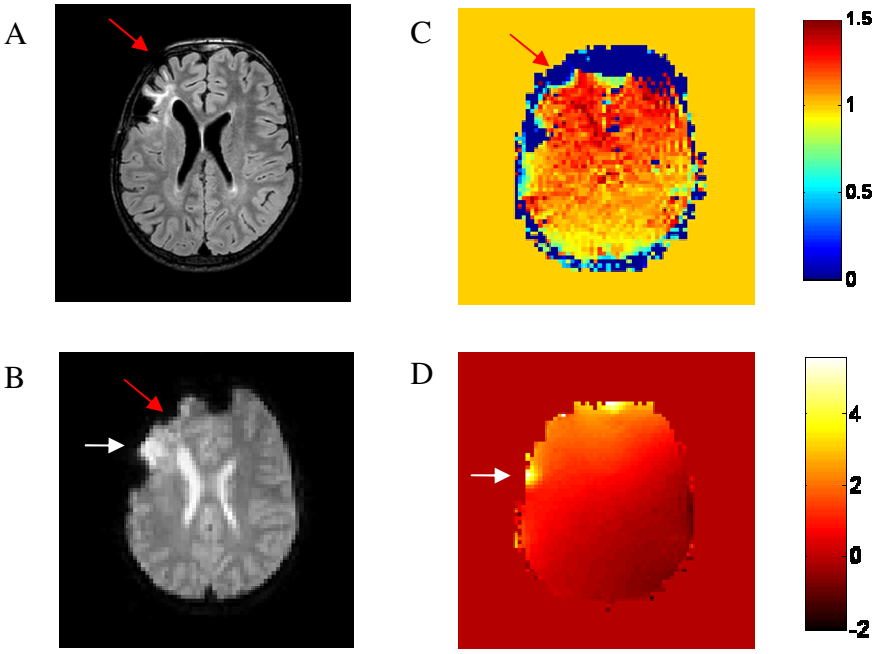

Figure 5. 15: A. Anatomical images, B. Echo-planar images, C. Simulated BOLD sensitivity maps, and D. Pixel shift map.

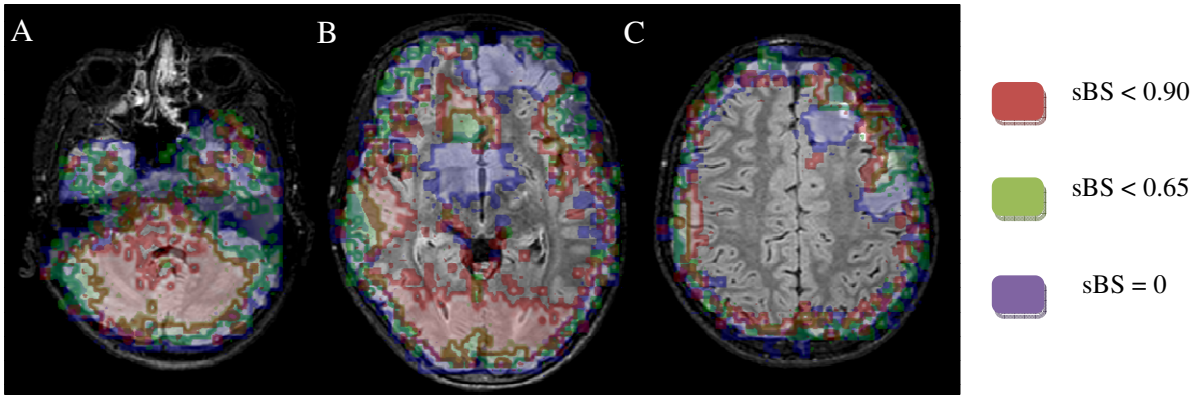

Figure 5. 16: A, B, C, anatomical images with overlaid maps of BOLD sensitivity values for three different slices.

Figure 5.16 shows anatomical images of the patient overlaid with BOLD sensitivity values for three different slices. Three different levels of sBS are shown.

6 Discussion

In this chapter, the results from Chapter 5 will be discussed and analyzed. First the motivation for the project will be discussed.

The problem of susceptibility artifacts in echo-planar imaging is well known. Inhomogenities in the magnetic field can cause geometric distortions and steeply varying susceptibility gradients can severely reduce the BOLD sensitivity and achievable BOLD contrast. Many solutions to this problem have been approached, still, there is no general consensus on what method best addresses these issues.

Some imaging parameters can be changed to limit susceptibility artifacts. A lower magnetic field will reduce artifacts, as will a shorter TE and smaller voxels; however all of these parameters are intrinsic to BOLD imaging and are necessary to achieve an observable BOLD effect (5). Carefully choosing slice tilt and spatial resolution may recover signal from areas affected by signal loss. However, the parameters can normally only be optimized for one specific region of interest, and other areas may actually loose BOLD sensitivity (30). The same is true for shimming which is applied to make the magnetic field as homogenous as possible. Even after shimming there will often remain substantial local field differences, not least because optimal shimming can only be attained for one point in the volume (12) and image intensity and BS in other areas may decrease (11).

A case has been made for using magnetic field maps to correct for distortion due to susceptibility effects (6); however, signal voids cannot be corrected for with this method (31) and Ojemann et al. (5) suggest that signal loss is a greater effect than distortion. In addition, the correction methods are not perfect and there is a risk that the corrected images will lead to misinterpretations (32). For these reasons this project will focus on using magnetic field maps to identify artifacts and areas at risk of low BS, rather than correcting for these artifacts. In this way one avoids definite conclusions being drawn on an unsound basis.

BOLD fMRI is already an important part of basic neuroscience research, and its use in clinical applications is increasing. Whatever the aim of the BOLD analysis is, it is important to be aware of the techniques flaws, in addition to its possibilities.

6.1 Matlab Field Maps vs. FSL Field Maps

Phase unwrapping is required for applications in many different fields; there are even several applications within the MRI field that necessitate robust unwrapping algorithms, such as chemical shift mapping and velocity measurements for MR angiography, in addition to magnetic field mapping. Many unwrapping algorithms have already been developed; some specialized in unwrapping for MRI use (27). Still, it was decided in this project that, as far as possible, the unwrapping algorithm used should be self-produced. The main reason for this was ensuring the transparency of the entire process of generating field maps. The unwrapping process is fundamental to generating high-quality field maps, and these field maps were again fundamental for both aims in this project. In this light it was felt to be worth the time invested to avoid a ‘black-box’ in the core of the project.

The overall correlation between the self-produced method and the FSL method was good. The PRELUDE algorithm used by FSL was based on a clustering method, making it more time efficient. However, the iterative technique employed in the Matlab method was somewhat simpler and easier to implement. Due to the limited time available it was decided that the iterative technique served the purposes of this project adequately.

The line profiles in Figure 5.1, illustrate the concept of phase unwrapping and to what extent that has been accomplished for these images. The line profiles are seen to have appreciably improved after the unwrapping process; the profiles become much smoother after the unwrapping. Figure 5.1-A and C show the phase images before the unwrapping; the image taken at a longer echo time, C, seems to have larger phase differences in a more complex way. When the echo time is longer multiple wrappings can occur. B and D show the phase images after unwrapping and it can be seen that the image with a shorter echo time was unwrapped in a better way than the image with a long echo time. This seems reasonable since the phases developed in that image are more complicated.

The results from Section 5.1 show that the field maps generated by the FSL method were somewhat better than the self-produced field maps. Figure 5.2 shows the two main types of irregularities between the two methods. The first type, highlighted with black arrows in Figure 5.2-B, includes pixels that clearly have been wrongly unwrapped; however, these are almost always located outside the brain. For fMRI analysis, only areas inside the brain are of interest, and if a brain extraction tool had been applied to the images, these irregularities would more than likely not have been visible on the finished field map.

The second type of irregularity is of a more serious kind and is highlighted by the white arrow in Figure 5.2-B. These irregularities are often located in areas where the original phase maps were very complicated with fast changing phases. These problems are also seen in the FSL generated field maps, albeit to a lesser extent. Although these artifacts witness of an imperfect unwrapping routine, they are usually easy to identify in the finished field maps and will likely not lead to any misinterpretations of the field maps. The point can also be made that these deviances will occur in areas where the susceptibility gradient is steep, and will only further illustrate what areas of the brain will be exposed to artifacts due to inhomogeneities in the magnetic field.

Figure 5.2-C shows the percent deviation between the two methods for generating field maps. These deviations are mostly caused by inaccuracies in the conversion process when the files were imported to FSL and are generally seen to be small. The deviation in percent is seen to be large in areas highlighted by the black arrows, these are areas that have low phase values and the inaccuracies from the conversion process will be relatively larger, but are in practice negligible.

6.2 Ability of Field Maps to Predict Artifacts

Figure 5.3 shows field maps together with anatomical and EPI images for four different slices. When comparing the images it can be observed that areas with darker colors toward either end of the spectrum mark areas where artifacts can be spotted in the EPI images. These artifacts are especially pronounced in areas around the temporal and frontal regions of the brain. These are regions that are close to air cavities and bone structures and are therefore likely to be affected by susceptibility effects. These results match well with results from literature (5), (12), (33). In the areas severely affected by artifacts, the deviation from the B0 field is on the order of a couple of ppm. This seems reasonable and correlates well with what is found in literature (34).

If the goal of an fMRI experiment is to observe activity in for example the frontal lobe, or other areas especially affected by susceptibility artifacts, the identification and estimation of such artifacts is especially important to avoid false negative results. The results presented in Section 5.2 are representative for the general tendency found throughout the volume and also for the other subject. The frequency maps give a good indication of where the absence of signal cannot automatically be interpreted as an absence of activity following,

for example, stimuli to the patient. However, the BOLD sensitivity model, which is discussed in Section 6.7, is more suited to guide these decisions.

Although the maps illustrate in a satisfactory way where artifacts are likely to be found, they do not easily distinguish between whether these artifacts will manifest as distortions or signal loss. This information can be found by examining what causes the different types of artifacts. Varying sequence parameters and registering the effects was found to be useful in this endeavor.

6.3 Artifact Dependence on Bandwidth

The effect of the bandwidth in the phase encoding direction on EPI image artifacts was discussed in Section 2.3.2. The pixel bandwidth denotes the difference in frequencies between adjacent pixels. Any source of inhomogeneities in the magnetic field that leads to frequency differences above the pixel bandwidth will lead to artifacts. As a consequence, lower bandwidths will lower the threshold at which artifacts will occur. If the voxel dimensions are small enough, compared to the magnitude of the field differences, the resulting artifact will be pixel shifts; if not signal loss is a more likely outcome as the spin distribution within a voxel cancels out the signal.

Figure 5.4-A and B shows the anatomic image and the field map, respectively, for a slice. Figure 5.4-C and D shows EPI images and pixel shift maps for three different bandwidths. Comparing the EPI images with the anatomical image, and each other, the presence of artifacts is seen to increase with decreasing bandwidth. The deviation from the main magnetic field, illustrated by the field map in Figure 5.4-B, is the same for all three bandwidths. However, the same frequency difference has a larger impact on the images acquired with a smaller bandwidth; this fact is illustrated by the pixel shift maps. The effect of bandwidth on the presence of susceptibility artifacts illustrated here is well documented in literature (35), (36).

Comparing the EPI images and the pixel shift maps there is a clear correlation between where artifacts are observed and where they are estimated to occur. The magnetic field maps used to detect artifacts do not separate between whether signal loss or geometric distortions are more likely to occur. Turning the field map into a pixel shift map can only estimate to what degree image distortion would happen if it were the prevailing artifact. However, the maps give a good indication of where the problem areas are.

The bandwidths chosen in this project are around what is common in echo-planar imaging, around 30 Hz/pixel. As seen in Figure 5.4, the pixel shift map for the image with the smallest bandwidth, 21.7 Hz/pixel shows a maximum pixel shift of about 5. With a voxel dimension of 3 mm this can lead to a misregistration of a pixel of 1-2 cm. A pixel shift of this magnitude can cause problems for the BOLD fMRI analysis, as will be discussed in Sections 6.7-6.9.

6.4 Artifact Dependence on Echo Time

Keeping the bandwidth constant, the other parameter that was chosen to vary was the echo time, TE. As seen in Figure 5.5-C the echo time varies significantly across the slice. This is due to susceptibility gradients in the phase encoding direction that alter the position of the echo in the acquisition window. As was explained in Section 3.1.2, the effect of the gradients depends on the polarity. The middle image illustrates the effects of both negative and positive gradients. The blue arrow marks a region where a negative local gradient implies a Q-value, as defined in Equation 3.3, larger than 1 and a decrease in image intensity and echo time. This

effect is seen particularly in the orbitofrontal cortex and the superior frontal lobes corresponding well with what has been observed in literature (21). There are steep susceptibility gradients in these areas due air/bone/tissue interfaces.

The green arrow points to a region where the echo time is longer than the nominal 35 ms, because of a positive local susceptibility gradient in the phase encoding direction. This implies a Q value smaller than 1. Equation 3.5 implies an increase in image intensity because of this, but no such effect can be observed. This discrepancy is explained by Equation 4.5, which shows the final expression for the simulated image intensity. Because of the increased TE, the through-plane spin-dephasing effect caused by susceptibility gradients in the slice selection direction is greater and will decrease the image intensity. If the susceptibility gradient in the phase encoding direction is large enough, the echo may be shifted outside the acquisition window, and all signal will be lost, as is the case near the sinuses on the left side of the brain for all three echo times. The echo time is seen to go abruptly from a high value to zero.

When comparing the EPI images taken at different echo times, the effect of through-plane dephasing becomes evident. Table 5.1 displays intensity values for two ROIs in each EPI image. The red ROI is located in an area affected by a positive susceptibility gradient, while the blue ROI was placed in an area affected by a negative gradient. As expected, the blue ROI generally has a lower intensity than the red ROI. In addition, when comparing the ROIs across echo times, the image intensity for each ROI decreases with increasing echo time. As the nominal echo time increases, there is a greater effect of through-plane spin-dephasing and the image intensity decreases. Geometric distortions can also be observed to be worse at higher TE, but the main susceptibility effect seems to be signal loss due to through-plane spin-dephasing and decrease in SNR, this is consistent with what is found in literature (5). With a longer echo time the adverse effects of the susceptibility gradients have a longer time to develop, out-weighing the potential positive effects caused by the in-plane gradient.

Although image intensity losses caused by through-plane gradients can be minimized by reducing the echo time, Equation 3.3 shows that the effect of gradients in the phase encoding direction on the BOLD sensitivity is independent of the echo time, and so reducing the nominal echo time will not necessarily recover the BOLD sensitivity even though some image intensity is recovered. This has been demonstrated at 2T by Gorno-Tempini et al. (24).

The results presented in Section 5.3 show the importance of choosing sequence parameters, like TE and bandwidth, with care. However, the space in which these parameters can be adjusted is rather limited. Many of the parameter settings that lead to severe artifacts in EPI sequences are essential to achieve a detectable BOLD signal. A long echo time is needed to let contrast differences develop between areas with oxyhemoglobin and areas with deoxyhemoglobin. A small bandwidth is necessary to achieve acceptable time resolution. A strong magnetic field will increase the differences between active and resting areas of the brain, thereby increasing BOLD contrast, but will in addition lead to larger field inhomogeneities, increasing the occurrence of artifacts. The results presented, illustrate the balancing act that is needed to achieve an fMRI image with an acceptably low level of artifacts and yet a satisfactory BOLD signal (5). It also shows the importance of elucidating the problems that often occur in BOLD fMRI so that the analysis is as reliable as possible.

6.5 Fat Shift Direction

The results presented in Section 5.4 illustrate how the parameter fat shift direction can be used, to some degree, to influence the appearance of susceptibility effects. The parameter

will also affect chemical shift artifacts; however, as mentioned in Section 4.2, the fat signal was suppressed in all the EPI sequences in this project.

Figure 5.6 shows anatomical images and EPI images for two different fat shift directions for four different slices. Throughout the slices, artifacts are drawn toward the front of the brain for the posterior fat shift direction and toward the back of the brain when the fat shift direction was set to anterior. This is to be expected as susceptibility artifacts are shifted in the opposite direction of chemical shift effects.

Signal accumulation may result when signal is shifted from one location to another and added to the signal already there. Depending on what areas of the brain are of special interest in a study; the fat shift direction can be chosen to avoid the worst artifacts in significant areas of the brain. For example, the parameter is often set to posterior to avoid the occurrence of high signal at the border of the frontal sinus, while an anterior direction can be chosen to avoid high signal at the border of the petrous bones. Both the sinuses and the petrous bones are sources of susceptibility artifacts, as discussed in Section 2.4.2. In the EPI sequences acquired in this project, the fat shift direction was set to posterior to avoid signal accumulation in the frontal lobe.

Figure 5.6 also illustrates how some susceptibility artifacts can be difficult to detect. When examining the EPI images for both directions together, more artifacts can be identified than if the images had been considered separately. If only images from one of the directions is observed, certain pixels appear to be unaffected by the artifacts, but if the EPI image with the opposite fat shift direction also is taken into account it becomes clear that the validity of the pixel cannot necessarily be trusted.

Figure 5.6 illustrates an additional point. Observing the artifacts from slice to slice, it becomes clear that the amount of artifacts is greater in the slices lower in the brain compared to further up. This is to be expected as the upper slice is further away from areas that are known to induce susceptibility artifacts such as the sinuses and the petrous bone.

6.6 T2* Map

T2* is a parameter that combines the transverse relaxation phenomenon, T2, caused by interactions between spins, and static field inhomogenities. Therefore, the variation in T2* across the volume can be seen as illustrative of inhomogenities in the field and susceptibility effects.

Figure 5.7-A and C shows T2* maps for a slice in the lower part of the brain and a slice from higher up in the brain, respectively. B and D show histograms of the values for the same slices. In the lower slice there is a large distribution of different T2* values, especially the orbitofrontal and anterior temporal lobes seem to have T2* values even below 20 ms. In the upper slice the values are much more concentrated, the main bulk of the pixels have T2* values between 30 and 55 ms. These values are closer to the nominal value of T2*, which is given by Wansapura et al. (25) to be about 50 ms in gray matter at 3 T. The large difference in T2* distribution between the upper and lower slice found here is consistent with the results found by Gorno-Tempini et al. (24). The lower slice is likely to be more affected by susceptibility gradients than the upper slice due to its proximity to air filled cavities and bone and these gradients lead to a reduction in the transverse relaxation time.

The areas that are most affected by susceptibility gradients are of most interest in this project, especially the frontal lobe. There is vast variation in T2* values in this area, both variation within the area and variation in relation to nominal T2* values for grey matter. When planning a BOLD fMRI sequence the choice of echo time is partially based on the T2*

value of the tissue being imaged; as the variation in T2* values found here illustrates, this is not always a straightforward task.

Still, from Figure 3.2 in Section 3.1.2, it can be observed that the there is a quite broad maximum for what TE value gives the optimal BOLD sensitivity. For a T2* value of 40 ms, TE values between 30 and 60 ms give a BOLD sensitivity of 90 % or more. This implies that the TE value chosen can deviate somewhat from the T2* value and still give an acceptable BS.

6.7 BOLD Sensitivity

In a typical BOLD fMRI survey the goal is to detect activation of the brain following the execution of tasks by a subject or the exposing of the subject to stimuli. Gradient-echo EPI is the sequence of choice because of unparalleled time resolution and better BOLD contrast than the similar spin-echo EPI. However, as was discussed in Section 2.3.2, GRE-EPI is prone to artifacts that make the detection of brain activity a more complicated task. In a given BOLD exam there is a risk of false negative results; false negative and positive results were discussed in Section 3.1.1. The presence of artifacts can make it difficult to conclude that there is no activity even if no signal has been detected. It is important to note that simulated BOLD sensitivity maps are not directly connected to brain activity; these maps only reveal the likelihood of detecting the BOLD signal if it is there (37).

The method behind creating BOLD sensitivity maps was discussed in Section 4.8. Again magnetic field maps are used, in this case to map the components if the susceptibility gradients throughout the volume. The effect of susceptibility gradients on image quality depends on what direction the gradients are in, as discussed in Section 3.1.2. A gradient in the read-out direction will likely not have an effect on the EPI images because of the high bandwidth in that direction. For this reason the effect of this gradient was disregarded when generating the BOLD sensitivity maps. Equation 3.1 states that the BOLD sensitivity depends on the effective echo time and the image intensity. The effect of susceptibility differences on the echo time was discussed in Section 6.4; their effect on the image intensity is discussed in Section 6.7.1.

6.7.1 Simulated Image Intensity Maps

Figure 5.8 shows anatomical images, A, EPI images, B, simulated image intensity maps, C, and pixel shift maps, D, for four different slices. The expressions for Q, SII and ψ, Equations 3.3, 4.5 and 4.6, respectively, show the dependence of the simulated image intensity on the susceptibility gradients in the phase encoding and slice selection directions.

The EPI images can be seen as measured image intensity maps, and they should be expected to correlate reasonably well with the simulated image intensity maps. The overall pattern in both sets of intensity maps is similar; however, the magnitude of the signal loss is generally greater in the simulated intensity maps. This divergence between the measured and simulated intensity maps has also been observed by others, although the importance of this deviance has been downplayed (11), (12).

In some regions, signal can be observed even though the simulations predict complete signal loss. Part of this deviance can be explained by geometric distortions. As shown in Sections 5.2 and 5.3, deviances in the magnetic field can cause spatial misregistration. It is possible that some of the signal detected in regions in the measured image intensity maps where the simulated image intensity predicts zero intensity, originates from another area. The pixel shift maps shown in Figure 5.8-D are an expression for how far a pixel can be

misregistrated due to offsets in the magnetic field. The maximum pixel shift is seen to occur near the region of interest. In these areas, the pixel shift is of about three to four pixels, this corresponds to a spatial shift in the phase encoding direction of about 1 cm, given a pixel dimension of 3 mm. And so, geometric distortions can account for some of the differences observed between the measured and simulated image intensity maps.

It is unlikely that this discrepancy is caused by geometric distortions in the slice direction. In the EPI sequences, an interleaved scan order was employed. Neighboring slices were always acquired a relatively far apart temporally. Limiting possible crosstalk between slices.

The different types of signal loss caused by susceptibility gradients in the phase encoding direction were discussed in Section 3.1.2. The red arrow in slice 11 in Figure 5.8-C shows type 1 signal loss; as is characteristic for this type of signal loss, there is a sudden transition between high image intensity and zero image intensity as the effective echo time is shifted outside of the acquisition window (37). Signal loss of type 2 is highlighted by the blue arrow. In this case the effective echo time is still within the acquisition window, but the sampling of k-space is changed in a way that causes a decrease in the image intensity. As illustrated by the simulated image intensity map from slice 21, in Figure 5.8-C, the overall effect of the susceptibility gradients seems to be to increase the image intensity slightly, higher up in the brain.

The intensity loss highlighted by the blue arrow in Figure 5.8-C, is also partly caused by a reduction in the image intensity caused by spin dephasing due to the susceptibility gradients in the slice selection direction. Figure 5.9 show the effect of both components of the susceptibility gradient on the simulated image intensity for slice 11, separately. The effect of the through-plane component, shown in Figure 5.9-D, is for the most part negligible, but in the orbitofrontal cortex this gradient has a substantial negative effect on the image intensity. The component of the susceptibility gradient in the phase encoding direction also has a considerable effect in this region, but in this case the effect on the intensity is positive. However, as the simulated image intensity maps of the same slice show, the image intensity in this area is zero. This is because the gradients in the phase encoding direction also affect the effective echo time as discussed in Section 6.4, shifting it outside the acquisition window making detection of signal impossible.

Z-shimming is often used to reduce the effects of through-slice susceptibility gradients. However, as seen from figure 5.9-D, the magnitude of these gradients vary significantly across the brain and can only truly be compensated for in a limited region of the brain at a time. In addition, the compensation gradient used for z-shimming will cause additional dephasing, and in some areas decrease the image intensity (12).

6.7.2 Simulated BOLD Sensitivity Maps

The effect of susceptibility gradients on the image intensity was discussed in Section 6.7.1. The effect of susceptibility gradients in the phase encoding direction on the BOLD sensitivity are greater and more widespread than for the image intensity since BS also depends on the echo time which is also affected by these susceptibility gradients. This fact is clearly illustrated when Figures 5.8-C and 5.10-C are compared. The areas that are predicted to have a decreased BOLD sensitivity in Figure 5.10, are areas that are known to be particularly vulnerable to susceptibility effects, for example the orbitofrontal cortex and the superior temporal lobes (21).

When it comes to the extent of complete signal loss, the simulated image intensity and the simulated BOLD sensitivity are equally affected. The graph in Figure 6.1 shows the BOLD sensitivity as a function of the susceptibility gradient in the phase encoding direction.

BS is set to 100% in the absence of susceptibility gradients. The numerical values shown in the figure are only valid for a volume acquired with the particular sequence parameters shown in the table, but the general tendency holds for all volumes. If the gradient is too large in the positive or negative direction the effective echo time will be shifted outside the acquisition window. The conditions for these critical gradients were described by Equations 4.8 and 4.9. For the EPI sequence discussed in this section, the basis sequence used in this project, the acquisition window was relatively narrow. The echo time was 35 ms, the start of the window was at about 26 ms and the end at 44 ms, this implies that relatively small gradients in the phase encoding direction could lead to complete signal drop out and loss of BOLD sensitivity.

The BOLD analysis in a BOLD fMRI experiment is generated on the basis of EPI images. As discussed in Section 6.7.1, these images are affected by geometric distortions to some extent. And these distortions will almost certainly compromise the accuracy of the BOLD analysis; therefore contradictions may arise between the activity maps derived from the BOLD analysis and the BOLD sensitivity maps. This will be investigated further in Sections 6.9 and 6.10.

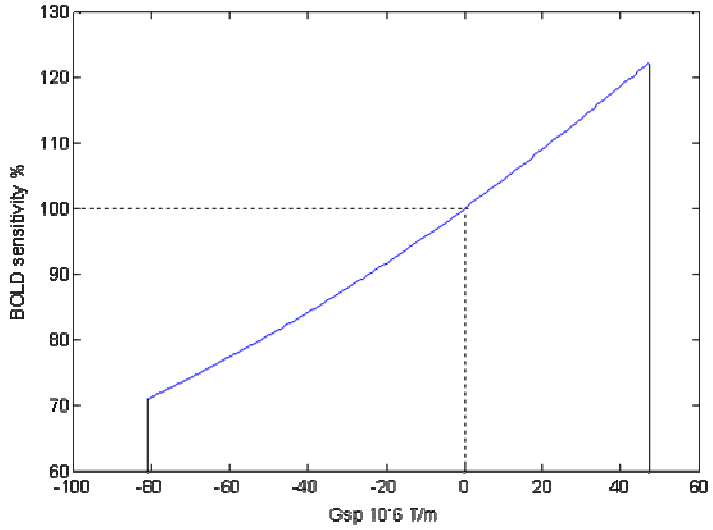

TC	35 ms
Δt	0.4256 ms
t_{start}	25.87965
t_{end}	44.12035

Figure 6. 1: Simulated BOLD sensitivity dependence on the susceptibility gradient in the phase encoding direction, G_{sp} for an EPI sequenced with the parameters given in the table. BS is given as a percentage of the value at G_{sp}=0.

The signal to noise ratio, SNR, will decide what amount of type 2 signal loss can be tolerated before the signal cannot be detected. As discussed in Section 3.1.1, signal change caused by the BOLD effect during activation is quite small, usually between two to four percent. The intrinsic SNR in an EPI sequence is often relatively large, but even so, a signal change of only a couple percent will be difficult to detect (33). If the BOLD sensitivity is appreciably lowered it will compromise the already limited detection power of the BOLD experiment as the BOLD signal is reduced to the level of noise. The direct consequences this will have in general for BOLD exams will be discussed further in Section 6.8 and for the special cases of the FRONT project and the epilepsy patient in Sections 6.9 and 6.10, respectively.

6.8 Acceptable BOLD Sensitivity

The BOLD sensitivity maps' implications for the BOLD analysis need to be investigated further. The maps by themselves give a qualitative idea of the effect of susceptibility gradients. The impact of susceptibility gradients on the BOLD sensitivity was discussed in a qualitative way in Section 6.7.2. The gradients reduce the signal-to-noise ratio and therefore affect the ability of the BOLD experiment to detect changes in brain activity (33). However, for the BS maps to be a truly valuable component of the process, the effect needs to be connected to the detectable BOLD signal in a more quantitative way.

One way to quantize the impact of the change in BOLD sensitivity on the BOLD signal is for a threshold to be set for how much the BOLD sensitivity can be reduced before the integrity of the experiment is compromised. Different values of this threshold can be found in literature. De Panfilis and Schwarzbauer (12) operate with a threshold of a BS of 50 %, although this is in the context of using BOLD sensitivity maps to compare different acquisition methods. At any rate the threshold will have to depend on the signal change available in each particular BOLD fMRI experiment and on the noise level. It seems reasonable that a BOLD response of 3% can tolerate a lower BOLD sensitivity than a response of 2%. At some point the response will be undetectable as it is reduced to such a level that it is impossible to separate from noise. When BOLD results are analyzed it is important to know if the absence of activity can be directly inferred from the absence of signal, or if susceptibility gradients make the detection of signal impossible.

Figure 6.2, shows a schematic of a typical BOLD response. The signal change is about 2 %, while the noise level is just under 1 %. A response like this would likely not be observable in a region with BOLD sensitivity close to 50 %. A reduction in BOLD sensitivity because of susceptibility gradients can therefore lead to false negative results in the BOLD analysis.

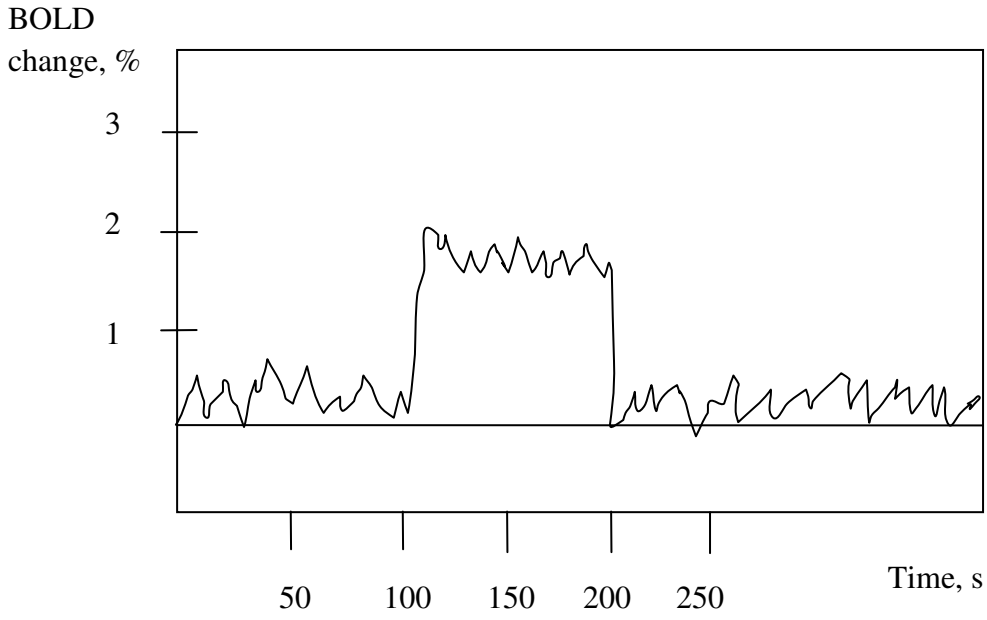

Figure 6. 2: Schemtaic of the BOLD response to a task or stimuli.

The basis for the BOLD effect was briefly discussed in Section 3.1.1. For activity in a certain part of the brain to be determined, the difference between resting states and active states has to be statistically significant (18). If the BOLD sensitivity in an area is reduced because of susceptibility gradients, the difference between active and resting states that is required to determine significance will increase and some voxels that are in reality activated may be overlooked because of strict statistical demands.

6.9 Case: FRONT

BOLD fMRI has since its inception been an important tool in the field of neuroscience research. In the FRONT project, BOLD fMRI was employed together with other tools to investigate the effect of frontal brain injury on certain neurological abilities. Since the frontal lobe is especially vulnerable to susceptibility effects, the BOLD sensitivity maps could contribute valuable information about the validity of the BOLD analysis in this region.

Areas where the BS maps can contribute the most are areas where there is complete loss of BOLD sensitivity due to in-plane gradients shifting the effective echo time outside of the acquisition interval. This type of BOLD sensitivity loss will not be affected by an additional susceptibility gradient in the slice direction; the estimated sensitivity is zero in any case. In Section 3.1.1, the different types of errors that can occur in the BOLD analysis were discussed. In neurological research the statistical analysis is specifically designed to prevent false positives. Basic neuroscience relies on activation maps that mark areas where one is confident there is activation. A voxel is set to inactive if the signal change between stimulus and baseline is statistically insignificant. If the area is affected by loss in BOLD sensitivity due to susceptibility gradients this can result in false negative results, voxels that were in reality activated are set to inactive.

Figure 5.11 shows BOLD sensitivity maps and activation maps for one patient and one healthy control. The BOLD sensitivity maps show two clear dropout regions on either side of the frontal lobe for the patient. Considering the BS maps it seems clear that it cannot be concluded that the patient lacks activation in the frontal lobe. The failure to detect activation can be because of the loss of BS in this region. The healthy control is seen to have a strong activation in the same region, particularly on the left side. The patients in the FRONT study all had some form of frontal lobe brain injury. Many had undergone previous surgeries which left them with metallic clips or scars that can contribute further to the susceptibility gradients already present. It was therefore especially useful to observe the activity maps together with BS maps for these subjects.

The BS maps can also be used to assess if the activation maps generated from the BOLD analysis give false positive results, or at least if activations can have been shifted from their correct position. Figure 5.12 shows BOLD sensitivity maps and activation maps for one patient and one healthy control together with pixel shift maps. The slice was from a lower part of the brain, and both BS maps show considerably more dropout in BOLD sensitivity. For both subjects clear activation is seen in areas where the BS maps predicts complete sensitivity dropout. There can be several reasons for this discrepancy. First, the activation maps and the BS maps had to be coregistered manually, inevitably leading to some inaccuracies. Secondly, the discussion from Section 6.7.1 also applies here. The activation maps are based on a series of EPI images that are affected by image distortion as a result of susceptibility differences. The slices shown in Figure 5.12 are taken from the lower part of the brain, affected to a substantial degree by susceptibility differences. The length of the green line in Figure 5.12-C is approximately 2 cm. The pixel shift map in Figure 5.12-D shows that this region has relatively large pixel shift values and it is likely this kind of geometric distortion is

responsible for some of the deviances between the activity maps and the BS maps. In Figure 5.12-B it can be observed that the patients anatomical image, with the activation map overlaid, shows some activation outside of the brain, this strengthens the likelihood that the activity maps are either inaccurately coregistered or that there was some distortion in the EPI images.

6.10 Case: Epilepsy

The results presented in Section 5.8 illustrate how simulated BOLD sensitivity maps can contribute to the presurgical planning process. The purpose of the BOLD analysis conducted on this patient was to guide in the planning of an impending operation. Operations to cure epilepsy are elective, as epilepsy is not a life threatening condition. Therefore it is extra important to map activity and the location of important centers in the brain, so that serious surgery related morbidity can be avoided (20). These results can be taken into account when deciding how the operation should be performed, or even if it should be performed at all.

When the BOLD exam is conducted for clinical purposes, the data should be analyzed differently than if the exam is conducted for basic neuroscience studies (8). There is a fundamental difference between the use of BOLD fMRI in research projects and for clinical applications. False positive and negative results were discussed in Section 3.1.1. In research applications, the statistical analysis is performed in such a way as to avoid false positive results. This emphasis can increase the frequency of false negative results. For research purposes false negative results may not have very serious effects, as the results are not the basis for diagnosis or further treatment of a patient. However, in clinical fMRI, for the individual patient, false negative or false positive results can have severe consequences. When planning the removal of, for example, an epileptic focus to relieve of epilepsy seizures, a false negative error in the BOLD analysis may lead the surgeon to remove too much tissue, possibly leading to a loss of function for the patient. On the other hand, a false positive result may result in the removal of too little tissue, thereby reducing the chances of complete loss of symptoms and cure. In cases such as these, a BOLD sensitivity map can be a valuable companion to the BOLD activation map. Considering the two maps together will give a more correct interpretation of the BOLD data.

The language centre is usually located near the area that was the target for this operation, see Figure 4.4. The activity maps in Figures 5.13 and 5.14 show orange activation blobs near the targeted area of the operation. These maps indicate that the language centre is in this region. If these activation maps are accurate it would imply that an epilepsy focus resection surgery could damage the language centre of the patient, leading to functional losses after the surgery. And for the surgery to be allowed to be performed, an ECoG procedure would most likely need to be conducted during the surgery. This is an unpleasant alternative, and it is possible that BOLD sensitivity maps could contribute important information so that this procedure could be avoided. The activation blob seen in Figure 5.14 seems to be located in an area shown to have a high BOLD sensitivity on the BS map. It is possible that the high BS in this region causes the activation to be artificially high, for example by combining with stimulus correlated noise or motion. If this connection is proved to be valid, BS maps can in the future potentially help in avoiding the use of the ECoG procedure. However, this aspect would need to be studied further.

There are some inconsistencies between the activation maps and the BOLD sensitivity maps that need to be addressed. On the right side of the brain, in Figure 5.13-B, there seems to be activation, marked by the white arrow, in an area where the BS map predicts complete

loss of BOLD sensitivity. There are several factors that can cause this deviation. First, recall the discussion of the deviance between simulated and measured image intensity maps in Section 6.7.1. Deviations in the magnetic field, in addition to altering the movement through k-space, can also cause geometric distortions in the EPI images, as discussed in Sections 6.2 and 6.3. The BOLD analysis is of course based on EPI images and the accuracy of the analysis can therefore be compromised. Figure 5.13-C shows a pixel shift map, generated from a magnetic field map for the slice. The pixel shift map is seen to have a high value in the relevant area, with a pixel shift of around 4. With a pixel dimension of 3 mm, this would lead to a signal shift of just over 1 cm in the anterior direction, which could be the reason for why activity is detected in a region where zero BOLD sensitivity is expected.

In addition, the coregistration between the BS maps and the activity maps was imperfect, this cannot explain gross differences like the one in Figure 5.13, the error will be limited to a couple of pixels. However, it implies that there will not be perfect correlation between the BS and activation maps in any case. In 5.13-A, some activation can be seen in the white matter, even though brain activity is supposed to be limited to grey matter; this can indicate that there are slight problems coregistering the activation maps with the MR images.

Until now, only cases where the susceptibility artifacts were caused by susceptibility differences between structures in the scull have been an issue. But in analogy with the discussion in Section 2.3.2, any metallic object in the region being imaged has the potential to cause artifacts. In the case of the epilepsy patient, several metallic clips from a previous operation caused severe signal dropout effects in the EPI images. This would of course affect the expected BOLD sensitivity and the analysis and interpretation of the BOLD signal. In Figure 5.15, the effect of metallic objects on the images is clearly illustrated. Some of the signal absence is a result of brain tissue having been removed during a previous surgery. The red arrows highlight a region where both the EPI image and the anatomical image are seen to have artifacts in the form of signal loss. But, as expected from the discussion in Section 2.3, the EPI image is affected to a larger degree. Figure 5.15-C shows the simulated BOLD sensitivity map of the slice, and the effect of the metallic clip on the left side of the brain is clear. Complete loss of BOLD sensitivity can be seen in the vicinity of the clips, although the region seems to be fairly well demarcated. However, on the edges there is a region where the BS is markedly reduced, this reduction can possibly affect the possibility of detecting BOLD signal in the area.

The white arrow in Figure 5.15-B, highlights a region where there seems to occur signal accumulation in the EPI image. If the pixel shift map, Figure 5.15-D, is surveyed, a region of high pixel shift can be observed just below the signal accumulation. Shifts of up to 5 pixels, 1.5 cm, are predicted in this region, which may account for the accumulation of signal that is observed.

Figure 5.16 illustrates one method of visualizing the reduced BOLD sensitivity caused by susceptibility gradients. The figure shows anatomical images for three different slices with three different levels of BOLD sensitivity overlaid. The levels shown can be adjusted according to the BOLD signal and noise levels in each particular BOLD experiment, so that each particular experiment's threshold can be determined.

From the results presented it seems that simulated BOLD sensitivity maps and pixel shift maps together, can contribute significantly to the process of quality assurance of the BOLD analysis that is derived from the EPI images.

6.11 Sources of Error

The field map used to generate the BOLD sensitivity map is acquired early in the MRI protocol before the EPI images. Motion of the patient between the two sequences can result in the field map no longer being valid for the fMRI volumes. Mannfolk et al. (37), however, concluded that, in the presence of typical motion, the BOLD sensitivity maps acquired from the field maps were still valid and could safely be used to estimate the BOLD sensitivity.

Inadequate or erroneous unwrapping of the phase images used to create the field maps, could become a following error when the BS maps and pixel shift maps are generated. However, as was discussed in Section 5.1, methods exist for unwrapping phase images almost perfectly (27). Where problems do arise, is where the original phase images were particularly complicated as a result of a quickly changing magnetic field, or in other words steep susceptibility gradients. Artifacts in these areas will lead to even steeper gradients and it is likely that either the general tendency of the BS maps will be preserved or the errors will be easy to spot. Even so, it is imperative that the field maps are quality checked before being used to generate BOLD sensitivity and pixel shift maps.

As described in Section 4.8, in order to obtain transverse gradient maps of the susceptibility gradient in the slice direction, a coregistration had to be performed between the axial and the sagittal dual echo sequences. Because of rounding there is a limit to the accuracy with which the slice gradient values can be transposed into the transverse plane. This accuracy will obviously improve with better resolution; however, this will in turn increase the duration of the unwrapping algorithm. In addition, acquiring the EPI images and the dual echo images with the same matrix size has practical benefits.

As discussed in Section 6.6 and illustrated in Figure 5.7; the value of T2* is well known to vary across the brain, both as a function of intrinsic properties and inhomogenities in the magnetic field (38). More accurate expressions for the simulated image intensity, SII, and simulated BOLD sensitivity, sBS, could therefore be achieved by introducing a varying T2*. However, the T2* mapping technique described in Section 4.7 would not be adequate as some of this variation is already accounted for through the expressions for the effect of the through-plane susceptibility gradients. A special mapping technique would therefore have to be developed in order to avoid counting the same effect twice. In analogy to other studies estimating BOLD sensitivity a constant T2* value was employed in the generation of BOLD sensitivity maps in this project (13), (12).

As discussed in Section 6.7, the possible effects of the magnetic susceptibility gradient in the read-out direction were neglected when generating the simulated BOLD sensitivity maps. The effect of a gradient, $\frac{\partial B}{\partial x}$, in the read direction is given by the following condition (30):

$$\frac{\partial B}{\partial x} > \frac{\pi}{\gamma * \Delta x * TE} \tag{6.1}$$

where Δx is the pixel dimension in the read direction. If 6.1 is satisfied, BS would be zero, otherwise there is no affect of the susceptibility gradient in the read direction. For common values of Δx and TE, the value of $\frac{\partial B}{\partial x}$ would have to be in order of magnitude ~5 mT/m, this is unlikely to be the case. As shown in Section 5.3, the effective echo time does vary throughout the brain; however, the TE would have to change so drastically that it would most certainly fall outside of the acquisition interval in any case. Excluding the susceptibility effects in the

read-out direction does therefore not seem to be a source of error in the generation of BOLD sensitivity maps.

In addition to neglecting the susceptibility gradient in the read direction and the variation in T2*, the BOLD sensitivity model developed by Deichmann et al. (21), does not consider the effects of patient movement and physiological noise. These have the potential to affect the accuracy of the BOLD model; however, Balteau et al. (30) concluded that for the parameters used in their experiments, similar to the ones used in this project, the approximation was valid. The field of BOLD sensitivity is still active, and new developments may eventually integrate these aspects into the model.

7 Conclusion and Outlook

7.1 Conclusion

Echo-planar imaging is today a very important part of the magnetic resonance imaging arsenal. Although this project has focused on the problems that are intrinsic to EPI, it is important to remember what a powerful tool this sequencing method can be. Years of research and development have been successful in eliminating some of the artifacts that plague EPI, but several problems persist. Both main goals of this project were aimed at identifying what problems can be expected when employing EPI for BOLD fMRI so that proper considerations can be made. In this project, methods for investigating the effects of susceptibility differences on EPI image quality and on BOLD sensitivity have been elucidated. It has been shown how magnetic field maps and BOLD sensitivity maps can improve the quality of the BOLD analysis by accounting for the effects of susceptibility differences.

In Sections 5.2-5.4, and 6.2-6.5, the use of magnetic field maps to indentify common artifacts in echo-planar imaging, such as signal loss and geometric distortions, caused by inhomogenities in the magnetic field, were illustrated and discussed. The idea behind the magnetic field maps is relatively simple and so is using the field maps to detect potential regions in EPI images where caution should be exercised when interpreting the images.

Echo-planar imaging is today most used in the field of functional magnetic resonance imaging. This project has focused particularly on the use of the blood oxygenation level-dependent effect to investigate brain activation. Through the theory presented in Section 3.1.2 and the results presented in Section 5.6, it is clear that the effect of susceptibility differences on BOLD is more comprehensive than the effect these differences have on the image intensity. Using simply the EPI images to predict the BOLD sensitivity would likely lead to erroneous conclusions about BS. BOLD sensitivity maps were generated and discussed in Sections 5.6 and 6.7 respectively; both the occurrence and distribution of BOLD sensitivity losses predicted by the maps were seen to correlate well with the general findings from other projects. And so it was found that the BS maps, together with magnetic field maps and pixel shift maps, work well as indicators of the quality of the BOLD fMRI experiment.

In Section 5.8, BOLD sensitivity maps were generated based on the data collected from the FRONT project. It has been shown that these maps contribute valuable information about the quality of the BOLD fMRI experiment. Depending on the level of the BOLD response, a reduction in BOLD sensitivity, as illustrated by the BS maps, may compromise the credibility of the experiment. The BOLD sensitivity map generated in Section 5.10, from the data collected from the epileptic patient, illustrate how these maps can become an important tool in the use of BOLD fMRI in presurgical planning. Through these two case studies it has been demonstrated how BOLD sensitivity maps can contribute valuable information to BOLD fMRI applications within both neuroscience and clinical neurology.

The method for generating field maps was laid out in Sections 4.4-4.5, in Section 4.8 it was discussed how these maps could be used to generate simulated BOLD sensitivity maps. All the code was programmed in Matlab, a common mathematical programming language. SPM is a free software package in Matlab and FSL is open source. Nordic ICE can be replaced by any software that reads dicom images and can export in alternative formats. Implementing these methods as an additional aspect of the BOLD analysis should therefore be straight forward. Compared with a standard MR scanning protocol, the only additional

sequences needed would be two dual echo sequences, one in the axial direction and one in the sagittal direction, adding only minutes to the total scan time. The data from the FRONT project showed how the magnetic field maps generated by the MRI scanner can be used directly, if a sufficiently short ΔTE is used the need for unwrapping can be circumvented.

In conclusion, the use of magnetic field maps and BOLD sensitivity maps as a means of assuring the quality of the BOLD fMRI analysis seems to be both feasible and effective.

7.2 Outlook and Future Work

BOLD fMRI is today far more commonly employed in the field of neuroscience than in clinical practice. Clinical applications are becoming more and more common; however, there are additional concerns in the clinical use of BOLD fMRI compared to use in basic neurological research. Standards and guidelines need to be established and trials need to be conducted. Routines need to be established for both data acquisition and processing. It is important to identify the limitations of BOLD fMRI and possible adverse effects. The work presented in this project is one step on the way in facilitating the use of BOLD fMRI for clinical applications.

In this project there was only a limited amount of time available for testing the methods developed on actual data, whether clinical or research related. Future work should therefore focus on applying the methods in both research projects and in the clinic, as well as finding ways of validating the predictions made by the magnetic field maps and simulated BOLD sensitivity maps. It would be particularly interesting to see how sBS maps can contribute to the BOLD analysis that is performed ahead of surgical removal of tumors.

More specifically, the tendency towards loss of BOLD sensitivity towards the posterior parts of the brain and the general positive effect of in-plane gradients higher up in the brain are interesting aspects to study. The presence of activity in areas with zero BOLD sensitivity should be investigated further. It would also be interesting to investigate if high BOLD sensitivity in a region, combined with stimulus correlated noise or motion, can produce false positive results.

In reference to the FRONT project it would be interesting to see if BOLD sensitivity maps and pixel shift maps combined can explain any deviances between the activity maps generated from the BOLD fMRI data and the other methods. It would likely improve the quality of the BOLD analysis if BOLD sensitivity could be included as a covariate in the analysis, comparing the sBS with the BOLD signal level and the noise level of the particular BOLD experiment. It could also be interesting to look at tendencies across patients and controls, respectively, by conducting a group analysis of the BS results for the two groups. And see if any general tendencies in the BOLD sensitivity could be found.

From the pixel shift maps shown, it is clear that there is some uncertainty in the spatial location of the activity detected in a BOLD analysis, due to geometric distortions. Several techniques have been developed for EPI distortion correction, and perhaps one of these techniques could be implemented by a future master student, to make the BOLD analysis more reliable.

References

1. **Mansfield, P., Pykett, I.L., Morris, P.G.** Human whole body line-scan imaging by NMR. *British Journal of Radiology.* 51, 1978.

2. **Lauterbur, P. C.** Image formation by induced local interactions: Examples employing nuclear magnetic resonance. *Nature.* 242:190-191, 1973.

3. **Mansfield, P.** Multi-planar image formation using NMR spin echoes. *Journal of physics.* 10, 1977.

4. **Ogawa, S., Lee,T.M., Nayak, A.S., Glynn, P.** Oxygenation-sensitive contrast in magnetic resonance image of rodent rat brain at high magnetic fields. *Magn. Reson. Med.* 44, 1990.

5. **Ojemann, J. G., Akbudak, E., Snyder, A. Z., McKinstry, R.C., Raichle, M. E., Conturo, T. E.** Anatomic localization and quantitative analysis of gradient refocused echo-planar fMRI susceptibility artifacts. *NeuroImage.* 6, 1997.

6. **Jezzard, P., Balaban, R.** Correction for geometric distortion in echo planar images from B0 field variations. *Magnetic Resonance in Medicine.* 34, 1995, 1.

7. **Barmet, C., De Zanche, N., Wilm, B. J., Pruessmann, K. P.** A transmit/receive system for magnetic field monitoring of in vivo MRI. *Magnetic Resonance in Medicine.* 2009, 62:269-276.

8. **Stippich, C.** *Clinical Functional MRI: Presurgical Functional Neuroimaging.* New York : Springer Verlag, 2007. 0942-5373.

9. **Detre, J. A.** Clinical applicability of functional MRI. *Journal of Magnetic Resonance Imaging.* 2006, 23:808-815.

10. **Jezzard, P., Matthews, P. M., Smith, S. M.** *Functional MRI: An introduction to methods.* Oxford : Oxford university press, 2001. 0192630717.

11. **Cusack, R., Russell, B., Cox, S., De Panfilis, C., Schwarzbauer, C., Ansorge, R.** An evaluation of the use of passive shimming to improve frontal sensitivity of fMRI. *NeuroImage.* 2005, 24:82-91.

12. **De Panfilis C., Schwarzbauer C.** Positive or negative blips? The effect of phase encoding scheme on susceptibility-induced signal loss in EPI . *NeuroImage.* 25, 2005.

13. **Deichmann, R., Gottfried, J.A., Hutton, C., Turner, T.** Optimized EPI for fMRI studies of the obitofrontal cortex. *NeuroImage.* 2003, 19.

14. **Bjørnerud, A.** The Physics of Magnetic Resonance Imaging. Oslo : s.n., 2008.

15. **Vlaardingerbroek, M.T., den Boer J.A.** *Magnetic Resonance Imaging.* s.l. : Springer Verlag, 2004.

16. **Westbrook, C.** *MRI in Practice.* Oxford : Blackwell Publishing Ltd, 2005.

17. **Haacke, E. M., Brown, R. W., Thompson, M. R., Venkatesan, R.** *Magnetic Resonance Imaging: Physical principles and sequence design.* New York : John Wiley & sons, 1999. 0-471-35128-8 .

18. **Buxton, R. B.** *Introduction to Functional Magnetic Resonance Imaging.* Cambridge : Cambridge University Press, 2009.

19. **Martin, E. A.** *Oxford concise colour medical dictionary.* Oxford : Oxford university press, 2007. 978-0-19-280699-4.

20. **Moonen, C.T.W., Bandettini, P.A.** *Functional MRI.* Berlin : Springer-Verlag, 2000. 3-540-67215.

21. **Deichmann, R. Josephs, O. Hutton, C. Corfield D. R., Turner, R.** Compensation of susceptibility-induced BOLD sensitivity losses in echo-planar fMRI imaging. *NeuroImage.* 2002, 15.

22. **Cusack, R., Brett, M., Osswald, K.** An evaluation of the use of magnetic field maps to undistort echo-planar images. *NeuroImage.* 18, 2003.

23. **Chavez, S., Xiang, Q., An, L.** Understanding phase maps in MRI: A new cutline phase unwrapping method. *IEEE Transactions on Medical Imaging.* 2002, Vol. 21, 8.

24. **Gorno-Tempini, M.L., Hutton, C., Josephs, O., Deichmann, R., Price, C., Turner, T.** Echo time dependence of BOLD contrast and susceptibility artifacts. *NeuroImage.* 2002, 15:136-142.

25. **Wansapura J.P, Holland S.K, Dunn R.S, Ball W.S.** NMR relaxation times in the human brain at 3T. *Journal of Magnetic Resonance Imaging.* 9, 1999.

26. **Krüger, G., Kastrup, A., Glover, G. H.** Neuroimaging at 1.5 T and 3.0 T: Comparison of oxygenation-sensitive magnetic resonance imaging. *Magnetic Resonance in Imaging.* 45, 2001.

27. **Jenkinson, M.** Fast, automated, N-dimensional phase-unwrapping algorithm. *Magnetic Resonance in Imaging.* 49, 2003.

28. **Smith, S.M.** Fast robust automated brain extraction. *Human Brain Mapping.* 2002, 17(3):143-155.

29. **Collignon, A., Maes, F., Delaere, D., Vandermeulen, D. Suetens, P. and G. Marchal.** Automated multi-modality image registration based on information theory. [bokforf.] Y.,

Barillot, C. and Di Paola, R. Bizais. *Information Processing in Medical Imaging.* Dordrecht, The Netherlands : Kluwer Academic Publishers., 1995.

30. **Balteau, E., Hutton, C., Weiskopf, N.** Improved shimming for fMRI specifically optimizing the local BOLD sensitivity. *NeuroImage.* 2010, 49:327-336.

31. **Norris, D.G.** Principles of magnetic resonance assessment of brain function. *Journal of Magnetic Resonance Imaging.* 2006, 23:794-807.

32. **Lipschutz, B., Friston, K. J., Ashburner, J., Turner, R., Price, C.J.** Assessing study-specific regional variations in fMRI signal. *NeuroImage.* 2001, 13:392-398.

33. **Devlin, J. T., Russell, R. P., Davis, M. H., Price, C. J., Wilson, J., Moss, H. E., Matthews, P. M., Tyler, L. K.** Susceptibility-induced loss of signal: Comparing PET and fMRI on a semantic task. *NeuroImage.* 2000, 11:589-600.

34. **Hunsche, S., Sauner, D., Treuer, H., Hoevels, M., Hesselmann, V., Schulte, O., Lackner, K., Volker, S.** Optimized distortion correction of epi-based statistical parametrical maps for stereotactic neurosurgery. *Magnetic Resonance Imaging.* 2004, 22:163-170.

35. **Oehler, M. C., Schmalbrock, P., Chakeres, D., Kurucay, S.** Magnetic susceptibility artifacts on high-resolution MR of the temporal bone. *American Journal of Neuroradiology.* 1995, 16:1135-1143.

36. **Le Bihan, D., Poupon, C., Amadon, A., Lethimonnier, F.** Artifacts and pitfalls in diffusion MRI. *Journal of magnteic resonance imaging.* 24, 2006.

37. **Mannfolk, P., Nilsson, M., Ståhlberg, F., Wirestam, R., Olsrud, J.** Assessment of spatial BOLD sensitivity variations in clinical fMRI using field maps. s.l. : ESMRMB, 2009.

38. **Clare, S., Francis, S., Morris, P. G., Bowtell, R.** Single-shot T2* measurement to establish optimum echo time for fMRI: Studies of the visual, motor, and auditory cortices at 3.0 T. *Magnetic Resonance in Medicine.* 2001, 45:930–933 .

39. **Ogawa, S., Tank, D. W., Menon, R., Ellermann, J. M., Kim, S. G., Merkle, H., Ugurbil, K.** Intrinsic signal changes accompanying sensory stimulation: functional brain mapping with magentic resonance imaging. *Proc. Natl. Acad.* 1992.

40. **Cusack, R. Papadakis, N.** New robust 3-D phase unwrapping algorithms: Application to magnetic field mapping and undistortiong echoplanar images. *NeuroImage.* 2002, 16:754-764.

Appendix A

Abbreviations and Expressions

μ	Magnetic moment
γ	Gyromagnetic ratio for hydrogen
Axial	Plane that divides the body into head and tail portions
B_0	Main magnetic field
BOLD	Blood Oxygenation Level Dependent
BS	BOLD Sensitivity
BW	Bandwidth
CBV	Cerebral Blood Volume
CBF	Cerebral Blood Flow
$CMRO_2$	Cerebral Metabolic consumption Rate
ECoG	Electrocoricography
EPI	Echo-Planar Imaging
fMRI	Functional Magnetic Resonance Imaging
FoV	Field of View
FSL	Fmrib Software Library, a software library containing image analysis and statistical tools for functional MRI
GRE	Gradient-Echo sequence
Hz	Hertz, unit of frequency
Lateralization	Specialization of function between the left and right hemispheres of the brain
Matlab	Matrix Laboratory, a programming language specially developed for handling matrices
MRI	Magnetic Resonance Imaging
NICE	nordic Image Control and Evaluation, an MR-image processing and analysis software
Resection	Surgical removal of a portion of any part of the body
Sagittal	Plane that divides the body into left and right portions
SE	Spin-Echo sequence
SENSE	Sensitivity Encoding
SPIR	Spectral Presaturation with Inversion Recovery
SPM	Statistical Parametric Mapping, a software that uses statistical methods to analyse functional MRI data
T	Tesla, unit for magnetic field strength
T1	Longitudinal relaxation time
T2	Transverse relaxation time
T2*	T2 including dephasing due to magnetic field inhomogenities
TE	Echo Time
TR	Repetition Time
WFS	Water fat shift

Appendix B

The two-sample t significance test

A t-test is a statistical hypothesis test in which the test statistic follows a Student's t distribution in the null hypothesis is true. If the null hypothesis $H_0 : \mu_1 = \mu_2$, then the following equation computes the two-sample t statistic:

$$t = \frac{\bar{x}_1 - \bar{x}_2}{\sqrt{\frac{s_1^2}{n_1} + \frac{s_2^2}{n_2}}}$$

Where $\bar{x}_1$ and $\bar{x}_2$ are the means of the two populations, s_1 and s_2 are the estimates of the standard deviations of the two populations and n_1 and n_2 are the sample sizes. When using t statistics in a BOLD fMRI analysis, the two populations represent active and resting states respectively. The higher the t-value, the more likely there is a significant difference between the resting and the active state. Once a t-value is determined, a p-value can be found using a table of values from the Student's t-distribution. If the corresponding p-value is below a chosen threshold, usually the 0.01, 0.005 or 0.001 level, then the null hypothesis can be rejected, and the difference between the two states is statistically significant at the chosen level.

Appendix C

Matlab Code

B.1 Unwrapping algorithm

```
function unwrap_bet

% Input: dualecho and bet
% Output: pixel shift maps, magnetic field maps in T and in Hz

folder = uigetdir('C:\Documents and Settings\nybruker\Mine dokumenter\MATLAB\opptak\','Declare folder with dicom files');
folder_bet = uigetdir('C:\Documents and Settings\nybruker\Mine dokumenter\MATLAB\opptak\','Declare folder with bet files');
list=dir(strcat(folder,'\*.dcm'));
cd(folder);
ant=size(list);
antallbilder=ant(1);
s=30;
t=1;
A=zeros(50,2);
for q=1:2:antallbilder
if q<=antallbilder
filename=list(q).name;
else
break
end
info=dicominfo(filename);
imtype=info.ImageType;
verdi = strncmp(imtype, 'ORIGINAL\PRIMARY\PHASE MAP\P\FFE', 25);
eval(['info' num2str(s) '=info;'])
if verdi==1
bildenr=info.InstanceNumber;
IM1 = dicomread(list(bildenr).name);
IM2 = dicomread(list(bildenr+1).name);
cd(folder_bet)
navn2 = ['load -ASCII bet_sag' num2str(s) '.mat'];
eval(navn2);
bet = eval(['bet_sag' num2str(s)]);
cd('..')
[r_dim, c_dim]=size(IM1);
nymatrise1=zeros(size(IM1));
nymatrise2=zeros(size(IM1));
maks=double(max(max(IM1)));
maks2=double(max(max(IM2)));
null=(maks)/2;
null2=(maks2)/2;
% Rescaling pixels between -pi og pi
for p=1:r_dim
for l=1:c_dim
if bet(p,l)~=0
nymatrise1(p,l)=((double(IM1(p,l))-null)/null)*pi;
end
if bet(p,l)~=0
nymatrise2(p,l)=((double(IM2(p,l))-null2)/null2)*pi;
end
end
end
for u=1:2
bilde=eval(['nymatrise' num2str(u)]);
diffbildefor=(imsubtract(nymatrise2,nymatrise1));
k=zeros(c_dim,r_dim); grad=zeros(c_dim,r_dim);
% Generating quality map
```

```
for h=1:2
bw=edge(bilde);
for m=2:(r_dim-1)
for n=2:(c_dim-1)
gjsn=(bilde(m,n)+bilde(m,n+1)+bilde(m+1,n)+bilde(m+1,n+1)+bilde(m-1,n)+bilde(m,n-1)+bilde(m-1,n-1)+bilde(m-1,n+1)+bilde(m+1,n-1))/9;
if bilde(m,n) && bilde(m,n+1) && bilde(m+1,n) && bilde(m+1,n+1) && bilde(m-1,n) && bilde(m,n-1) && bilde(m-1,n-1) && bilde(m-1,n+1) && bilde(m+1,n-1)
k(m,n)=(((bilde(m,n)-gjsn)^2)+(bilde(m,n+1)-gjsn)^2+(bilde(m+1,n)-gjsn)^2+(bilde(m+1,n+1)-gjsn)^2+(bilde(m-1,n)-gjsn)^2+(bilde(m,n-1)-gjsn)^2+(bilde(m-1,n-1)-gjsn)^2+(bilde(m-1,n+1)-gjsn)^2+(bilde(m+1,n-1)-gjsn)^2)/9;
else
k(m,n)=10;
end
if k(m,n)> 2.5 && k(m,n)<10 && bw(m,n)
k(m,n)=k(m,n)-(k(m,n)-0.3);
end
end
end
% Eliminates pixels with zero standard deviation
for l=1:c_dim
for p=1:r_dim
if k(l,p)==0
k(l,p)=10;
end
end
end
k=abs(k);
[gradintx,gradinty]=gradient(bilde);
% Eliminates problems from zero pixels
for l=1:c_dim
for p=1:r_dim
grad(l,p)=abs((gradintx(l,p)*gradinty(l,p))*k(l,p));
if bilde(l,p)==0
grad(l,p)=20;
end
end
end
% Find start pixel
[verdi1,rader] = min(k);
[verdi2,kollonne] = min(verdi1);
strpktkol = kollonne;
strpktrad = (rader(kollonne));
disp('Performing unwrapping ...');
colref1=strpktkol;
rowref1=strpktrad;
snupkt=3.4;                          % Treshold value
negsnupkt=-3.4;
topi=2*pi;
unwrapped_binary=zeros(size(IM1));     % Unwrapped pixels marked as 1
visited_binary=ones(size(IM1));        % Visited pixels marked with 0
unwrapped_binary(rowref1, colref1)=1;  % Start pixel marked as unwrapped
tic;
for l=1:c_dim                        % Zero pixels marked as visited
for p=1:r_dim
if bilde(l,p)==0 || diffbildefor(l,p)==0
visited_binary(l,p)=0;
end
end
end
if h==1
kval=grad;
else
kval=k;
end
w=0;       % Counting variable
```

```
%Loop until there are no adjoining pixels or they all lie on the border
while sum(sum(visited_binary(2:r_dim-1,2:c_dim-1)))~=0 && w<(r_dim*c_dim)
w=w+1;
%Obtain coordinates of adjoining unwrapped phase pixels
[r_unwrapped, c_unwrapped]=find(unwrapped_binary);
temp=size(r_unwrapped);
limk=100*ones(size(IM1));
for i=1:temp(1)
if visited_binary(r_unwrapped(i),c_unwrapped(i))==1
limk(r_unwrapped(i),c_unwrapped(i))=kval(r_unwrapped(i),c_unwrapped(i));
end
end
[verdipix1,rad] = min(limk);
[verdipix2,kollonne] = min(verdipix1);
c_active = (kollonne);
r_active = (rad(kollonne));
% Ignore pixels near the border
if r_active<=r_dim-1 && r_active>=2 && c_active<=c_dim-1 && c_active>=2
% Check that pixel hasn't already been used to unwrap
if visited_binary(r_active, c_active)==1
% Mark pixel as used
visited_binary(r_active, c_active)=0;
% Check pixel below first
if (bilde(r_active, c_active)-bilde(r_active+1, c_active))>snupkt && unwrapped_binary(r_active+1, c_active)==0 && bilde(r_active+1,
c_active)~=0
if (bilde(r_active, c_active)-bilde(r_active+1, c_active))>(snupkt+topi)
if (bilde(r_active, c_active)-bilde(r_active+1, c_active))>(snupkt+2*topi)
bilde(r_active+1, c_active)=bilde(r_active+1, c_active)+6*pi;
else
bilde(r_active+1, c_active)=bilde(r_active+1, c_active)+4*pi;
end
else
bilde(r_active+1, c_active)=bilde(r_active+1, c_active)+2*pi;
end
unwrapped_binary(r_active+1, c_active)=1;
elseif (bilde(r_active, c_active)-bilde(r_active+1, c_active))<negsnupkt && unwrapped_binary(r_active+1, c_active)==0 &&
bilde(r_active+1, c_active)~=0
if (bilde(r_active, c_active)-bilde(r_active+1, c_active))<(negsnupkt-topi)
if (bilde(r_active, c_active)-bilde(r_active+1, c_active))<(negsnupkt-2*topi)
bilde(r_active+1, c_active)=bilde(r_active+1, c_active)-6*pi;
else
bilde(r_active+1, c_active)=bilde(r_active+1, c_active)-4*pi;
end
else
bilde(r_active+1, c_active)=bilde(r_active+1, c_active)-topi;
end
unwrapped_binary(r_active+1, c_active)=1;
else
unwrapped_binary(r_active+1, c_active)=2;
end
% Check pixel down to the right
if (bilde(r_active, c_active)-bilde(r_active+1, c_active+1))>snupkt && unwrapped_binary(r_active+1, c_active+1)==0 && bilde(r_active+1,
c_active+1)~=0
if (bilde(r_active, c_active)-bilde(r_active+1, c_active+1))>(snupkt+topi)
if (bilde(r_active, c_active)-bilde(r_active+1, c_active+1))>(snupkt+4*pi)
bilde(r_active+1, c_active+1)=bilde(r_active+1, c_active+1)+6*pi;
else
bilde(r_active+1, c_active+1)=bilde(r_active+1, c_active+1)+4*pi;
end
else
bilde(r_active+1, c_active+1)=bilde(r_active+1, c_active+1)+2*pi;
end
unwrapped_binary(r_active+1, c_active+1)=1;
elseif (bilde(r_active, c_active)-bilde(r_active+1, c_active+1))<negsnupkt && unwrapped_binary(r_active+1, c_active+1)==0 &&
bilde(r_active+1, c_active+1)~=0
```

```
if (bilde(r_active, c_active)-bilde(r_active+1, c_active+1))<(negsnupkt-topi)
if (bilde(r_active, c_active)-bilde(r_active+1, c_active+1))<(negsnupkt-4*pi)
bilde(r_active+1, c_active+1)=bilde(r_active+1, c_active+1)-6*pi;
else
bilde(r_active+1, c_active+1)=bilde(r_active+1, c_active+1)-4*pi;
end
else
bilde(r_active+1, c_active+1)=bilde(r_active+1, c_active+1)-2*pi;
end
unwrapped_binary(r_active+1, c_active+1)=1;
else
unwrapped_binary(r_active+1, c_active+1)=2;
end
% Check pixel to the right
if (bilde(r_active, c_active)-bilde(r_active, c_active+1))>snupkt && unwrapped_binary(r_active, c_active+1)==0 && bilde(r_active,
c_active+1)~=0
if (bilde(r_active, c_active)-bilde(r_active, c_active+1))>(snupkt+topi)
if (bilde(r_active, c_active)-bilde(r_active, c_active+1))>(snupkt+4*pi)
bilde(r_active, c_active+1)=bilde(r_active, c_active+1)+6*pi;
else
bilde(r_active, c_active+1)=bilde(r_active, c_active+1)+4*pi;
end
else
bilde(r_active, c_active+1)=bilde(r_active, c_active+1)+2*pi;
end
unwrapped_binary(r_active, c_active+1)=1;
elseif (bilde(r_active, c_active)-bilde(r_active, c_active+1))<negsnupkt && unwrapped_binary(r_active, c_active+1)==0 && bilde(r_active,
c_active+1)~=0
if (bilde(r_active, c_active)-bilde(r_active, c_active+1))<(negsnupkt-topi)
if (bilde(r_active, c_active)-bilde(r_active, c_active+1))<(negsnupkt-4*pi)
bilde(r_active, c_active+1)=bilde(r_active, c_active+1)-6*pi;
else
bilde(r_active, c_active+1)=bilde(r_active, c_active+1)-4*pi;
end
else
bilde(r_active, c_active+1)=bilde(r_active, c_active+1)-2*pi;
end
unwrapped_binary(r_active, c_active+1)=1;
else
unwrapped_binary(r_active, c_active+1)=2;
end
% Check pixel above to the right
if (bilde(r_active, c_active)-bilde(r_active-1, c_active+1))>snupkt && unwrapped_binary(r_active-1, c_active+1)==0 && bilde(r_active-1,
c_active+1)~=0
if (bilde(r_active, c_active)-bilde(r_active-1, c_active+1))>(snupkt+topi)
if (bilde(r_active, c_active)-bilde(r_active-1, c_active+1))>(snupkt+4*pi)
bilde(r_active-1, c_active+1)=bilde(r_active-1, c_active+1)+6*pi;
else
bilde(r_active-1, c_active+1)=bilde(r_active-1, c_active+1)+4*pi;
end
else
bilde(r_active-1, c_active+1)=bilde(r_active-1, c_active+1)+2*pi;
end
unwrapped_binary(r_active-1, c_active+1)=1;
elseif (bilde(r_active, c_active)-bilde(r_active-1, c_active+1))<negsnupkt && unwrapped_binary(r_active-1, c_active+1)==0 &&
bilde(r_active-1, c_active+1)~=0
if (bilde(r_active, c_active)-bilde(r_active-1, c_active+1))<(negsnupkt-topi)
if (bilde(r_active, c_active)-bilde(r_active-1, c_active+1))<(negsnupkt-4*pi)
bilde(r_active-1, c_active+1)=bilde(r_active-1, c_active+1)-6*pi;
else
bilde(r_active-1, c_active+1)=bilde(r_active-1, c_active+1)-4*pi;
end
else
bilde(r_active-1, c_active+1)=bilde(r_active-1, c_active+1)-2*pi;
end
```

```
unwrapped_binary(r_active-1, c_active+1)=1;
else
unwrapped_binary(r_active-1, c_active+1)=2;
end
% Check pixel above
if (bilde(r_active, c_active)-bilde(r_active-1, c_active))>snupkt && unwrapped_binary(r_active-1, c_active)==0 && bilde(r_active-1,
c_active)~=0
if (bilde(r_active, c_active)-bilde(r_active-1, c_active))>(snupkt+topi)
if (bilde(r_active, c_active)-bilde(r_active-1, c_active))>(snupkt+4*pi)
bilde(r_active-1, c_active)=bilde(r_active-1, c_active)+6*pi;
else
bilde(r_active-1, c_active)=bilde(r_active-1, c_active)+4*pi;
end
else
bilde(r_active-1, c_active)=bilde(r_active-1, c_active)+2*pi;
end
unwrapped_binary(r_active-1, c_active)=1;
elseif (bilde(r_active, c_active)-bilde(r_active-1, c_active))<negsnupkt && unwrapped_binary(r_active-1, c_active)==0 && bilde(r_active-
1, c_active)~=0
if (bilde(r_active, c_active)-bilde(r_active-1, c_active))<(negsnupkt-topi)
if (bilde(r_active, c_active)-bilde(r_active-1, c_active))<(negsnupkt-4*pi)
bilde(r_active-1, c_active)=bilde(r_active-1, c_active)-6*pi;
else
bilde(r_active-1, c_active)=bilde(r_active-1, c_active)-4*pi;
end
else
bilde(r_active-1, c_active)=bilde(r_active-1, c_active)-2*pi;
end
unwrapped_binary(r_active-1, c_active)=1;
else
unwrapped_binary(r_active-1, c_active)=2;
end
% Check pixel above left
if (bilde(r_active, c_active)-bilde(r_active-1, c_active-1))>snupkt && unwrapped_binary(r_active-1, c_active-1)==0 && bilde(r_active-1,
c_active-1)~=0
if (bilde(r_active, c_active)-bilde(r_active-1, c_active-1))>(snupkt+topi)
if (bilde(r_active, c_active)-bilde(r_active-1, c_active-1))>(snupkt+4*pi)
bilde(r_active-1, c_active-1)=bilde(r_active-1, c_active-1)+6*pi;
else
bilde(r_active-1, c_active-1)=bilde(r_active-1, c_active-1)+4*pi;
end
else
bilde(r_active-1, c_active-1)=bilde(r_active-1, c_active-1)+2*pi;
end
unwrapped_binary(r_active-1, c_active-1)=1;
elseif (bilde(r_active, c_active)-bilde(r_active-1, c_active-1))<negsnupkt && unwrapped_binary(r_active-1, c_active-1)==0 &&
bilde(r_active-1, c_active-1)~=0
if (bilde(r_active, c_active)-bilde(r_active-1, c_active-1))<(negsnupkt-topi)
if (bilde(r_active, c_active)-bilde(r_active-1, c_active-1))<(negsnupkt-4*pi)
bilde(r_active-1, c_active-1)=bilde(r_active-1, c_active-1)-6*pi;
else
bilde(r_active-1, c_active-1)=bilde(r_active-1, c_active-1)-4*pi;
end
else
bilde(r_active-1, c_active-1)=bilde(r_active-1, c_active-1)-2*pi;
end
unwrapped_binary(r_active-1, c_active-1)=1;
else
unwrapped_binary(r_active-1, c_active-1)=2;
end
% Check pixel to the left
if (bilde(r_active, c_active)-bilde(r_active, c_active-1))>snupkt  && unwrapped_binary(r_active, c_active-1)==0 && bilde(r_active,
c_active-1)~=0
if (bilde(r_active, c_active)-bilde(r_active, c_active-1))>(snupkt+topi)
if (bilde(r_active, c_active)-bilde(r_active, c_active-1))>(snupkt+4*pi)
```

```
bilde(r_active, c_active-1)=bilde(r_active, c_active-1)+6*pi;
else
bilde(r_active, c_active-1)=bilde(r_active, c_active-1)+4*pi;
end
else
bilde(r_active, c_active-1)=bilde(r_active, c_active-1)+2*pi;
end
unwrapped_binary(r_active, c_active-1)=1;
elseif (bilde(r_active, c_active)-bilde(r_active, c_active-1))<negsnupkt && unwrapped_binary(r_active, c_active-1)==0 && bilde(r_active,
c_active-1)~=0
if (bilde(r_active, c_active)-bilde(r_active, c_active-1))<(negsnupkt-topi)
if (bilde(r_active, c_active)-bilde(r_active, c_active-1))<(negsnupkt-4*pi)
bilde(r_active, c_active-1)=bilde(r_active, c_active-1)-6*pi;
else
bilde(r_active, c_active-1)=bilde(r_active, c_active-1)-4*pi;
end
else
bilde(r_active, c_active-1)=bilde(r_active, c_active-1)-2*pi;
end
unwrapped_binary(r_active, c_active-1)=1;
else
unwrapped_binary(r_active, c_active-1)=2;
end
% Check pixel below to the left
if (bilde(r_active, c_active)-bilde(r_active+1, c_active-1))>snupkt && unwrapped_binary(r_active+1, c_active-1)==0 && bilde(r_active+1,
c_active-1)~=0
if (bilde(r_active, c_active)-bilde(r_active+1, c_active-1))>(snupkt+topi)
if (bilde(r_active, c_active)-bilde(r_active+1, c_active-1))>(snupkt+4*pi)
bilde(r_active+1, c_active-1)=bilde(r_active+1, c_active-1)+6*pi;
else
bilde(r_active+1, c_active-1)=bilde(r_active+1, c_active-1)+4*pi;
end
else
bilde(r_active+1, c_active-1)=bilde(r_active+1, c_active-1)+2*pi;
end
unwrapped_binary(r_active+1, c_active-1)=1;
elseif (bilde(r_active, c_active)-bilde(r_active+1, c_active-1))<negsnupkt && unwrapped_binary(r_active+1, c_active-1)==0 &&
bilde(r_active+1, c_active-1)~=0
if (bilde(r_active, c_active)-bilde(r_active+1, c_active-1))<(negsnupkt-topi)
if (bilde(r_active, c_active)-bilde(r_active+1, c_active-1))<(negsnupkt-4*pi)
bilde(r_active+1, c_active-1)=bilde(r_active+1, c_active-1)-6*pi;
else
bilde(r_active+1, c_active-1)=bilde(r_active+1, c_active-1)-4*pi;
end
else
bilde(r_active+1, c_active-1)=bilde(r_active+1, c_active-1)-2*pi;
end
unwrapped_binary(r_active+1, c_active-1)=1;
else
unwrapped_binary(r_active+1, c_active-1)=2;
end
end
end
end
end
eval(['bilde' num2str(u) '=bilde;' ])
t=t+1;
end
diffbilde=imsubtract(bilde2,bilde1);
% B0-kart
deltaTE=2.3*10^-3;          % s
gyro=2.67663694*10^8;       % rad*Hz/Tesla
bandwidth=42.1;             % Hz/pixel
% Magnetic field map in HZ
frekkart=diffbilde/(deltaTE*2*pi);
```

```
% Pixels hift map
pixshift = frekkart/bandwidth;
% Magnetic field map in T
kart=diffbilde/((deltaTE)*gyro);
e(:,:,:,s) = pixshift;
% Save fieldmap in T as .mat
cd ('Fieldmap')
navn=['Fieldmap' num2str(s) '.mat'];
save(navn, 'kart', '-ASCII')
cd('..')
eval(['Kart' num2str(s) '=frekkart;'])
A(s,1)=max(max(pixshift));
A(s,2)=min(min(pixshift));
toc;
s=s+1;
end
end
fremax=max(max(A));
absfremin=abs(min(min(A)));
range=fremax+absfremin;
Matrise(1,1)=fremax;
Matrise(1,2)=absfremin;
Matrise(1,3)=range;
% Save fieldmap in Hz as dicom
cd ('Dicom_fieldmap')
for i=1:(s-1)
frekkart=eval(['Kart' num2str(i)]);
inform=eval(['info' num2str(i)]);
frekkart=((frekkart+absfremin)/range)*4094;
min(min(frekkart));
max(max(frekkart));
RGB16 = uint16(round(frekkart));
if i<10
dicomwrite(RGB16, ['Fieldmap0' num2str(i) '.dcm'], inform);
else
dicomwrite(RGB16, ['Fieldmap' num2str(i) '.dcm'], inform);
end
end
save -ascii Matris.dat Matrise
cd('..')
figure,montage(e, 'DisplayRange', []), title('Pixelshiftkart'), impixelinfo
```

B.2 T2* map

```
function t2stjerne_ylva

% Generating a map of T2*
% Input: 2 images pr slice at different TE and BET

folder = 'C:\Documents and Settings\nybruker\Mine dokumenter\MATLAB\Opptak_etter_Nice\Ylva\dual_echo_ms_21';
folder2 = 'C:\Documents and Settings\nybruker\Mine dokumenter\MATLAB\Opptak_etter_Nice\Ylva\dual_echo_ms_21\BET';
TE1 = 3.2;
TE2 = 5.5;
r_dim = 80;
c_dim = 80;
T2 = double(zeros(c_dim,r_dim));
histogram = zeros(151);
t=1;
for q = 1:36          % q denotes slice number
cd(folder)
navn_TE1 = ['IM' num2str(2*q-1) '.dcm'];
int1 = double(dicomread(navn_TE1));
navn_TE2 = ['IM' num2str(2*q) '.dcm'];
```

```
int2 = double(dicomread(navn_TE2));
% Read BET images
cd(folder2)
navn2 = ['load -ASCII bet' num2str(q) '.mat'];
eval(navn2);
bet = eval(['bet' num2str(q)]);
for p=1:r_dim
for l=1:c_dim
if abs(log(int1(p,l)./int2(p,l)))>0.01
if bet(p,l)~=0
T2(p,l) = (TE2-TE1)./log(int1(p,l)./int2(p,l));
else
T2(p,l) = 0;
end
end
end
end
% Generate histogram
for p=1:r_dim
for l=1:c_dim
verdi = round(T2(p,l));
if verdi<=150 && verdi>0
histogram(verdi)=histogram(verdi)+1;
end
end
end
cd ('T2-star')
if t<10
navn=['TETO' num2str(t) '.mat'];
save(navn, 'T2', '-ASCII')
else
navn=['TETO' num2str(t) '.mat'];
save(navn, 'T2', '-ASCII')
end
cd('..')
t=t+1;
end
```

B.3 Susceptibility gradient in slice direction

```
function slice_grad_epilepsi

% Input: Fieldmaps in sagittal direction
% Output: Slice gradient in the transverse plane
% x,y and z are the coordinates in the sagittal images
% x1, y1 and z1 are the coordinates for the axial slices

folder_fieldmap_slice = 'C:\Documents and Settings\nybruker\Mine
dokumenter\MATLAB\Opptak_etter_Nice\Epilepsi_0705\dual_echo_sag\Fieldmap_bet';
folder_slice_gradient = ('C:\Documents and Settings\nybruker\Mine
dokumenter\MATLAB\Opptak_etter_Nice\Epilepsi_0705\dual_echo_sag\Slice_gradient');
ant_slices = 54;
rdim=80;
cdim=80;
for i = 1:ant_slices
cd(folder_fieldmap_slice)
navn = ['load -ASCII Fieldmap' num2str(i) '.mat'];
eval(navn);
fieldmap_slice = eval(['Fieldmap' num2str(i)]);
[gradx, grady] = gradient(fieldmap_slice, 0.003, 0.003);
grady = -grady;
eval(['vert' num2str(i) '=flipud(grady);' ])
end
```

```
for z=1:48
slice_transverse = double(zeros(rdim,cdim));
for x=2:rdim-1
for y=2:cdim-1
x1 = round(0.001*x-1*y+0.005*z+82.995);
y1 = round(0*x+0.005*y+1*z+24.678);
z1 = round(-1*x-0.001*y+0*z+67.899);
if z1<ant_slices && z1>0 && x1<cdim && y1<rdim
current = eval(['vert' num2str(z1)]);
slice_transverse(y,x) = current(y1, x1);
end
end
end
slice_transverse=flipud(slice_transverse);
cd(folder_slice_gradient)
navn=['slice_grad' num2str(z) '.mat'];
save(navn, 'slice_transverse', '-ASCII')
end
```

B.4 BOLD sensitivity maps

```
function bold_sensitivity

% Generates BOLD sensitivity maps

folder_fieldmap = 'C:\Documents and Settings\nybruker\Mine
dokumenter\MATLAB\Opptak_etter_Nice\Epilepsi_0705\dual_echo_ax\Fieldmap_bet';
folder_slice_grad = 'C:\Documents and Settings\nybruker\Mine
dokumenter\MATLAB\Opptak_etter_Nice\Epilepsi_0705\dual_echo_sag\Slice_gradient';
folder_EPI = ('C:\Documents and Settings\nybruker\Mine dokumenter\MATLAB\Opptak_etter_Nice\Epilepsi_0705\EPI');
% Parameters
gyro = 42.576*10^6;           % Hz/Tesla If 42 is used 2*pi is dropped in Q
delta_t = 1.0466*10^-3;       % Interecho spacing s
delta_z = 3*10^-3;            % Slice thickness
FoV = 240*10^-3;              % m
tc = 35*10^-3;                % Echo time s
T2 = 50*10^-3;                % Relaxation time of gray matter at 3T s tatt fra Zwaag
dyn_scans = 75;
t_start = 12.5328*10^-3;      % Time after excitation when acquisition starts s
t_end = 57.4672*10^-3;        % Time after excitation when acquisition ends s
t=1;                          % Counter
r_dim = 80;
c_dim = 80;
TC = double(tc*ones(c_dim,r_dim));
TE = double(zeros(c_dim,r_dim));
SII = double(zeros(c_dim,r_dim));
sBS = double(zeros(c_dim,r_dim));
Q = double(zeros(c_dim,r_dim));
F = double(zeros(c_dim,r_dim));
factor = double(zeros(c_dim,r_dim));
qval = double(zeros(c_dim,r_dim));
for q = 1:35        % q denotes slice number
% Read fieldmap axial
cd(folder_fieldmap)
navn = ['load -ASCII Fieldmap' num2str(q) '.mat'];
eval(navn)
field_map = eval(['Fieldmap' num2str(q)]);
% Read EPI images
cd(folder_EPI)
if q<3
navn_epi = ['Image#0' num2str(10+(q-1)*dyn_scans) '.dcm'];
```

```
else
navn_epi = ['Image#' num2str(10+(q-1)*dyn_scans) '.dcm'];
end
epi = dicomread(navn_epi);
% Read slice gradient map
cd(folder_slice_grad)
navn = ['load -ASCII slice_grad' num2str(q) '.mat'];
eval(navn);
slice = eval(['slice_grad' num2str(q)]);
% Generating Q
[gradx, grady1] = gradient(field_map, 0.003, 0.003);
grady = -grady1;
for p=1:r_dim
for l=1:c_dim
Q(l,p) = 1-(gyro*delta_t*FoV*grady(l,p));
end
end
% Generating actual TE-map
for p=1:r_dim
for l=1:c_dim
if abs(Q(l,p))>0.2
TE(l,p) = TC(l,p)/Q(l,p);
end
if TE(l,p)>t_end || TE(l,p)<t_start
TE(l,p)=0;
end
end
end
% Generating F
for p=1:r_dim
for l=1:c_dim
F(l,p) = (slice(l,p)*TE(l,p)*gyro*2*pi*delta_z)/(4*sqrt(log(2)));
factor(l,p) = exp(-(F(l,p)^2));
end
end
% Generating simulated sensitivity map
limit_n=(((1-tc/t_end))/(gyro*delta_t*FoV));
limit_u=(((1-tc/t_start))/(gyro*delta_t*FoV));
for p=1:r_dim
for l=1:c_dim
if  abs(Q(l,p))>0.2
SII(l,p) = exp(-(TE(l,p)-TC(l,p))/T2)/Q(l,p)*factor(l,p);
elseif Q(l,p)==1
SII(l,p)=1;
end
if grady(l,p)<limit_u || grady(l,p)>limit_n
SII(l,p)=0;
end
end
end
% BOLD sensitivity map
for p=1:r_dim
for l=1:c_dim
sBS(l,p) = SII(l,p)*TE(l,p)/TC(l,p);
end
end
x(:,:,:,t) = sBS;
t=t+1;
end
figure, montage(x, 'DisplayRange', []), title('SBS'), caxis([0 1.5]), colormap(jet), impixelinfo
```